Light-trapping and Superhydrophobic Plant Surfaces
–
Optimized Multifunctional Biomimetic Surfaces for Solar Cells

Dissertation

Zur

Erlangung des Doktorgrades (Dr. rer. nat.)

der

Mathematisch-Naturwissenschaftlichen Fakultät

der

Rheinischen Friedrich-Wilhelms-Universität Bonn

vorgelegt von

Anna Julia Schulte

aus

Meschede

Bonn, Mai 2012

Angefertigt mit Genehmigung der Mathematisch-Naturwissenschaftlichen Fakultät der Rheinischen Friedrich-Wilhelms-Universität Bonn.

1. Gutachter: Prof. Dr. Wilhelm Barthlott

2. Gutachter: Prof. Dr. Kerstin Koch

Tag der Promotion: 22.08.2012

Erscheinungsjahr: 2012

Preface and Acknowledgements

Contents

1 General Introduction

1.1 Plant surfaces as model for biomimetic light-trapping surfaces

In a process spanning over 400 millions years of evolution, plants have developed multifunctional surfaces that are highly adapted to environmental conditions [Koch et al. 2010; Koch and Barthlott 2009; Koch et al. 2009; Barthlott 1991]. Nature provides several millions varieties of plant species resulting in an extreme diversity of functionalized surfaces, which are often characterized by a hierarchically structured architecture [Barthlott and Ehler 1977]. These sophisticated surface designs may protect leaves against contaminations or mechanical stress, play an important role in the plant's hydrologic balance, protect the metabolic system against harmful radiation or support the optical attractiveness of flowers [Koch et al. 2010; Bargel et al. 2006]. The architecture and chemistry of these surfaces determine their functionalities. Analysis of these optimized biological surfaces could be the key to optimizing technical surfaces. Over the last years these functionalized plant surfaces have often been used as models for the development of e.g. self-cleaning (Lotus-Effect) or air retaining (Salvinia-Effect) biomimetic surfaces [Barthlott et al. 2010; Cerman et al. 2009; Barthlott and Neinhuis 1997; Neinhuis and Barthlott 1997]. Yet the technical potential of the optical properties of plant surfaces has only been examined marginally.

1.2 Light-trapping in leaf and flower surfaces

The surfaces of light harvesting plant organs are particulary interesting, especially the surfaces of leaves and petals. Because of their energy harvesting through photosynthetic processes, scientific investigations have paid more attention to the examination of the optical properties of leaves [Riederer 2006; Brodersen and Vogelmann 2007; Sims and Gamon 2002; Combes et al. 2007; Knapp and Carter 1998; Smith et al. 1997; Woolley 1971; Lee et al. 1990; Lee and Graham 1986]. Plants collect sunlight as an energy source, more specifically electromagnetic radiation. The total energy (E; in eV) emitted from the sun is composed of many wavelengths and therefore appears white to the human eye and is described by

$$E = h \cdot \frac{c}{\lambda} \tag{1.1}$$

where h is Planck's constant ($\frac{eV}{s}$), c is the speed of light in vacuum ($\frac{m}{s}$) and λ is the wavelength (μm). The different wavelengths can be separated by passing light through a dispersive medium, i.e. water or glass, which results in the occurrence of a rainbow based on the varying velocities of light. The wavelengths in the visible spectral range (380 to 780 nm) are seen by us as different colours (blue to red). Wavelengths which are shorter (< 380nm, starting with ultraviolet radiation) as well as longer (> 780nm, starting with infrared radiation) than the visible spectrum can't be detected by the human eye [Hecht 2001].

The radiation send out by the sun (surface colour temperature about 6000 K) could be compared to the radiation send out by a black body at a temperature of 5800 K and ranges from 140 nm (high energy UV-C radiation) to about 10 cm (low energy microwaves) [Hecht 2001]. However,
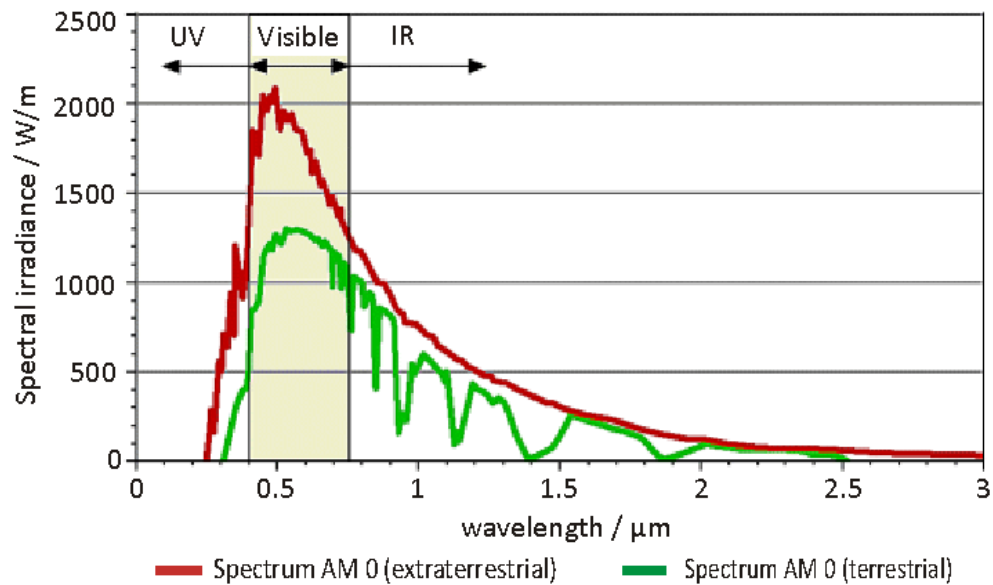
Figure 1.1: Comparison of sun spectal irradiance ($\frac{W}{m^2}$) outside the earth's atmosphere (AM 0) to the sun spectral irradiance reaching the earth's surfaces (AM 1.5); figure source: volker-quaschning.de

radiation striking the surface of the earth is affected by atmospheric effects, such as absorption and scattering. Local variations in the atmosphere, like water vapour, clouds, and pollution, but also the angle of incidence, the season of the year and the time of day, affect the intensity of terrestrial radiation [Wagemann and Eschrich 2010] (Figure 1.1). Thus, the radiation which strikes the earth's surface depends on the angle of approach. To get comparable values for radiation intensity Air Mass (AM) values are defined, which quantify the reduction in the power of light passing through the atmosphere. When the sun is directly overhead, Air Mass is 0 (AM 0). The most important standard value is AM 1.5, when the sun is positioned in a 48.2° angle to the earth surface normal.

Plants generally process electromagnetic radiation in the blue (400-480 nm) and yellow through red (550-700 nm) spectral range. These wavelengths are absorbed by photosynthetic reaction centres that contain chlorophyll a and chlorophyll b [Sitte et al. 2008] and are processed together with carbon dioxide to become organic compounds and oxygen. In contrast the absorption in the green range (480 to 550 nm) is low (Fig. 1.2); as a result leaves appear green.

Carotenoides also play a role in the photosynthetic reaction centres by enhancing the absorption in the blue/green range of around 500 nm [Pfündel et al. 2006]. They are usually synthesised and located in plastids. In green leaves these plastids are usually absent, but they have been found in some extreme shade plants [Hebant and Lee 1984; Lee and Graham 1986]. Further pigments, absorbed in the visible range, are anthocyanins (absorbance between 500 to 550 nm) and betalains (absorbance peaks near 480 nm, between 530 and 550 nm as well as between 270 and 280 nm). If they occur in a leaf, then they are located in the vacuoles and accumulated in the upper leaf epidermis [Pfündel et al. 2006].

Before the light is absorbed by the pigments within the leaf it must be transmitted across the outermost surface of the epidermal cells. How much light is transmitted into the leaf depends on the leaf's surface structuring. For plants in low-light environments, reduction of the specular surface reflection, which coincides with an increased transmittance of light, is of particular importance. Endler [1993] examined different light habitats (plant composition of a habitat) and their light environment (irradiance spectra within a habitat). The examination of shade in tropical rainforests shows that spectral distribution is rich in the middle wavelengths (green or yellow-green)
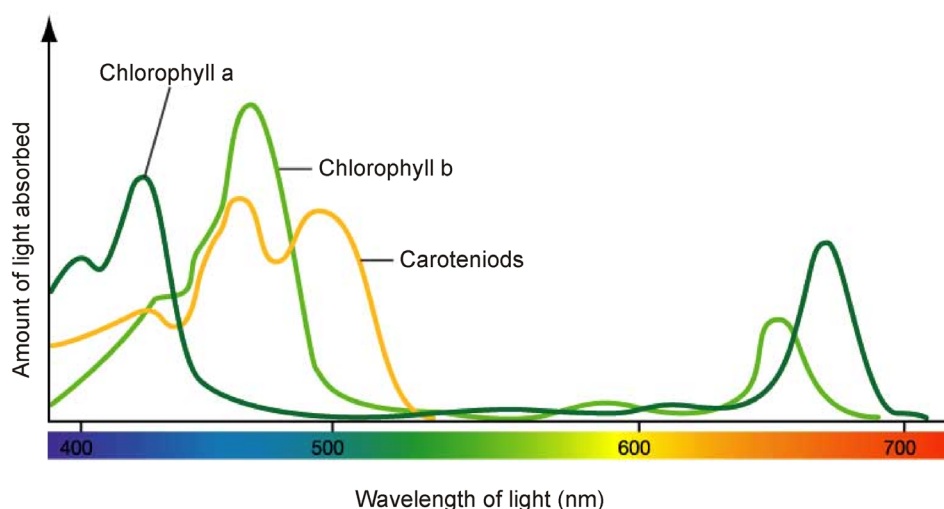
Figure 1.2: Absorption spectra of the leaf pigments chlorophyll a, chlorophyll b and caroteniodes; figure source: www.plantingscience.org

and also above 680 nm (red and near infrared). The light intensity within the forest shade varies but is in general markedly reduced (Fig. 1.3).

For this reason, low-light plants developed strategies for collecting as much of the available light as possible. Bone et al. [1985] examined tropical shade plants and postulated that uneven surfaces probably improve light-harvesting by decreasing specular reflection; they found lower reflectance values in light-focusing shade leaves as compared to sun leaves. Additionally, Martin et al. [1989] estimates that convex epidermal cells increase the capturing of light even from low angles by minimizing the specular reflection from the leaf surface. This reduction of the specular reflection is caused by multiple reflections between convexly shaped epidermal cells (Fig. 1.4).

Flowers also absorb sunlight, but they do this in order to be more colourful and attractive for pollinators [Whitney et al. 2011; Bernhard et al. 1968; Exner and Exner 1910]. In this process the favoured wavelengths are in the visible spectral range as well as the UV range (280 to 380 nm). Which wavelengths are favoured depends on the absorption properties of the pigments involved. A flower that is perceived as yellow contains pigments that absorb blue and green light, allowing the yellow light to pass through and out of the petal [Glover 2007]. The more light strikes a pigment, the more intense the colour signal will be. The most prominent pigments in flowers are flavonoids. They give flowers which are ivory and creamy (flavonols and flavones), yellow and orange colours are from aurones and chalcones, and the red-pink-purple-blue range result from anthocyanins [Glover 2007]. These water soluble pigments accumulate in the vacuole of epidermal cells [Kay et al. 1981]. Further existing pigments are the betalains, which only occur in the Caryophyllales [Glover 2007; Pfündel et al. 2006] or the carotenoids; which are much more widespread but less significant as floral pigments. The caroteniods are lipid-soluble and an essential component of the photosynthesis [Glover 2007].

To get colour intense petals, the surfaces have to (I) reflect less light, (II) disperse the transmitted light to the floral pigments and then (III) send it out of the leaf. In 1910 Exner and Exner postulated that the structure of a flower surface must be able to do this. The surface structure
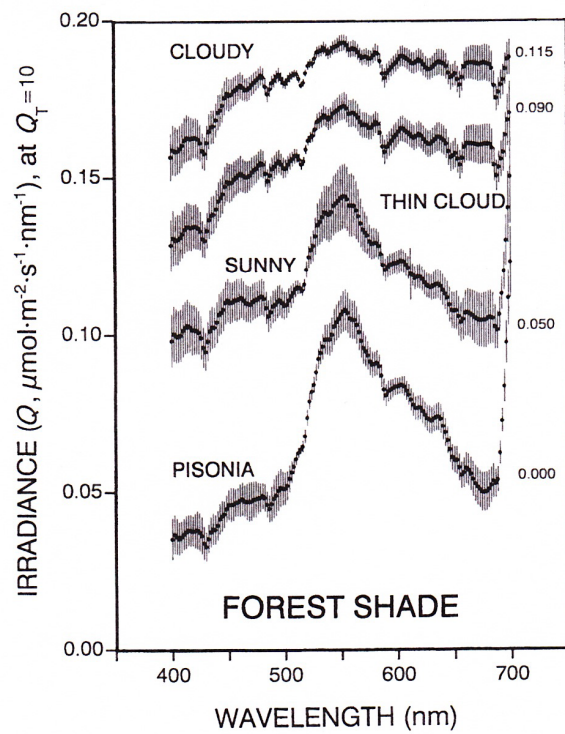
Figure 1.3: Forest shade spectra under varying weather conditions after [Endler 1993].
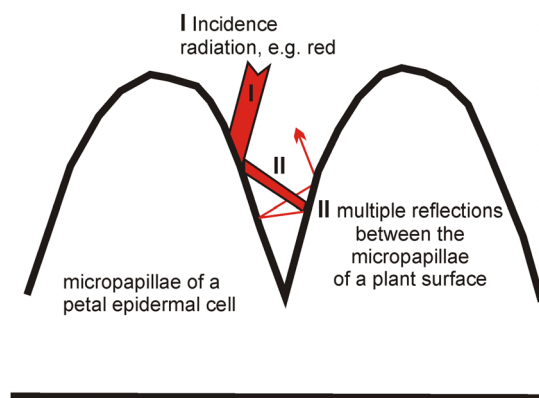
Figure 1.4: Multiple reflections at convex shaped epidermal cells. Drawing modified after Bernhard et al. [1968] based on the data from Exner and Exner [1910].
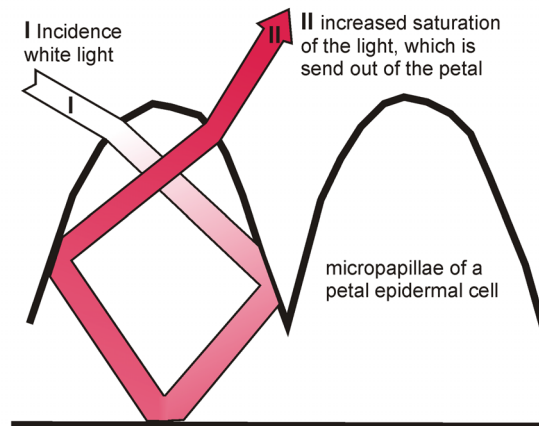
Figure 1.5: Path lengthening effect caused by the micropapillae of petal surfaces. Drawing modified after Bernhard et al. [1968] based on the data from Exner and Exner [1910]

reduces the specular reflection at the surface level as well as forming path directing of the light within the flower petal [Bernhard et al. 1968], saturating the flower colour (Fig. 1.5).

Thus, the development of hierarchically structured surfaces, especially in low-light plants and colour intensive petals, seems to offer a greater advantage in light harvesting processes and an benefit in pollinator attraction. These biological surfaces could be used as models for technical light trapping surfaces, such as the surfaces of solar cells.

1.3 Light-trapping in solar cell surfaces

Solar cell surfaces have to cope the same problems as plant surfaces. Optical losses reduce the power from a solar cell by lowering the short-circuit current. Optical losses occur when light is reflected on the front surface, or when it passes the solar cell without beeing absorbed.

Like plants, solar cells also capture in the visible spectral range, but additionally in the near infrared (from 400 up to 1000 nm). The spectral response of a solar cell is comparable to the quantum efficiency (Figure 1.6). The quantum efficiency gives the number of electrons output by the solar cell as compared to the number of photons incident on the device, while the spectral response is the ratio of the current generated by the solar cell to the power incident on the solar cell [Wagemann and Eschrich 2010] [www.pveducation.org].

To minimize optical losses on the surface of a solar cell different attempts were made to optimize their surfaces. One possibility is the use of an anti-reflective coatings (ARC) applied to the solar cell surface. These coatings are thin layers of a dielectric material, which cause destructive interference resulting in a zero reflection. The thickness of these anti-reflection coatings has to be one quarter the wavelength of the incoming wave, i.e. to eliminate reflectance over a broad spectral range multiple layers of different AR layers have to be applied [Wagemann and Eschrich 2010]. This results in extensive and expensive preparation.

A second possibility is the reduction of reflection using special texturing at the solar cell surface. Surface textures are able to reduce reflections by increasing reflections between surface structures, instead of sending them from the cell [Wagemann and Eschrich 2010]. In this context two different layers can be structured in a solar cell. First the Si-Wafer, and then a glass substrate on top of the solar cell. The principal design of a solar cell is shown in Figure 1.7. Surface texturing can be generated in different ways, i.e. *via* anisotropic etching of a single crystalline substrate
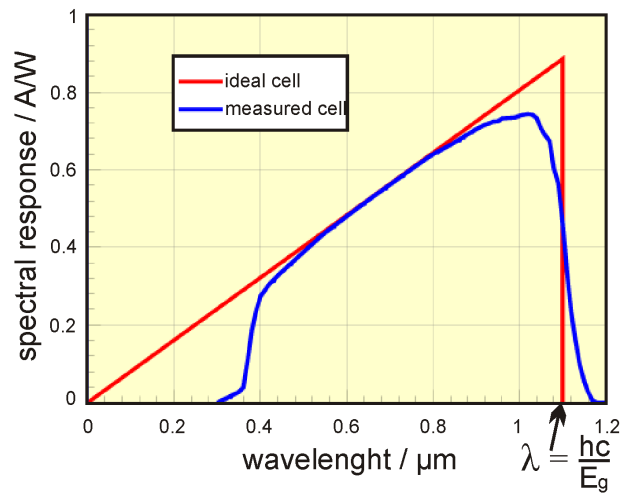
Figure 1.6: Spectral response of a silicon solar cell under glass; figure source: pveducation.org
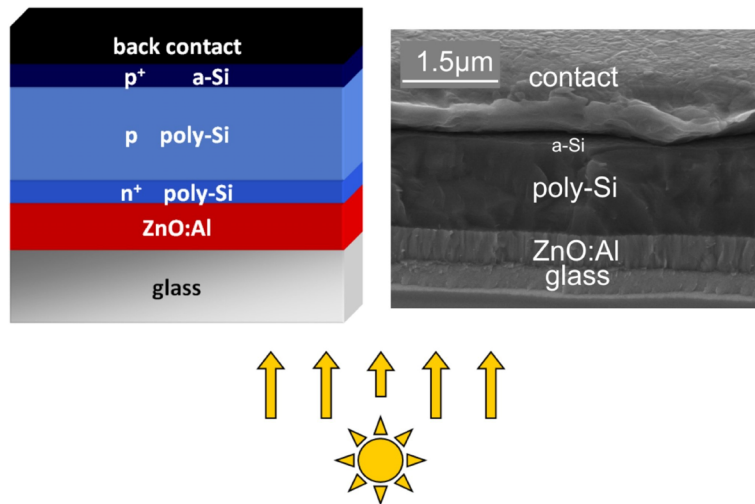
Figure 1.7: Principal design of a polycrystalline thin-film solar cell on a glass substrate; figure source: helmholtz-berlin.de

[Holdermann 2002]. Commonly used textures in industry are 'random pyramids', shown in Figure 1.8 A and 'inverted pyramid' textures, shown in Figure 1.8 B, which are realized directly in the silicon substrate [Campbell and Green 1987; Sun et al. 2008]. However, multicrystalline wafers can be textured using photolithographic techniques as well as by mechanically sculpting the front surface using dicing saws or lasers [Wenham and Green 1986]. These structures are also introduced for the upper cover glass, in order to minimize the reflection on the glass substrate. Some working groups made them from an additional polymer layer on top of the glass substrate [Choi and Huh 2010].

Optical losses can furthermore be reduced by increasing the optical path length in the solar cell (light trapping). Light trapping within the solar cell describes the process, by which the optical path length of a photon within the device is several times higher than the actual device thickness. This leads the incoming photon to stay in the material for a much longer time; consequently the absorption will increase. An optimal path length is about 50 times longer than the device thickness [Wagemann and Eschrich 2010]. Light trapping usually depends on the angle at which the incidence light penetrates the solar cell. Textured surfaces not only reduce surface reflection
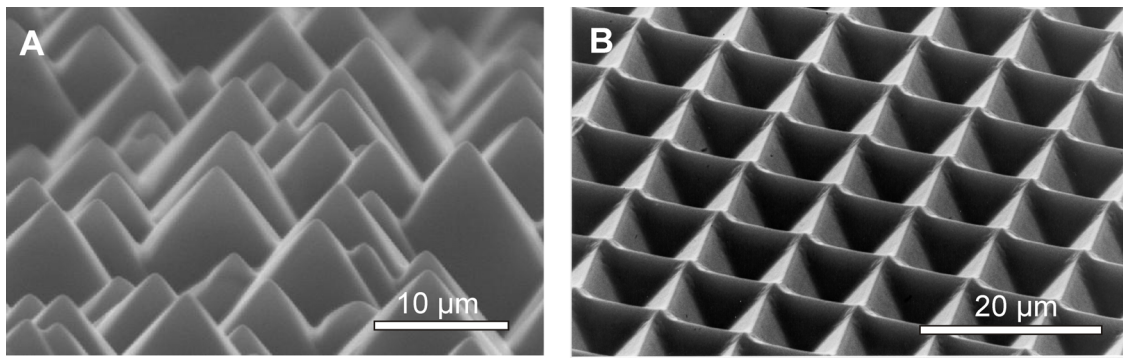
Figure 1.8: SEM micrograph of textured silicon surfaces: 'random pyramids' (A) and 'inverted pyramids' (B); figure source: pveducation.org
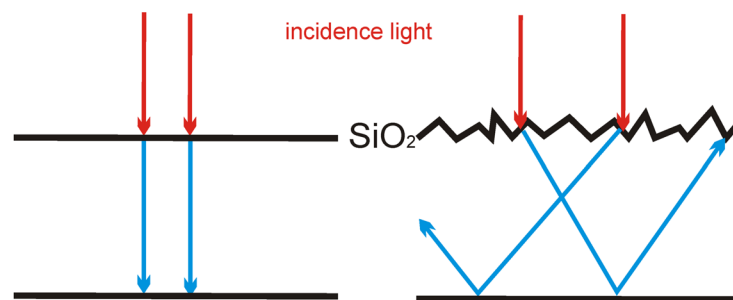
Figure 1.9: Light-trapping in solar cells: comparison of the optical path of the light within a smooth (A) and a structured (B) technical material. Light's path in the structured material is much longer than in the smooth material.

by multiplying reflections, but also capture the low angle light in silicone, resulting in an optical path lengthening (Fig. 1.9).

Remarkable similarities are to be found in the strategies used for reducing optical losses in plant and solar cell surfaces. However, plants had more than 400 millions of years to optimize their anti-reflective and light-harvesting surfaces.

2 Aims of this thesis

Plants developed highly adapted hierarchically structured surfaces. Especially in terms of their optical and wetting properties, plant surfaces could be used as models for the optimization of light-trapping and water-repellent solar cells. Though different solar cell surface textures have been proposed, a real biomimetic technical surface based on plant surface design is still missing. Out of this, the idea arose of developing a biomimetic light harvesting surface following the model of hierarchically structured plant surfaces. Therefore this study analyses the optical and wetting properties of hierarchically structured leaf and flower surfaces as well as their replicas. The aim of this work is the development of new light trapping biomimetic surface architectures for the optimization of high efficient solar cells combined with superhydrophobic (self-cleaning) properties. Thus, the presented thesis is divided into three sections with the subsequent research questions:

Fabrication of transparent biomimetic replicas for optical analyses (Chapter 3). The optical properties of plant organs like leaves and petals are very complex. Multiple reflections on the plant surface as well as within the organs make it difficult to analyse the influence of surface architecture alone on the spectral properties. In this chapter the plant surface structuring is separated from the biological model using the replication technique introduced by [Koch et al. 2008], modified for the fabrication of transparent surface replicas for optical examinations. A material has to be found which combines a good replication performance with transparent properties. To avoid air inclusions, often occurring in particular at surfaces with high aspect ratio micropapillae and dens nanofolds on top, a vacuum chamber should be developed.

Spectral properties of hierarchically structured biomimetic replicas (Chapter 4). For the optical optimization of high efficient solar cells, appropriate plant models must first be chosen. Which plant surfaces are qualified and what does the surface structuring looks like? The chosen surfaces have to be characterized in their surface architecture as well as in their optical properties. So, how much light is reflected in the particular structuring? How do the surface structures determine the path of the transmitted light? Does the surface structuring of the replicas act as a light trap?

Wetting properties of anti-reflective biomimetic flower surfaces (Chapter 5). Multifunctional surfaces have become of great commercial and scientific interest. Especially the combination of superhydrophobicity (self-cleaning) and light-trapping could be of great interest in solar cell applications. This study reveals whether the analysed surfaces have the potential to generate such a multifunctional surface. How do the surface parameters have to be to provide superhydrophobicity? Is the combination with light trapping properties possible?

3 Replication of hierarchically structured plant surfaces: Fabrication of transparent biomimetic replicas for optical analyses

3.1 Introduction

The micro- and nanomorphology of plant surfaces determine their properties and functions, e.g. wetting properties, but also optical characteristics [Koch et al. 2009; Vogelmann 1993]. Especially the surface structures of light harvesting organs such as leaves and petals seem to support light absorption [Martin et al. 1989; Bone et al. 1985]. Determining the spectral properties (reflectance, transmittance or absorbance) of plant surfaces in intact leaves remains difficult, as they are complex systems [Smith et al. 1997]. Various compartments (e.g. cells and interspaces) composing different chemical substances (e.g. water, air, pigments) determine their optical properties. Multiple reflexions occur at the surface as well as within the organ [Jacquemoud and Ustin 2001]. Thus, analysing the role of surface structuring is still a challenge.

To examine the role of surface architecture in light-trapping, the surface structures have to be separated from the other parts of the plant, which influence the absorption. Previous investigations demonstrate that the moulding technique introduced by Koch et al. [2008, 2007] is particularly well suited to the transfer of topography from soft and fragile plant surfaces into a technical material. Up to now, a material is used, which possess a slight colouring. Further in the preparation of hierarchically structured petals, artifacts caused by air inclusions occur.

3.1.1 Cost-efficient biomimetic technical surfaces

Especially in the development of biomimetic surfaces this replication technique affords surface prototypes in a way that is both fast and cost efficient [Koch et al. 2008; Schulte et al. 2009]. The fabrication of such functional biomimetic surfaces becomes of great commercial and scientific interest [Koch et al. 2008], especially as existing methods for structuring and functionalizing technical surfaces often use expensive and extensive techniques such as wet and dry etching [Chattopadhyay et al. 2006; Youngblood and McCarthy 1999], hot embossing [Han and Wang 2011], electron and ion beam lithography or electrochemical deposition [Mlcak and Tuller 1994; Singh et al. 2002; Hozumi and Takai 1997]. The replication is a soft lithographic technique [Xia and Whitesides 1998; Whitesides et al. 2001] which is able to reproduce the surface architecture in a precise way. The moulding technique principal is a long established and well-known method of analysing the surface structures of plants or animals. Substances such as, for example, agrose respectively gelantine have been used [Martin et al. 1991; Crisp and Thorpe 1950]. But, these moulding materials did not replicate structures in nanometre dimensions. The development of new soft silicone moulding materials allows for this high performance replication [Schmid and Michel 2000; Quake and Scherer 2000]. High aspect ratio (height to width ratio) structures in sizes from a few nanometres [Koch et al. 2007; Gorb 2007] to several micrometres [Schulte et al. 2009] could be replicated.

3.1.2 Replication of biological surfaces

Several studies introduced different replication techniques for the fabrication of biomimetic functionalized surfaces. Especially in the production of superhydrophobic [Lee et al. 2010; Gao et al. 2009; Sun et al. 2005] and oil-repellent [Gosh et al. 2009] surfaces but also a few in the field of optical functionalized surfaces. In the development of biomimetic optical surfaces, up to now, animal surfaces were used as models much more than plant surfaces [Vukusic et al. 2007; Vukusic and Sambles 2003; Vukusic et al. 2001a,b; Parker 2009, 2004]. Of course, the replication techniques used there, depend on the stability of the models, as the scales of the wings of butterflies..

Anti-reflective surfaces have been investigated extensively by the 'moth eye' principle [Clapham and Hutley 1973]. The moth eye surface possesses anti-reflective sub-wavelength structures, which reduce surface reflexions to a minimum. Attempts to replicate such surface structures were made by different groups [Deniz et al. 2011; Chen et al. 2009]. Further, the colourful wings of butterflies were replicated in terms of transferring the structural colouring into a technical material [Kang et al. 2010; Lakhtakia et al. 2009; Saison et al. 2008]. These surfaces are typically of robust construction and withstand techniques requiring a strong vacuum [Bhushan and Her 2010]. However, the replication of plant surfaces is limited to techniques which do not destroy the often fragile surface structures [Koch et al. 2008].

The replication of plant surfaces for the purpose of developing optical surfaces was found less frequently. Martin et al. [1991] used a dental-impression material to make negative moulds of the adaxial surface of leaves. After the negative material was cured they used them to produce agarose positive replicas. These replicas were used for characterizing the lens properties of individual epidermal cells. Whitney et al. [2009a] analysed iridescence in flowers of the *Hibiscus trionum* and Tulipa species by replicating the surface structuring. They prepared the replicas using first a dental wax and as filling an epoxy resin. This method was introduced by Green and Linstead [1990]. Specifications concerning the replication performance of these materials were not provided.

The structural colour of red rose petals and their replicas was analysed by Feng et al. [2010]. For this analysis a polyvinyl alcohol (PVA) water solution was applied to the petal surface. After evaporation of the water the negative PVA film was peeled off and subsequently poured with a Polystyrene chloroform solution. With regard to the SEM pictures of the epidermal cells shrinking artifacts seem to occur, probably because of the long evaporation time in the first moulding step. For the replication of leaves and petals negative materials with short curing times must be preferred. Another two step moulding technique for the preparation of polymer replicas was presented by Lee et al. [2011]. Through nickel electroforming, dried biotemplates were moulded and negative moulds were thus prepared. Afterwards polydimethylsiloxane (PDMS) positive replicas were fabricated. In this technique vacuum preparation is required in the first moulding step. This results in a random collapsing of the epidermal cells. In order to cope with these problems the authors dried the biotemplates, which does not solve the problem as the result is the same: collapsed papillae cells.

Favoured materials for the fabrication of negative moulds are addition-curing dental waxes. Best results were found for the material President Light Body® Gel (ISO 4823, polyvinylsiloxane (PLB), Coltene Wahledent, Hamburg, Germany) [Schulte et al. 2009; Koch et al. 2008, 2007]. Also often found in the literature, is the silicone Sylgard (Sylgard (R) 184 Silicone Elastomer Kit, Dow Corning S.A., Sneffe, Belgium) [Lee et al. 2011; Gosh et al. 2009; Shin et al. 2004]. In fabricating the positive replicas different materials were used. The selection of the positive material depends on the replicas' intended use. Criteria including the desired functionalities of the final replica as well as the material's properties during the replication process are crucial. For instance Martin et al. [1991] used a soft, unstable material (agarose) in fabricating leaf replicas for the examination of the lens effect of epidermal cells. In contrast, Koch et al. [2008] produced stable epoxy resin replicas to examine the influence of surface structuring on the wetting properties of surfaces. The material used there was able to replicate structures in nanometre dimensions. Thus the replication performance is another criterion for choosing the right material. Even when there
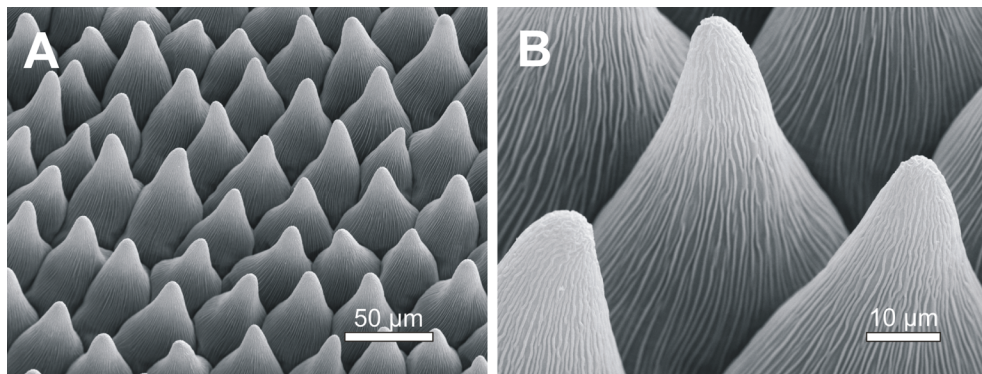
Figure 3.1: SEM micrographs of the surface structuring of *Viola tricolor* in 800x (A) and 1600x (B) magnification. Petal preparation was made *via* critical point drying

are several studies in which different resins were used as positive replication materials, there are no data on the precision of moulding process (replication performance).

3.1.3 Testing the replication performance

Koch et al. [2008] developed a method for analysing the moulding performance of materials in the replication of biological templates. In this method nanostructured surfaces were generated using plant wax crystals, which are then recrystallized on technical surfaces. Steps of 4 nm in height of the horizontally grown platelets will be replicated by different materials and their precision in replicating these steps should be examined.

3.2 Materials

3.2.1 Templates

For the development of a vacuum chamber, the upper surface (adaxial) sides of *Viola tricolor* petals were used, as air inclusions between this type of surface structure and the moulding material often occur. Plants were cultivated in the Botanic Gardens of the Rheinische Friedrich-Wilhelms-University (BGB). The registration number of *Viola tricolor* is BGB 27262-4-2004. A SEM picture of the surface structuring of *Viola tricolor* is shown in (Fig. 3.1). The petal was prepared by critical point drying (CPD).

Templates were made through octacosan-1-ol re-crystallization on silicon platelets of about 15 to 15 mm in order to characterize the new moulding material's replication performance. A low concentration solution (0.15 mass%) of the primary alcohol octacosan-1-ol (C28-ol, 99%purity; Sigma, Germany) in chloroform was applied to the substrate by dip coating. Subsequently, the templates were analysed using atomic force microscopy (AFM). Figure 3.2 shows the height and amplitude picture of a wax template (flat grown octacosan-1-ol crystal) analysed with an atomic force microscope (AFM).

3.2.2 Material for moulding

Two polysiloxanes were used for the fabrication of the negative moulds. First, the dental wax President Light Body® Gel (ISO 4823, polyvinylsiloxane (PLB), Coltene Wahledent, Hamburg, Germany) used in previous investigations. Then the silicon Sylgard (R) 184 Silicone Elastomer
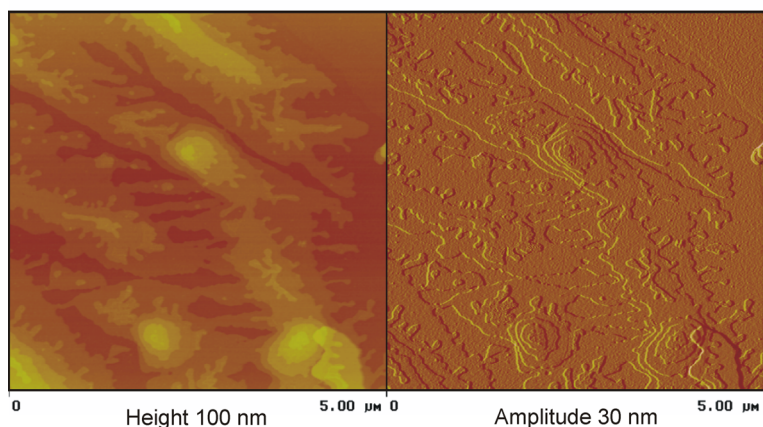
Figure 3.2: AFM pictures of a wax template of flat grown octacosan-1-ol crystals: height (left) and amplitude (right) picture.

Kit (Dow Corning S.A., Sneffe, Belgium) was chosen because of its low viscosity (300 mP) and thus good fluidity.

3.2.3 Fillings for the moulds

Two different fillings have been tested for their replication performance:

1. Epoxy resin (Epoxydharz L® , No. 236349, Conrad electronics, Hirschau, Germany) with hardener L (Härter L, No. 236365, Conrad electronics, Hirschau, Germany). Viscosity 700 mP. Mixing ratio 10 : 4.

2. Injecting resin EP (Reckli® , Chemiewerkstoff GmbH, Herne, Deutschland) with hardener B (Reckli® , Chemiewerkstoff GmbH, Herne, Deutschland). Viscosity 300 mP. Mixing ratio 3 : 1.

3.3 Methods

3.3.1 Scanning electron microscopy (SEM)

The surface structures of the templates and their replicas were investigated by SEM. Images were recorded using a CAMBRIDGE Stereoscan 200 SEM (Zeiss GMbH, Oberkochen, Germany), a digital image processing system (DISS 5, Version 5.4.17.0, Point Electronic GmbH, Halle, Germany) was used to visualize and measure the surface structures of the petals. Fresh plant material was dehydrated with ethanol and dried in a critical point dryer (CPD 020, Balzers Union, Balzers-Pfeifer GmbH, Aßlar). Replicas did not require special preparation because of their stability. All samples were sputter coated with a 30 nm gold layer (Balzers Union SCD 040, Balzers-Pfeifer GmbH, Aßlar) prior to SEM investigations.

3.3.2 Atomic force microscopy (AFM)

AFM measurements were performed using a Nano Scope IIa (Digital Instruments, Mannheim, Germany) in tapping mode with Al-coated silicon tapping-mode cantilevers (JPK-Instruments, Berlin, Germany). To identify the replication performance of the tested materials, height data
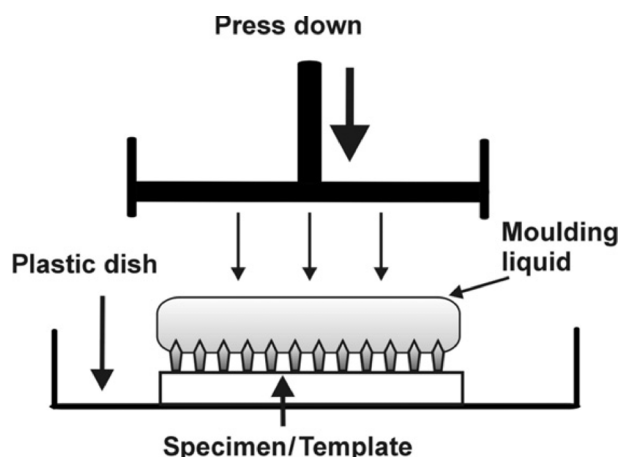
Figure 3.3: Schematic of the experimental set up of the first preparation step in moulding a plant surface [Koch et al. 2008].

were collected at the steps within the octacosan-1-ol crystals and their replicas. Height measurements were made with the program WSxM (Version 3.0, Nanotec Electronica, Madrid, Spain), using the image analysis tool Bearing. The results given are the median values of 10 crystal steps measured in an AFM scan size of $5 \times 5 \mu$m.

3.3.3 3D Light microscopy

The surface structures of the replicas were also investigated using the 3D light microscope. Images were recorded using a VHX 1000 digital microscope (Keyence Deutschland GmbH, Neu-Isenburg, Germany). Replicas were sputter coated with a 30 nm gold layer (Balzers Union SCD 040, Balzers-Pfeifer GmbH, Aßlar) prior to microscope investigations.

3.3.4 Contact angle measurements

The wettability of used filling materials (cured) was determined by static contact angel (CA) measurements (Dataphysics SCA 2.02, Filderstadt, Germany). These values should give additional information about the materials in terms of their use for the development of superhydrophobic replicas (Chapter 5). For this purpose, $5 \mu l$ droplets of de-mineralized water were applied to the material surface using an automatic dispenser controller. Contact angels were determined automatically using the Laplace-Young fitting algorithm. Measurements were carried out at room temperature (about $25°$). The material was characterized 2 days after curing. Average values and standard deviations were calculated from ten measurements (n=10).

3.3.5 Fabrication of the negative moulds

The replication technique used is a two-step moulding process, in which a negative is first generated and then a positive. For generating the negative replicas the template (biological sample) is in principal moulded with a polyvinylsiloxane dental wax (President light body Gel, ISO 4823, PLB; Coltene Whaldent, Hamburg, Germany). In the second step, the negative replicas were filled with a two-component resin. In this method the template surfaces are moulded by applying the negative material onto the template surface with a dispenser. The material is subsequently pressed onto the template with a pressure varying between 5 and 80 $\frac{g}{cm^2}$ [Koch et al. 2008]. The typical moulding process is shown schematically in (Fig. 3.3).
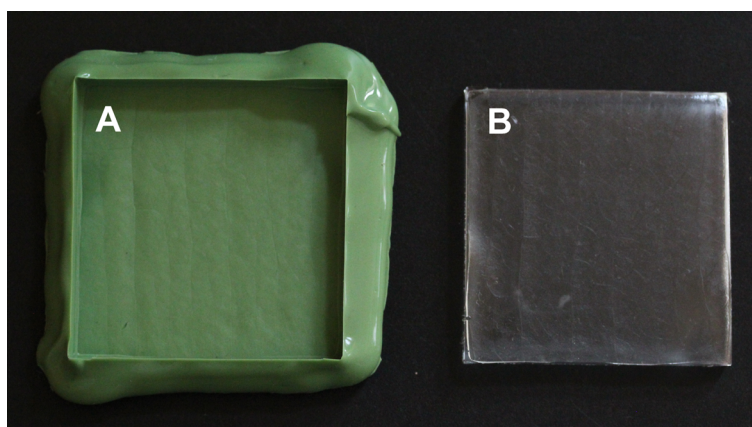
Figure 3.4: Replication of biological surfaces: Siloxane negative mould of a plant surface (A) and it's resin positive replica (B).

After a curing time of 5 minutes the elastic negative material is peeled off the templates. While the negative moulds of the petals need no further preparation, the negative moulds of the wax templates were washed in chloroform for 3-5 min and dried for 1-2 min at room temperature. This step is important as the wax crystals remain in the negative moulds after peeling them off the template. Afterwards, the negative replicas are bordered with the dental wax to get replica mould, which could be filled with epoxy resin (Figure 3.4). After this, the cleaned negatives are prepared for the next preparation step.

3.3.6 Fabrication of the positive replicas

In the next step the negative replicas were covered with a resin. Here the replication performance of a new material will be compared to the replication performance of a known one. Thus replicas made of epoxy resin [Koch et al. 2008] were compared to replicas made of an injection resin. To this end the epoxy resin and its hardener were mixed in a ratio of 10 : 4, while the injection resin and its hardener were mixed in a ratio of 3 : 1. Both mixtures were centrifuged at 30k rpm to eliminate air bubbles, which are produced during the mixing process and filled in the negative moulds. Subsequently, the filled replicas are positioned on a shaking device for 1h at 250 rpm, to reduce air bubbles produced during the filling process. The epoxy replicas were cured for 24h at room temperature while the injection resin replicas were cured for 48h at room temperature. After their individual curing times the replicas were peeled off the negatives. In total, five templates (petals as well as wax templates) were replicated and examined. Figure 3.4 shows exemplarily a positive replica prepared out of its negative mould.

3.4 Results

Modifications in the replication technique introduced by Koch et al. [2008] were required to fabricate biomimetic replicas and for the examination of their reflection and transmission properties. The results of this modification are presented in the following.

3.4.1 Replication performance of the positive materials

The replication performance of a new positive replication material has been investigated by replicating octocosan-1-ol wax platelets and measuring the step height of the flat monomolecular layers within the crystals. Figure 3.5 shows AFM height pictures as well as the associated section
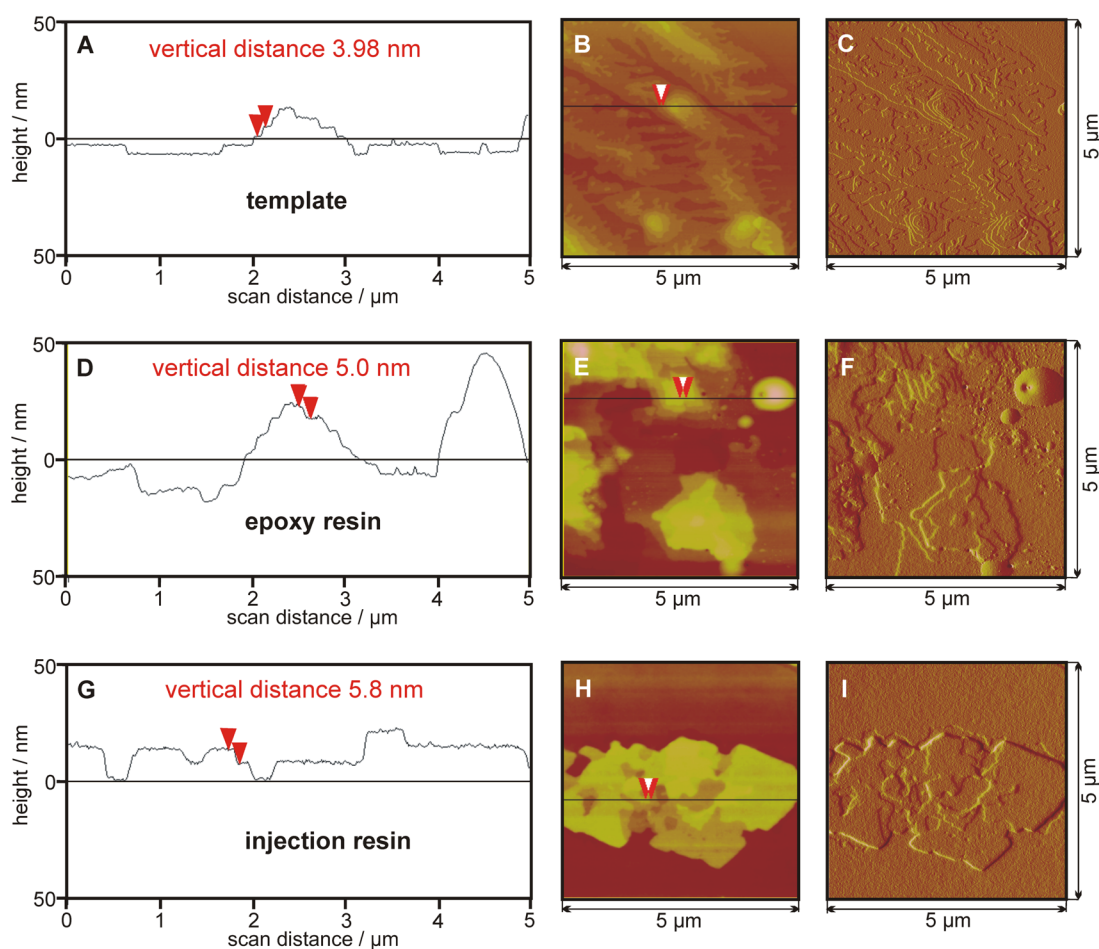
Figure 3.5: Section analyses of AFM height pictures of (A)flat grown octacosan-1-ol crystals and the corresponding height and amplitude pictures (B,C), section analyses of (D) epoxy resin replicas and the corresponding pictures (E, F) and analyses of (G) injection resin and the corresponding pictures (H, I).

analyses made of the template (Figure 3.5 A, B, C), its replica made of epoxy resin (Figure 3.5 D, E, F) and injection resin (3.5 G, H, I).

The median heights ($n = 10$) of the octacosan-1-ol platelets horizontally grown on two templates were analysed. The average platelet height on the first template was 4 ± 0.2 nm (Figure 3.5 A-C and Figure 3.6) and 4 ± 0.6 nm at the second template (only shown in Figure 3.6). The average height of the epoxy replicated platelets was 5 ± 0.9 nm for the first template (Figure 3.5 D-F and Figure 3.6) and 5.3 ± 0.9 nm for the second template(Figure 3.6). Further, the median height of the injection resin replicated platelets was 5.8 ± 0.8 nm for the first template (Figure 3.5G-I and Figure 3.6) and 5.4 ± 0.9 nm for the second template (Figure 3.6).

3.4.2 Vacuum application

The vacuum application chamber was developed to avoid air inclusions between the templates and the moulding material. This could happen during the first preparation step, while the negative material is being applied onto the template or during the second step, while the positive material is filled into the negative mould. This chamber was developed to be able using it in both replication
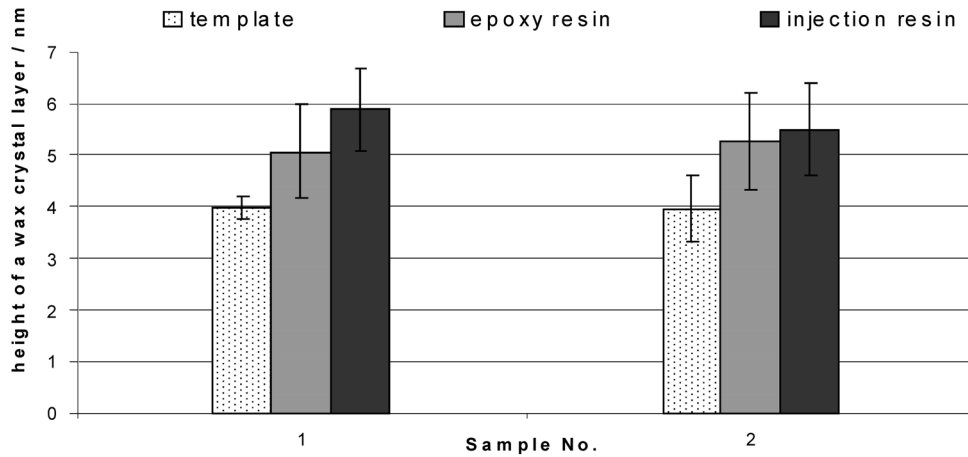
Figure 3.6: Average values and standard deviation (σ) of the crystal height of two templates and the replicas made of epoxy resin respectively injection resin.
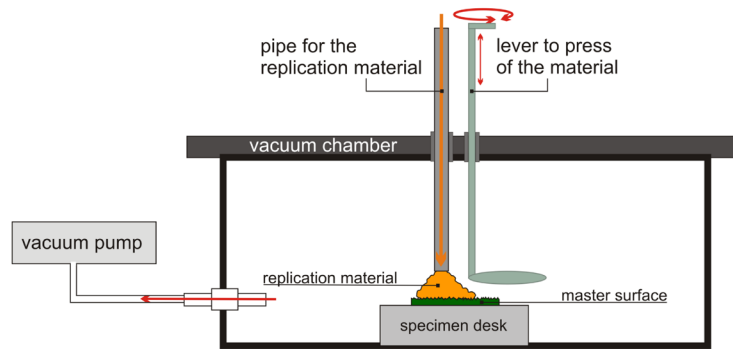
Figure 3.7: Schematic of the vacuum chamber.

steps, even when the application of the negative material onto a biological sample under vacuum is difficult as a high vacuum can cause the collapsing of the epidermal cells. Because of this only a low vacuum (20 mbar) was used to fabricate negative moulds of fragile biological samples. But, even when a vacuum application in the first step is possible, the work concentrates on the application of the positive material in the second step, as this is where most problems with air inclusions occur.

Two problems have to be solved in the development of a vacuum chamber. On the one hand, the chamber has to be closed while the replication material is applied to the template. The first problem is that even small gaps allowing air to get into the system, could hinder a controllable vacuum. Because of this a relatively small and manageable system had to be chosen first. A desiccator with two ports in the top cover and a port at the system's side was selected (schematically shown in Figure 3.7).

The first top port is used as a filling pipe for the replication material, consisting of a stable plastic tube (Polypropylen tube, length 10 cm, internal diameter 9 mm). The other was equipped with a lever to press the material down or influence its flow direction. At the side port a vacuum pump (Rd4 Vacuubrand GmbH & Co.KG, Wertheim, Germany) is attached to the system. The pressure inside the system was monitored with a manometer (DVR2 Vacuubrand GmbH & Co.

KG, Wertheim, Germany). Inside the vacuum chamber an elevated sample holder is positioned to bring the samples close to the filling pipe.

Generation of the negative moulds under vacuum

The ability to apply the negative material under vacuum could be of great interest in the replication of surface structures with undercuts. Here, biological samples where cut in to small samples ($1 \cdot 1 cm$) and secured on a glass slide using double-faced adhesive tape. The prepared samples were positioned within the desiccator at the sample desk. After closing the desiccator's top cover, the pipe was filled with the mixed two-component dental wax. Immediately afterwards the vacuum pump was switched on and a vacuum was drawn to about 20 mbar. During this process the negative material flowed from the pipe and was automatically applied to the template surface. Care must be taken to ensure that the vacuum does not fall under 20 mbar as the dental wax would be boiled. When the template is covered with the dental wax, the lever could be additionally used to press the material onto the template, thus the material spreads over the whole template and a smooth back side of the negative could be fabricated. Under vacuum the applied dental wax needs 15-20 min to cure, which is much longer than under ambient conditions (curing time about 5 min). After curing the negative mould is peeled off the template.

Generation of the positive replicas using vacuum

Air inclusions often occur on high papillated surfaces with additional cuticular folding on top (Figure 3.8 A). Application under vacuum is desirable to avoid such artifacts caused by air. In this the negative moulds of a template are positioned at the sample desk, directly under the application pipe of the closed top cover. The filing pipe is slightly pressed to an unstructured or unimportant area of the negative mould, filled with the mixed positive two-component resin and closed with a plug. Subsequently the vacuum pump is switched on. When the vacuum reaches about 20 mbar the pipe has to be lifted slightly and the resin flows out of the pipe into the negative replica. Here too care must be taken to ensure that the vacuum does not fall under 40 to 50 mbar as the epoxy resin would be boiled.

Figure 3.8 shows the SEM pictures of a positive replica of a *Viola* petal surface made under air conditions (A) and a positive replica made in vacuum conditions (B). In contrast to the replicas made at air (Figure 3.8 A), the replicas made under vacuum conditions possess no surface air inclusions (Figure 3.8 B). Repetitions of these positive replications show that the air bubble accumulation between the negative mould and the filling material could be considerably reduced because of the under pressure, even at low vacuum stages (20 mbar). It is furthermore assumed that the filling material flows more easily between the structuring than under ambient conditions as the negative replicas possess almost no artifacts.

3.4.3 Wetting properties of the negative materials

Static contact angle (CA) measurements were performed applying $5 \mu l$ water droplets to the smooth surface of the cured resins. From each material five samples were taken and two values were collected on each surface. Figure 3.9 shows the average CAs with their standard deviations. The epoxy resin has a median CA of $78.2 \pm 4.2°$ and the injection resin has a median CA of $77.1 \pm 3.46°$. Thus, the CAs of the compared materials do not differ significantly from each other.
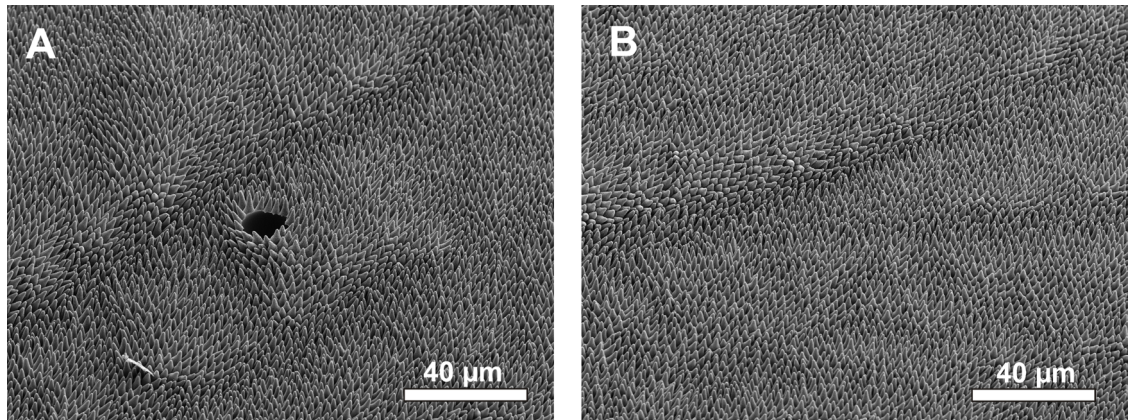
Figure 3.8: SEM Pictures of a *Viola* replica made at air (A) and at vacuum conditions (B). Replicas made in air often possess artifacts (holes in the replica) caused by air inclusions during the second preparation step. Application of the replication material under vacuum avoids these air inclusions.
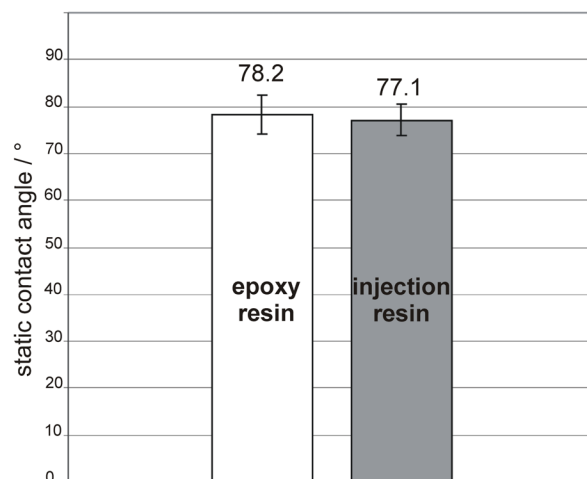
Figure 3.9: Static contact angles of the smooth epoxy and injection resin. Average values ($n = 10$) are given together with the standard deviation (σ).

3.5 Discussion

3.5.1 Replication performance of the materials

The values for the median height of the octacosan-1-ol platelets fit very well with the values shown by Koch et al. [2008], which also measured a median height of 4 nm. In contrast, the measured values of the epoxy replica or the injection resin (5 nm or 5.3 nm respectively) differ slightly from the measured values of the prepared replicas shown by Koch et al. [2008] (3.3 nm). This is probably a result of the different hardeners used. Koch et al. [2008] used hardener S while the replicas prepared here were made with hardener L. Some other slight variations, e.g. in room temperature or curing time, could perhaps result in these small differences. As compared to the epoxy replica, the injection resin replicas possess almost the same values (5.8 ± 0.8 nm and 5.4 ± 0.9 nm respectively). Both materials are able to replicate structures in nanometer dimensions. Slightly higher values could be caused by a marginal expansion of the resin during the curing process. Compared to the replication performance of the established epoxy resin the injection resin has the same replication performance and is therefore a suitable positive material in the replication process. Whitney et al. [2009b] also prepared replicas for optical investigations of plant surface structures. These replicas were prepared using the technique introduced by Green and Linstead [1990]. In this process a dental impression polymer was also used, but in contrast they used a two component dental polymer, which had to be mixed on a glass slide. The material used here is mixed automatically while dispensing it onto the plant surface. Previous studies with dental polymers mixed manually on a glass slide reveal, that air inclusions often occur within the dental material. These air inclusions can destroy the surface of the negative mould. The production of a high quality positive replica is hard to do. Further information about the replication performance of the positive material used was not provided. Green and Linstead [1990] reported on deficits in the replication of extremities (high aspect ratio structures). In contrast to the epoxy resin used by Koch et al. [2008] with a viscosity of 700 mP, the positive replication material used here (injection resin) has a clearly lower viscosity (300 mP). Because of this the material is more able to flow into cavities and high aspect ratio structures. A lack of surface features described by Green and Linstead [1990] could be avoided to a large extent. Additionally, these artifacts could be avoided by forcing the material down into the structures [Koch et al. 2008; Schulte et al. 2009].

3.5.2 Vacuum application

Green and Linstead [1990] also mentioned artifacts caused by air trapped between the template and the moulding materials. Using a vacuum chamber these air inclusions should be avoided as the pressure within the chamber is low (20 mbar in the first replication step and 40-50 mbar in the second replication step). Because of this the material is able to flow into the surface structures much better and air inclusions are avoided (Figure 3.8 B). Also, problems with the moulding of high aspect ratio surface structures could be handled using the vacuum chamber. In vacuum replication the strength of the vacuum is important. Results presented here show that a vacuum lower than 20 mbar, respectively, 40 -50 mbar cause a boiling of the moulding materials. Further, a strong vacuum is able to destroy the surface structuring of the fragile leaf and petal surfaces as shown by Lee et al. [2011] or Bhushan and Her [2010]. In addition, even if the curing time of the polymer is lengthened the replication process is relatively fast, the biological mater is not damaged by shrinkage as shown by Feng et al. [2010].

3.5.3 Wetting properties of the negative materials

In terms of generating superhydrophobic biomimetic surfaces knowledge of the CA of the replication material is of great importance. Both materials are defined as hydrophilic materials [Roach et al. 2008]. With respect to the wetting stages on rough surfaces proposed by Wenzel [1936] a

decreasing CA must be expected when a hydrophilic material is structured [Wenzel 1936]. However, the structuring of a hydrophobic material results in increased CAs. So in the fabrication of superhydrophobic biomimetic surfaces the surface structuring as well as the surface chemistry is important, i.e. the replicas have to become hydrophobic. Thus, in all probability, the polymer replicas have to be coated with a hydrophobic layer to get superhydrophobic replicas. This aspect will be examined and discussed in Chapter 5.

3.6 Conclusions

The fabrication of hierarchically structured biomimetic surfaces is of special interest in the envelopment of functionalized technical surfaces. Especially in the examination of the optical properties of plant surface structures transparent biomimetic replicas could be used to separate the surface structuring from the complex biological model. These replicas could be used as prototypes in the development of new light trapping surface designs. The modified replication technique introduced here is optimized for the fabrication of such surface prototypes. The replication performance of a new transparent material is tested in detail and the results show a high precision in replication even at nanometre dimensions. A vacuum chamber was then developed, which allows the application of the positive as well as the negative material under vacuum conditions. This results in far better replication as air bubble accumulation is almost eliminated. Artifacts in the surface structuring caused by these air inclusions are avoided. Compared to former replications techniques [Lee et al. 2011; Bhushan and Her 2010; Feng et al. 2010] a gentle technique is presented here, which does not destroy the fragile biological master.

In summary, the modified replication technique could be used for the fabrication of optically transparent, biomimetic surfaces. These replicas can be used for the examination of the optical properties of plant surface structures and therefore as prototypes for the development of high efficient light-trapping solar cell surfaces. Yet there are limitations in replica size, as the replicas as large as the plant surface models. Future research has to work on the large scale preparation of the biomimetic structures.

4 Spectral properties of hierarchically structured biomimetic replicas

4.1 Introduction

The outer surface of plants forms the first boundary, which interacts with the abiotic environment, e.g. light. Collecting energy is crucial for the survival of most plants. Leaves need to collect electromagnetic radiation through photosynthesis, i.e. to keep the metabolism running flowers need to harvest radiation in order to intensify their colouration to be more attractive for pollinators. The architecture of plant surfaces plays an important role in this light harvesting processes. The more light is reflected, the less light reaches the inner leaf compartments and the less energy can be captured. Especially in low light environments, plants need to develop strategies for optimized light harvesting, e.g. *via* optimized anti-reflective surfaces [Bone et al. 1985]. In this study 5 low-light plants and 4 colour intensive flowers were chosen and analysed as potential models for biomimetic light-harvesting surfaces in solar cell devices. Using the modified replication technique presented in Chapter 3, biomimetic surface replicas of the leaves and petals were generated.

In this thesis the term 'plant surface' is defined as the outermost structuring of leaves and petals, formed by the topography of epidermal cells with its overlying cuticle and additional coverings, e.g. wax layers. To understand the process of light capturing across the outer plant surfaces, the following morphological and physical aspects are relevant.

4.1.1 Physical fundamentals of surface optics

Physical consideration of the optical properties of whole leaves/petals are much more complex than the considerations of the surface only. Several studies pointed out two origins of reflected light in leaves. First the reflection from the cuticle/air interface and secondly light that enters the leaf and is reflected on the numerous air/cell interfaces inside the leaf [Vogelmann 1993; Gates and Tantraporn 1952]. The reflection from the cuticle/air interface does not pass the leaf interior and usually does not change spectrally [McClendon and Fukshansky 1990; King-Smith and Vanderbilt 1993] but partially in its polarization [King-Smith and Vanderbilt 1993; Woolley 1971]. The aspect of polarization seems to be important e.g. in remote-sensing in pollinator attraction. The amount of reflected light depends on the refractive index (RI) of the plant material. Wet plant cell walls possess an refractive index between 1.33 - 1.47 [Gausmann et al. 1974]. However, the light reflected on the air/cell interfaces passes the plant organ interior and changes it spectral composition because of the plant pigments and their absorption characteristics. Canopy reflectance models assume that whole leaf organs are Lambertain, i.e. perfect scatterers [Jacquemoud and Ustin 2001]. For the estimation of the optical properties (reflection and transmission of electromagnetic radiation) at the outermost plant surfaces some physical considerations are required.

If light (in the following the term light is used for the ultra violet, the visible spectrum as well for the near infrared) interacts at the interface of two media it will change its direction of propagation. Based on the law of conservation of energy, a combination of reflection and refraction can be observed. In contrast to the reflected part of the light, the transmitted light goes into the material of the second media. As mentioned above, the more light is reflected the less energy can be transmitted, i.e. collected. The amount of the reflected light depends on the
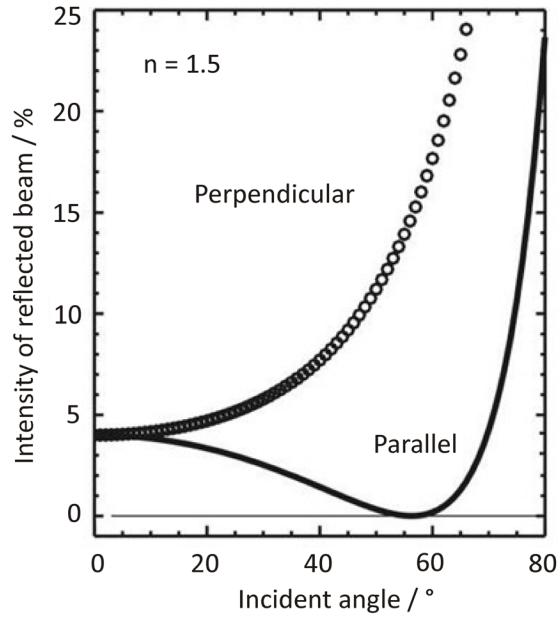
Figure 4.1: Theoretical reflectivity of a smooth surface with $n_1 = 1$ and $n_2 = 1.5$; figure source: what-when-how.com

angle of incidence and the refractive index (RI) of the media involved, e.g. air and glass, and is described by the Fresnel formulas. The reflectivity ($R(\lambda)$) for an angle of incidence perpendicular to the surface $R(\lambda)$ is described by the simplified Fresnel formula:

$$R(\lambda) = \left| \frac{n_1(\lambda) - n_2(\lambda)}{n_1(\lambda) + n_2(\lambda)} \right| \tag{4.1}$$

where $n_1\lambda$ and $n_2\lambda$ are the wavelength dependent refractive indices of the media involved. At angles of incidence $\neq 0$ the reflected beam is partially polarized. Figure 4.1 shows the theoretical reflectivity of the s-polarized (perpendicular) and p-polarized (parallel) light as a function of the angle of incidence for two media with $n_1 = 1$ (air) and $n_2 = 1.5$ (glass).

The calculated reflectivity of this medium (glass) is 0.04 (equivalent to 4%). For a transparent medium (glass) the absorption inside the medium is negligible and therefore the theoretical transmittance could be computed as 0.96 (96%). If a smooth and transparent surface is irradiated, specular reflection exist. In this case the incident light, the reflected light and the normal of the smooth surface lie in the same plane - the plane of incidence (Figure 4.2) [Hecht 2001].

The part of the light that crosses an interface of two media, e.g. air and glass, is changes its direction of propagation. This process is a product of the angle of incidence and refraction, which describes the change of the direction of a wave caused by a change in its speed. This correlation is described by Snell's law:

$$n_1 \cdot \sin \alpha_1 = n_2 \cdot \sin \alpha_2 \tag{4.2}$$

where α_1 is the angle of incidence and α_2 the angle of refraction, which is the angle of the transmitted light different to the surface normal (Figure 4.2).
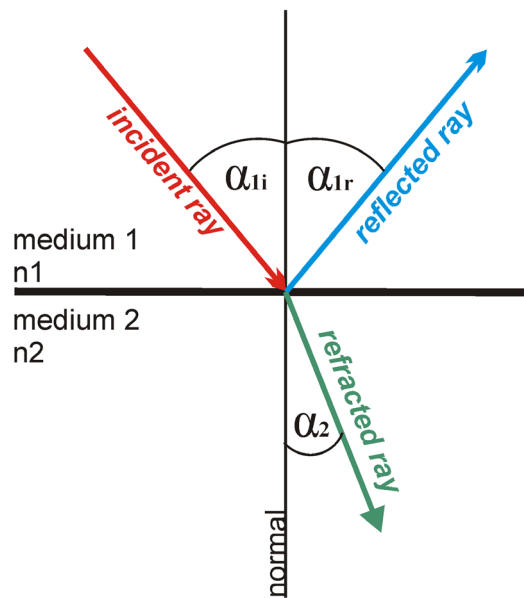
Figure 4.2: Refraction of light on an interface between two media with $n_1 = 1$ and $n_2 = 1.5$.
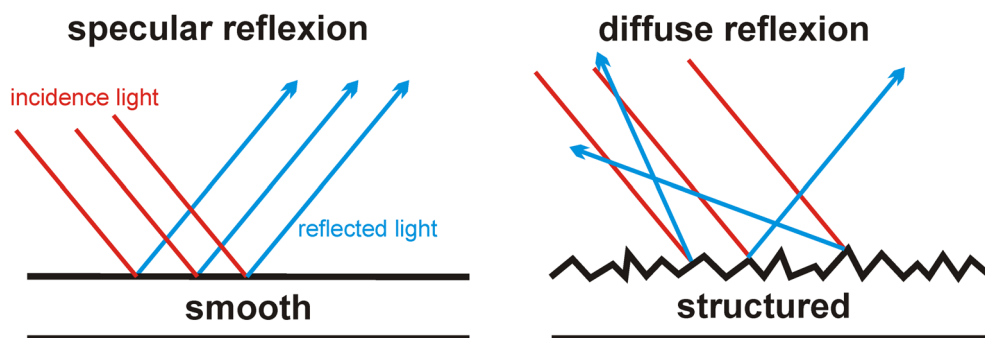
Figure 4.3: Specular and diffuse reflection on a smooth and a structured surface.

Additionally refraction depends on the wavelength of the light and is described as dispersion. Dispersion, i.e. $n = n(\lambda)$, could be observed if white light strikes a prism and the wavelength dependent refraction results in the splitting of the n different wavelengths, which could be perceived as a rainbow. Refraction in general occurs on surface structures, which are large in size compared to the wavelength of the incident light, e.g. the papillose cells on plant surfaces. As a consequence of this, the path of the transmitted light very much depends on the outermost curvature (the epidermal cell shape) of the leaves and flowers.

In contrast to specular reflection on a smooth surface, diffuse scattering occures on structured surfaces (Figure 4.3). In this case the incident light strikes the rough surface topography and the light will be reflected in different directions (scattering). The diffuse reflection patterns depend on the specific surface arrangement and have to be analysed individually. Perfect scatters, where the light is reflected equally in all directions, are called Lambertain.

Another physical aspect is the diffraction of light. Diffraction, occurs if a wave front is disturbed in its propagation by small objects, i.e. particles or pinholes. If light encounters a barrier, whether transparent or not, and the amplitude or its phase is changed, diffraction occurs. Diffraction is

Figure 4.4: Diffraction of a red and green laser beam at a pin hole projected onto a screen.

predicated on constructive or destructive interference, which describes the interaction of two or more electromagnetic waveforms, which are reinforced or cancelled as a result (Figure 4.4).

According to the wavelength and the barrier size, diffraction is more or less strong. The smaller the wavelength compared to the barrier, e.g. an aperture, the lower the diffraction. Diffraction gratings also occur on plant surfaces. As an example of nature, the petal cuticular striations of particular amplitude and frequency, e.g. found in *Tulipa*, cause iridescence [Whitney et al. 2009a].

4.1.2 Convexly shaped epidermal cells in plants

In this study in particular the optical properties of convexly shaped plant surfaces were investigated. Based on the theoretical considerations, the basic optical knowledge of convexly shaped epidermal cells is now presented.

Convexly shaped epidermal cells are known on the leaves of several species and widespread on the petals of flowers, especially in Angiosperms [Whitney et al. 2011; Koch et al. 2009; Barthlott and Ehler 1977]. Scanning electron microscopy analyses of the plant surface topography were carried out in major families such as the *Asteraceae* [Baagoe 1977], *Fabaceae* [Stirton 1980] or the *Asclepidaceae* [Ehler 1975]. Barthlott and Ehler [1977] described and classified the micromorphological sculptures and discussed their biological-ecological as well as their taxonomic-systematical significance.

After Barthlott and Ehler [1977], there are seven kinds of convexly shaped cell forms, which differentiate in their width (b) and height (h) ratio ($y = \frac{b}{h}$) and range from slightly convex to hairy. Studies by Kay et al. [1981] and by Christensen and Hansen [1998] found that conical cells occur on 75-80% of investigated angiosperm petals. On leaves they were found less frequently, but often in tropical herbs and understory plants as well as other species like the Lotus plant (*Nelumbo nucifera*) [Koch and Barthlott 2009; Bone et al. 1985; Lee and Graham 1986]. As mentioned above, these conically shaped cells can vary extremely in their shape [Koch et al. 2010; Barthlott and Ehler 1977]. As an example the papillated cells of *Calathea zebrina* leaves are shown in Figure 4.5.
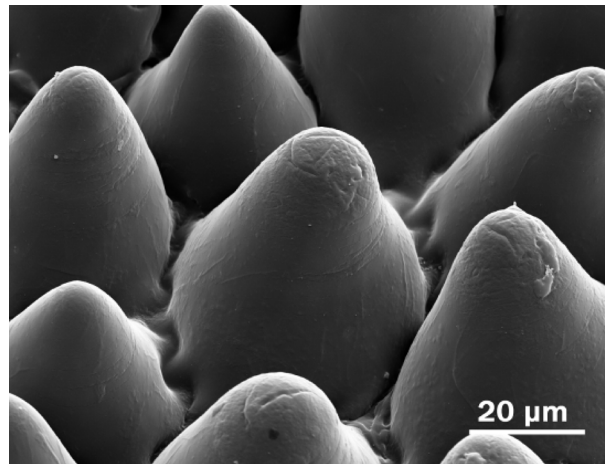
Figure 4.5: SEM picture of the convexly shaped (papillated) epidermal cells of *Calathea zebrina.*

Parameters like height, diameter and tip radius are as diverse as the structuring on top of the papillae, which can be anything from smooth to wax layer coated or arranged as a cuticular folding [Barthlott and Ehler 1977]. Though there have been several studies discussing the functions of convexly shaped cells, less is known about the exact surface parameters. Thus, there is a lack of information about the parameters of the micro- and nano-sculpturing on these surfaces.

4.1.3 Spectral properties of convexly shaped cells and their functionalities

Depending on the references used in the following, the terms 'conically shaped', 'cone shaped', 'papillated' or 'curved cells' were used as the authors used them in their papers. All these terms describe convex shaped cells, which are often not specified in their structural parameters. In the following the spectral properties and functionalities of convex shaped cells of plant surfaces are described.

Minimisation of the specular reflection on the plant surface.

Exner and Exner [1910] proposed that the primary function of the papillated epidermis of petals is to act as a light-trap for incident light by reducing the specular reflection on the surface [Bernhard et al. 1968]. This process is based on multiple reflections between the convex epidermal cells. The reduction of the specular reflection seems to play an important role, especially in low light environments, e.g. at the ground level of forests. Bone et al. [1985] examined tropical shade plants and postulated that uneven surfaces probably improves light-harvesting by decreasing specular reflection and found lower reflectance values in light focusing shade leaves as compared to sun leaves. Martin et al. [1989] additionally estimated that convex epidermal cells increase light collecting even from low angles of incidence by minimizing the specular reflection from the leaf surface. Investigations of Brodersen and Vogelmann [2007] gave detail information about reflectance values for the leaves of several understory plants irradiated with collimated and diffuse light. They pointed out that the average reflectivity of most leaves range from 3.5% at 450 nm, 4% at 650 nm, 7.8% at 700 nm and 45.8% at 750 nm, which is consistent with other studies [Knapp and Carter 1998; Gausmann et al. 1974; Woolley 1971]. Reflectance in the green range is variable, because it depends on the individual amount of pigmentation (chlorophyll) and leaf anatomy. Brodersen and Vogelmann [2007] measured values from 4.2% to 17.4% at 550 nm. They found that reflectance was typically lower in leaves with convexly shaped cells. However, a comparison between distinct leaves still seems difficult, because they differ in various aspects, like leaf thickness, amount of water, pigments or air spaces. Concerning the optical properties and

the thickness of sun and shade-adapted leaves, some studies showed that shade-adapted leaves had significantly lower leaf weights. Furthermore these leaves synthesized less chlorophyll per unit area, i.e. they used less chlorophyll for capturing the same quanta for photosynthesis [Lee et al. 1990]. It is postulated that, compared to the sun adapted species, the shade plants produce a radiation absorbing surface that is lighter and presumably metabolically less expensive to grow [Lee and Graham 1986].

Lens effect of convexly shaped epidermal cells.

The lens effect of curved cells, which describes the potential to focus light into the leaves is well-known [Brodersen and Vogelmann 2007; Myers et al. 1994; Chazdon and Pearcy 1991; Poulson and Vogelmann 1990; Martin et al. 1989; Bone et al. 1985; Haberlandt 1914]. First Haberlandt [1914] showed that leaf epidermal cells could act as lenses and focus light into the leaf. Vogelmann [1993] reviewed, pointing out that most epidermal cells focus light to some extent, but the most successful examples have been found in the leaves of shade plants [Martin et al. 1991; Poulson and Vogelmann 1990] and tropical herbs [Lee and Graham 1986; Bone et al. 1985]. In this process the curvature of the epidermal cells and the cell diameter play an important role. Poulson and Vogelmann [1990] proposed that the focused light is guided to populations of chloroplasts that were adapted to high light. Myers et al. [1994] confirmed this proposal. Martin et al. [1989] analysed the convex shaped epidermal cells of *Medicago sativa* leaves, which focus light within the upper region of the palisade parenchyma. They showed that covering the surface with a thin layer of a mineral oil is able to eliminate this epidermal focusing effect by eliminating the convex shaped form of the outer surface. Bone et al. [1985] proposed that the flowers of *Anthurium warocqueanum* are able to concentrate collimated light up to 20-fold and diffuse light 2-fold by the epidermal cell. Martin et al. [1991] were the first who analysed the lens properties of leaf surface replicas. They showed that agarose replicas focused light in a similar manner as the original epidermal cells and that the measured values (intensification factors and focal length) are comparable to the values from isolated epidermal layers.

Colour saturation of petals.

A further functionality is the ability to intensify the colouration in leaves and flowers. One example are the leaves of the moss *Schistostega* which grows in shallow caves and other dark places and appears intensely green when viewed from a perpendicular orientation [Toda 1918]. Further, there are several examples of colour intensification in flowers. Bernhard et al. [1968] reported that Exner and Exner [1910] had examined the epidermal cells of the petals of pansies and roses and pointed out, that because of their cone-shaped cells the total path of the light passing through the petal is longer as compared to papillated cells (Figure 1.5). The basal as well as the upper region of these papillated cells contain colour substances (pigments). These pigment filled cells act as a kind of colour filters. Consequently, higher cells create a longer path for the light within the petal and the outgoing light is more saturated. They got the impression that flowers with a brilliant, saturated colour stand a better chance of being seen and therefore have a higher reproduction success. Kay et al. [1981] examined 201 species of flowers from 60 families, where 79% have some form of cone shaped cells. It can be assumed that these conical-papillated cells increase the amount of light absorbed by the pigments in flowers and enhance the perceived colour of the petal. Noda et al. [1994] worked with *Antirrhinum majus* mixta mutants, which possessed flat hexagonal-based cells in contrast to the wild type with conically shaped epidermal cells. They proposed that the colour intensity depends on the specialized cell shape and showed that the mutant flowers appeared slightly paler and less velvety. It was shown that the wild type of *Antirrhinum* reflects significantly less light than the mutant and, thus, absorbs significantly more light. Gorton and Vogelmann [1996] also showed that the conical-papillated cells of *Antirrhinum* petals enhance the visible colouration by focusing the light into the region of the epidermis where the pigments are contained. Glover and Martin [1998] worked on the biological relevance of this

colour intensification and found that conical petal cells significantly enhance a flower's chance of being visited by a pollinator. They showed that flat celled flowers had significantly fewer fruits than conical-papillated celled flowers. This result was also found in white flowers. Whitney et al. [2011] also reported on the subtle colour enhancing in specialized (cone-shaped) epidermal cells and additionally referred to some further functionalities of conical shaped epidermal cells. These functionalities will be illustrated briefly in the following paragraph.

Further functionalities

Since the examination of the lotus effect it is known that conical epidermal cells have an important influence on surface wetting [Wagner et al. 2003; Barthlott and Neinhuis 1997; Neinhuis and Barthlott 1997]. In addition to their surface chemistry, conical shaped and papillated surface structures could result in diverse surface wetting regimes, i.e. from superhydrophobic to super-hydrophilic [Koch and Barthlott 2009]. The wetting of papillated surfaces is introduced in detail in Chapter 5. Moreover, Kevan and Lane [1985] proposed that the shape of petal epidermal cells are used as a tactile guides and cues by insects in their discrimination between different kinds of flowers. Examinations of Comba et al. [2000] indicate, that bees distinguished between the two genotypes of *Antirrhinum* petals of the mutants (flat cells) and the wild type (conically shaped cells) before and after landing (using as optical and tactile signal). They found that conical papillated surfaces absorb more direct sunlight than flat surfaces resulting in a higher flower temperature. Whitney et al. [2008] examined this warming effect of flowers. Even when they found only a small difference between floral temperature in petals with flat and conical shaped cells they suggested that a moderation of floral temperature is a significant factor in the production of conical petal cells.

4.1.4 Functionalities of the cuticular folding

Despite the cuticular folding on top of convex cells being well known since the late 19th century [Martin and Juniper 1970] and much being proposed concerning its likely functionalities, up until now relatively little is known about the their actual functionalities. Kay et al. [1981] postulated that over 50% of angiosperm species produce a striated cuticle over their petals. A fundamental classification of folding types was carried out by Barthlott and Ehler [1977]. The relevance of the cuticular folding in terms of mechanical stability [Bargel et al. 2006; Kay et al. 1981], good attachment for insects [Kevan and Lane 1985] and also increased attachment of pollen was discussed. Later studies showed, that the folds on top of cells are also able to decrease the attachment of insects and help to catch them, as in the example of *Nepenthes* pitcher plants Prüm et al. [2012b]. In contrast, the same working group found an increased attachment of insects on surfaces, which combined striations and conical cells [Prüm et al. 2012a].

In terms of their optical functionalities it was postulated that the cuticular folding, as well as the cell shape, is able to cause a reduction of surface reflection Kay et al. [1981]. Knoll [1938] showed with petals of *Viola* hybrids that the fundamental light scattering effect is caused by extremely papillated cells and proposed that the cuticular folds on top are able to cause an additional increase of this scattering. Barthlott and Ehler [1977] assumed that parallel folds cóuld act as a specific optical signal for pollinators. Thirty years later Whitney et al. [2009a] showed that these parallel folds cause iridescence generated through diffraction gratings using flower replicas. They postulated that this iridescence might increase the attractiveness of flowers.

4.1.5 Antireflective and light harvesting technical surfaces

Solar cell surfaces have to cope with the same physical problems as plant surfaces. Biological systems as well as technical systems try to reduce optical losses to increase the amount of collected

light. Thus, plant surface structures could be used as models for the optimization of solar cells as they are specialists at light harvesting.

One way of optimizing solar cells, is *via* the reduction of surface reflection. The more light is coupled into the solar cell, the higher the degree of energy transformation, means an increase in the efficiency of the cell [Wagemann and Eschrich 2010]. Currently there are two possibilities for reducing surface reflections: (I) covering the surface with an anti-reflective coating (ARC) and (II) by structuring the surface.

The principal of AR-Coatings is to reduce light reflection based on destructive interference. Therefore, the thickness of the coating is adapted to a quarter of the wavelength of the incident light, i.e. they work in a small spectral range. Moreover, they have to be adapted to the angle of incidence and the respective substrate, e.g. silicon or glass. Multi-layer coatings, which work in a broader spectral range, could be generated. But, these multiple layers are still extensive and expensive.

Structuring a surface is the second way to minimize surface reflections. Using different etching techniques a surface roughness can be created, e.g. pyramidal structures, which are bigger in size compared to the incoming wavelengths. Exactly as in the case of the structured plant surfaces, these pyramids cause a reduction of the amount of reflected light *via* multiple reflections between them (Figure 1.4). Further, these structures cause a lengthening of the light within the technical material (light-trapping) [Wagemann and Eschrich 2010].

Current scientific research works on anti-reflective coatings following the example of the nanostructured eyes of nocturnal moths [Yamada et al. 2011; Stavenga et al. 2006]. These surfaces possess nano pillars about 200 nm in height and 300 nm in distance, which are smaller than the incidenct light (visible wavelengths), and cause a continuous refractive index gradient, which results in a reduction of surface reflection. There are attempts to realize this surface structuring on solar panels in which different techniques are used to fabricate these structures [Koynov et al. 2006]. But, up to now there is no commercially available product on the marked.

Other groups worked on the development of anti-reflective and superhydrophobic surfaces. Often expensive and therefore extensive techniques are used. Cao et al. [2006] fabricated anti-reflective porous silicon surfaces with superhydrophobic properties, using different chemical etching techniques combined with fluoroalkylsilane self-assembly. They reached average reflection values of about 3% over the spectral range of 300 to 800 nm and contact angles of up to 161°. Faustini et al. [2010] combined anti-reflective and water repellent properties by coating a glass with nanoporous TiO_2 layers via sol-gel processing. These coatings are supposed to be easier to clean as they possess the photocatalytic properties of the TiO_2.

Double structured surfaces were prepared, e.g. by Chang et al. [2007]. They produced periodic subwavelength structures with enhanced hydrophobic behaviour by coating traditional inverted pyramid structures (Figure 1.8 B) with Teflon. At these surfaces a reflectance of 18% and contact angles of 135.9° were achieved. Even Choi and Huh [2010] used traditional pyramid structures and laser grooved surfaces to fabricate double structured anti-reflective, superhydrophobic surfaces. Traditionally produced expensive micro-pyramids were transferred into perfluoropolyether (PFPE) by a complex three-step replication technique. These surfaces reflect more than 2% of the incident light and possess contact angles of about 160° and a hysteresis of about 2°.

Here the transfer of evolutionary developed surface architectures from nature into modern technologies should result in new high efficiency surface architectures for solar cell applications. Therefore the influence of surface structuring on the optical properties of the leaves of shade adapted plant species and the petals of colour intensive flowers was examined. For that purpose the surface structuring was separated from the biological master by fabricating biomimetic replicas. Absolute reflectance values of the replicas should be compared with the microstructure parameters (I) cell height, (II) cell middle width, (III) cell distance, (IV) angle of the anticline of the cell and (VI) the tip radius of the cells. If it occurs, nano-structuring should also be characterised. Additional photogoniometric measurements should give information about the angle dependent
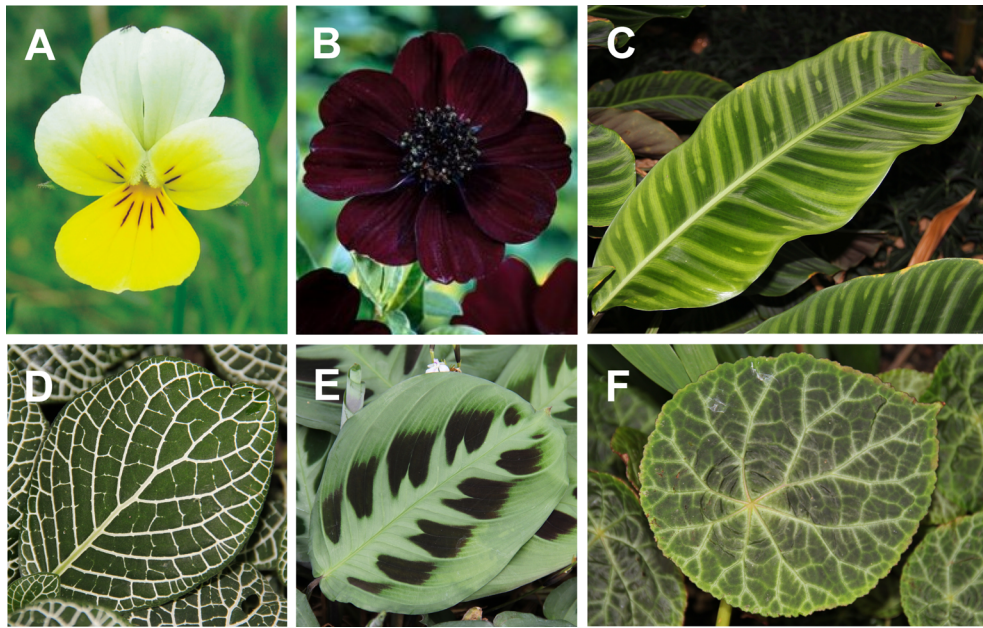
Figure 4.6: Macroscopic pictures of six of the chosen plants: *Viola tricolor* (A), *Cosmos atrosanguineus* (B), *Calathea zebrina* (C), *Fittonia verschaffeltii* (D), *Maranta leuconeura* (E) and *Begonia geogensis* (F). Sources of external pictures: treknature.com (Picture A), azweddingfloral.co (Picture B).

optical properties ('How does the light pass the surface structures of replicas?'), i.e. the light scattering properties of the biomimetic replicas. This analysis should give information about how technical surfaces could be optically optimized in terms of anti-reflection and light harvesting, e.g. for solar panels.

4.2 Materials and Methods

4.2.1 Biological surfaces

The structures of the upper surface (adaxial) side of 5 leaves of different low light plants and 4 different colour intensive flowers (petals) were investigated. Plants were cultivated in the Botanic Gardens of the Rheinische Friedrich-Wilhelms-University of Bonn (BGB) or commercially purchased. Their scientific names are given together with registration numbers of the (BGB) or the point of sale. Investigated leaves originate from 5 understory low-light herbs: *Begonia geogensis* (BGB 14466-7-1996), *Calathea zebrina* (BGB 1201), *Fittonia verschaffeltii* (BGB 11142), *Maranta leuconeura* (BGB 05028), *Pellonia pulchra* (BGB 18858-7-2002). Additionally the petals of 4 colour intensive flowers originate from *Anemone nemorosa* (BGB 11341), *Cosmos atrosanguineus* (BGB 29614-8-2008), *Rosa chinensis* (BGB 3089-9-1979), *Viola tricolor* (BGB 27262-4-2004) and *Viola x wittrockiana* hybrids (purchased from 'Pflanzen Breuer', Sankt Augustin, Germany). The surface structuring of *Viola tricolor* and *Viola x wittrockiana* hybrids do not differ significantly from each other. Thus, *Viola x wittrockiana* hybrids were also used, as they were available in larger numbers. Six of the examined plant species are shown in Figure 4.6.
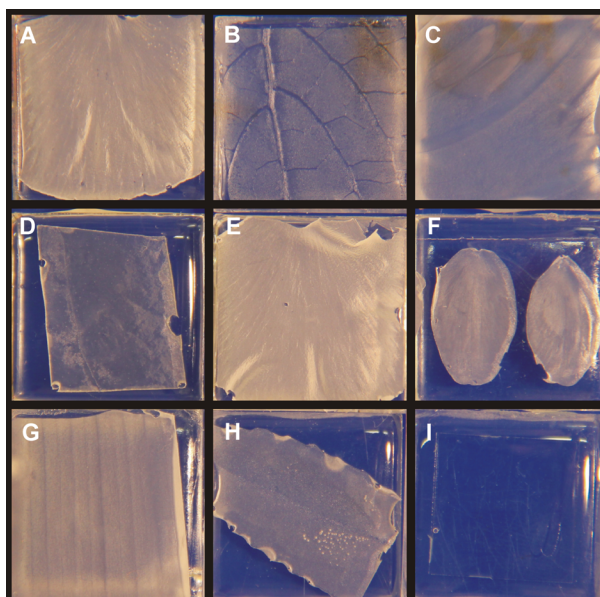
Figure 4.7: Macroscopic pictures of different transparent replicas laying on a blue background. Shown are the replicas of *Viola tricolor* (A), *Fittonia verschaffeltii* (B), *Maranta leuconeura* with the bright areas and dark spots (C), *Begonia geogensis* (D), *Rosa chinensis* (E), *Anemone nemorosa* (F), *Calathea zebrina* (G), *Pellonia pulchra* (H) and a smooth reference (I).

4.2.2 Technical surfaces

The replication technique introduced above (Chapter 3) was used for the fabrication of the biomimetic polymer replicas. Here the general technique is only briefly introduced and modifications, especially made for the optical measurements, are highlighted.

Transparent replicas

The replication technique is a two-step moulding process, in which a negative is first generated followed by a positive. For the generation of the negative replicas the master (biological sample) is moulded with a polyvinylsiloxane dental wax (President light body Gel, ISO 4823, PLB; Coltene Whaldent, Hamburg, Germany). In the second step the negative replicas were filled with a two-component injection resin (RECKLI Injektionsharz EP, RECKLI GmbH, Herne, Germany). After filling the negative replicas, the transparent epoxy resin had to dry for 48 h at 25° C. Afterwards hardening the positive replicas were peeled off from the negative replicas and further replicas were fabricated. In total five petals/leaves of each species were replicated and then examined. A selection of different replicas is shown in Figure 4.7.

Black replicas

For the examination of the reflection at the structured (upper) surface of the replicas non-transparent (black) replicas had to be generated (Figure 4.8). In these black replicas the reflections on the smooth back of the replica were suppressed by the black stain. In principal these replicas were prepared as described for the transparent replicas but in the second step 1.3 mass% of a black stain (Toolcraft 130 130-0, 886562-62, black, Conrad Electronic SE, Hirschau, Germany) was added. SEM analysis showed that the stain had no influence on the replication performance.
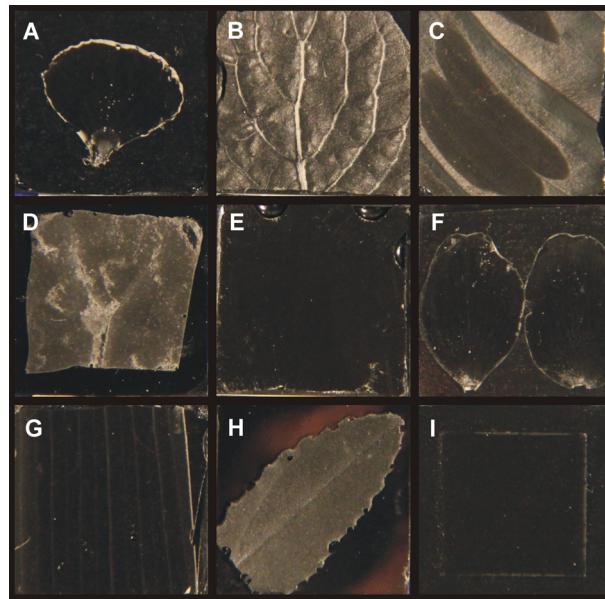
Figure 4.8: Macroscopic pictures of different black replicas: shown are the replica surfaces of *Viola tricolor* (A), *Fittonia verschaffeltii* (B), *Maranta leuconeura* with the bright areas and dark spots (C), *Begonia geogensis* (D), *Rosa chinensis* (E), *Anemone nemorosa* (F), *Calathea zebrina* (G), *Pellonia pulchra* (H) and a smooth reference (I).

4.2.3 Surface characterization

Scanning electron microscopy (SEM)

The surface structures of the biological samples and their replicas were investigated by scanning electron microscopy (SEM). Images were recorded using a CAMBRIDGE Stereoscan 200 SEM (Zeiss GmbH, Oberkochen, Germany). A digital image processing system (DISS 5, Version 5.4.17.0, Point electronic GmbH, Halle, Germany) was used to visualize and measure the surface structures of the petals. Fresh plant material was dehydrated with ethanol and dried in a critical point dryer (CPD 020, Balzers Union, Balzers- Pfeifer GmbH, Aßlar). On account of their stability the replicas did not require special preparation. To examine the height, mid width and tip diameter of the surface structures freeze fractures of the replicas were prepared and collected as shown in Figure 4.9. Prior to SEM investigations all samples were sputter-coated with a 30 nm gold layer (Balzers Union SCD 040, Balzers- Pfeifer GmbH, Aßlar).

Optical microscopy (OM)

The topography of the plant and replica surfaces was additionally investigated using a digital optical microscope. Images were recorded using a VHX-1000 Digital Microscope (Keyence Deutschland GmbH, Neu-Isenburg, Germany). The plant surfaces could be examined without further preparation. The replicas were covered with a 60 nm thick layer of gold.

4.2.4 Photogoniometric measurement system

With a spectrophotogoniometer the bidirectional spectral properties of leaves were analysed, i.e. the distribution of the reflected and transmitted light at surfaces could be examined angle dependent. Different goniometers were developed, for example by Combes et al. [2007]. The analyses with a photogoniometer are mostly of a qualitative character [Jacquemoud and Ustin 2001]. In
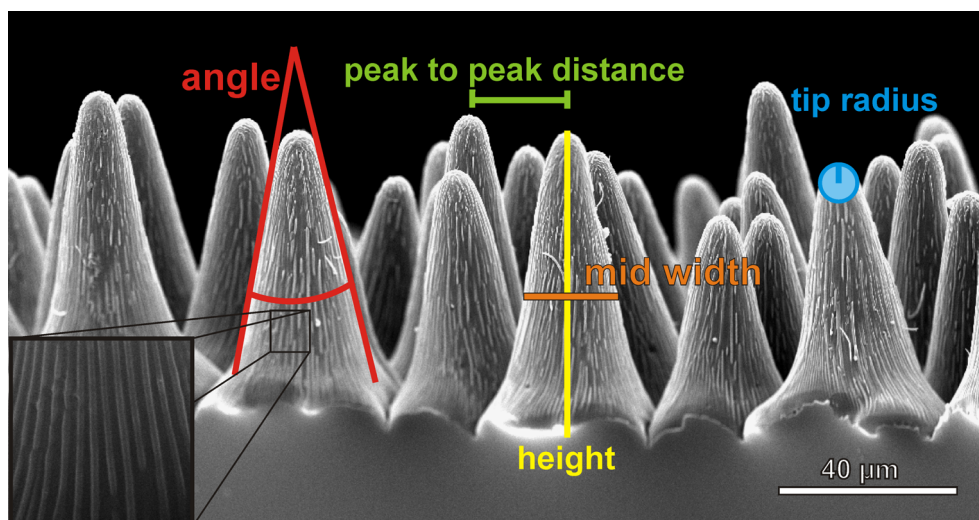
Figure 4.9: Micropapillae characteristics of the polymer replicas: collected data are papillae height, mid width, papillae angle, peak-to-peak distance and the tip (peak) radius. If occures the nanofolds were also characterized in their width and distance.
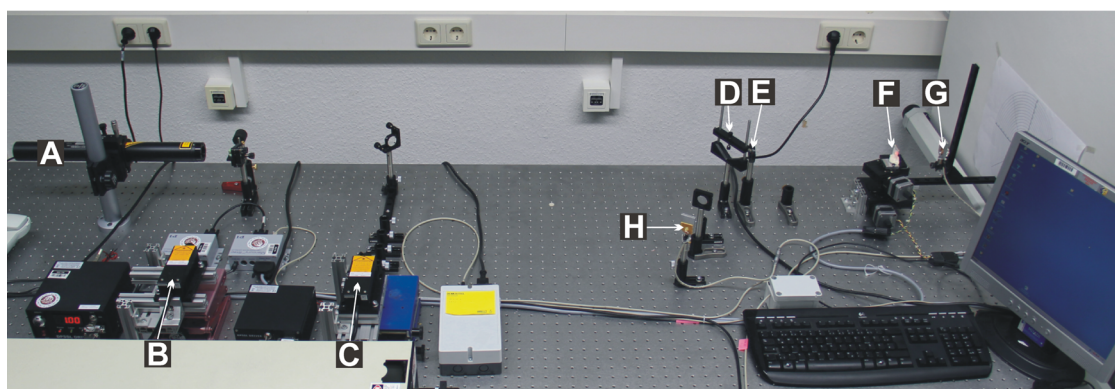
Figure 4.10: Set up Photogoniometer: red Laser (633 nm)(A), green laser (532 nm) (B), infrared laser (1064 nm) (C), beam splitter (D), aperture (E), movable sample holder with a sample (replica) on top (F), movable sample detector (G) and the static reference detector (H).

this study photogoniometric measurements were performed with a non-commercial optical setup essentially developed by Bay [2010] for the examination of the optical properties of the soft and hard tissue of teeth. Here the system was modified for the examination of the optical properties of biomimetic replicas. Setup modifications made here are the integration and adjustment of two additional visual lasers (red and green, further information see below), a revision of the computer program written with the visual programming language LabVIEW 8.6 (National Instruments, Austin TX, USA) and the extension of the axis for the horizontal movement of the sample detector. A picture of the setup is shown in Figure 4.10.

Principal setup

The schematic principal of the setup is shown in Figure 4.11. Setup modifications were carried out by the integration and adjustment of two additional continuouse wave emmitting laser systems (He-Ne laser, 633 nm and a frequency doubled Nd:YVO$_4$ laser, 532 nm), revision of the computer program written with the visual programming language LabVIEW 8.6 (National Instruments,
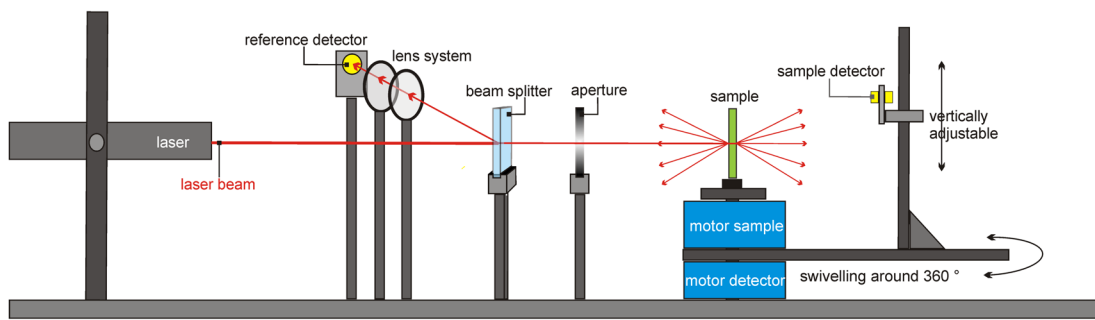
Figure 4.11: Schematic setup of the photogonimetric measurement system (laterally view).
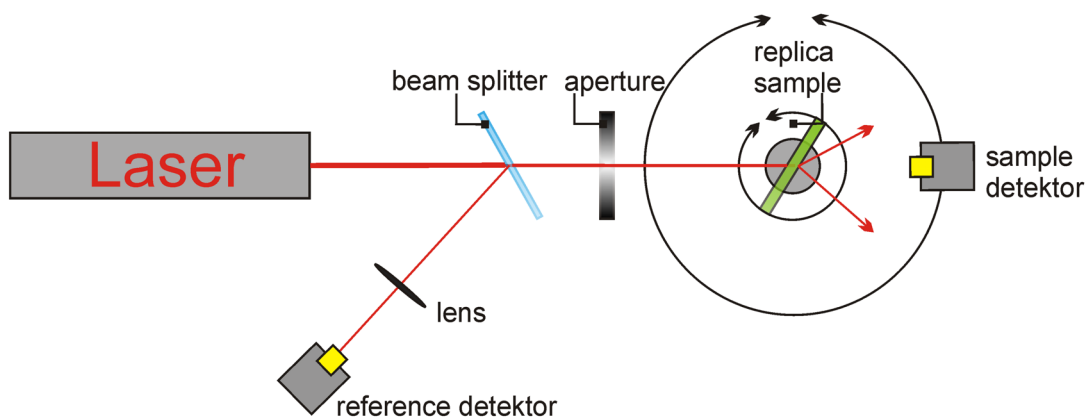
Figure 4.12: Schematic setup of the photogoniometric measurement system (top view).

Austin TX, USA) and the extension of the axis for the horizontal movement of the sample detector. Using this measuring system the angle dependent reflexion and transmission properties of transparent biomimetic replicas can be discovered. The spatial distributions of a laser beam sent to the surface of vertically mounted replicas can be detected at specific angular positions, as the replicas as well as the detector arm are independently movable.

Analysing the optical properties of transparent replicas a laser beam was sent across a beam splitter (BK 7 glass), through an aperture and then to the replica (sample) surface. The beam splitter was used as a reference and therefore only approximately 8% of the incident light was reflected to a second reference detector. The remaining part of the light (92%) was used for replica measurements. The reference signal gives information about the stability of the laser signal and warranted the reproducibility of different measurements. The transmitted beam (92%) passes through an aperture of 2 mm and immediately strikes the sample. The reflected and transmitted parts of the light were detected by the sample detector (Figure 4.12), which moves around the sample. The sample holder and the sample detector are independently movable. By moving the sample holder different angles of incidence could be realized, here measurements were carried out at a 0°, 20° and 40° angle of incidence. The detector was mounted at a distance of 91 cm, can be turned horizontally around the sample in a fixed plane and is adjustable in height (Figure 4.11). Measurements were made horizontally in steps of 1°. These horizontal measurements were carried out in different vertical planes (distance between each plane 5 mm). Reflection and transmission values were captured and the stepping motors were controlled using the visual programming language LabVIEW 8.6 (National Instruments, Austin TX, USA).
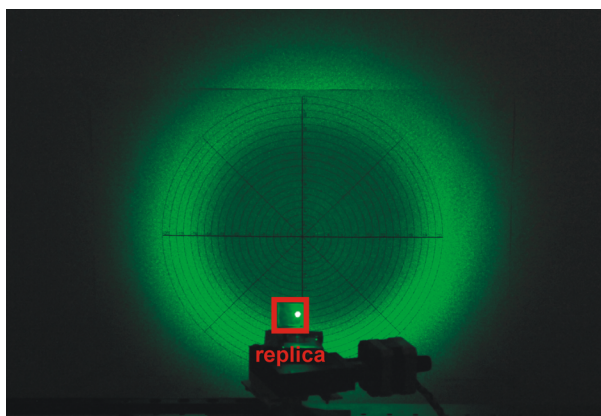
Figure 4.13: Transmission pattern (green ring) of a green laser beam send across a biomimetic replica (red box) of *Begonia geogensis*, projected onto a screen; angle of incidence 0°.

Radiation sources and detectors

Irradiation was performed using three different laser sources:

GREEN: Compact diode-pumped solid-state DPSS laser (CNI-532d-200-TTL-LED-3, Changchun New Industries Optoelectronics Technology Co., Ltd., Changchun, China) with a wavelength of 532 nm. A max output power of 250 mW was chosen for measurements.

RED: Polarized helium-neon laser (R-30991, HENe LAser, Newport Spectra-Physics GmbH, Darmstadt, Germany) with a wavelength of 633 nm and an max output of 5 mW.

INFRARED: Compact diode-pumped Nd:YVO$_4$ solid-state laser (MIL-III-1064nm-1W-9060111 (PO100401-01), Roithner Laser Technik GmbH, Wien, Östereich), with a wavelength of 1064 nm $\pm$10 nm. The emitted beam had a constant diameter of 2 mm. The max output was 1.36 W.

The red and green laser systems were used for the visual characterization of the transmission patterns, which were photographically documented (Figure 4.13). The IR laser and the related detector system (Germanium photodiodes (J16-5SP-R02M,LASER COMPONENTS GmbH, Olching, Germany)) were used for the angle dependent characterization of the transmission patterns. Depending on the amount of light transmitted at a specific position beyond the replicas, the photodiodes detected corresponding signal in volts (V). This current is sent to an analogue-digital card, which converts the incoming current to a dimensionless number proportional to the height of the current voltage.

Data analyses

Data were analysed using the numerical computing environment Matlab (MATLAB7$^{\circledR}$, R2009a, The MathWorks$^{\text{TM}}$) and SigmaPlot (Sigmaplot 11, Systat Software Inc.).

4.2.5 Total reflectance measurements using a spectrometer with an integrating sphere

The spectrophotometry is a well established method of characterizing the spectral properties of plants as well as technical surfaces [Lee et al. 1990; Lee and Graham 1986; Bone et al. 1985]. In combination with an integrating sphere, the absolute reflectance and transmittance values
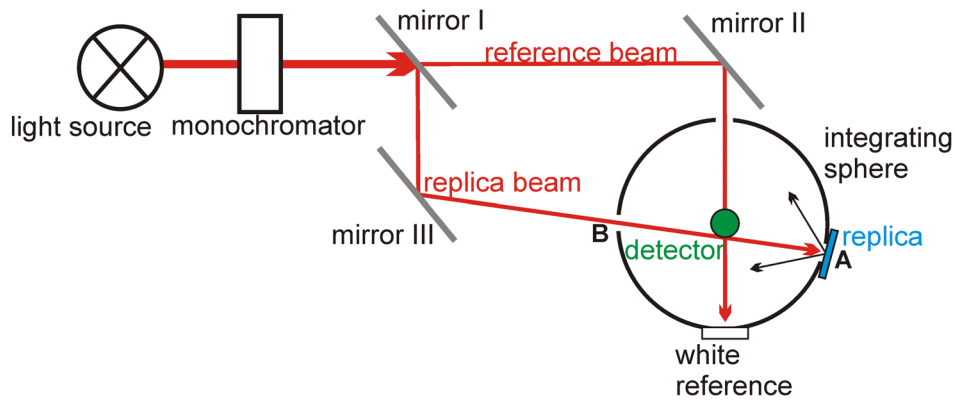
Figure 4.14: Schematic of the double beam spectrometer with an internal integrating sphere: replica sits behind the integrating sphere for reflection measurements. In transmission mode the replica would be positioned in front of the sphere.

of surfaces can be determined. These spheres are used to collect the directional-hemispherical reflectance or transmittance of surfaces irradiated with a beam (Figure 4.14).

Diffuse reflectance and transmittance measurements were acquired throughout the 300-800 nm spectrum using a commercial available double-beam spectrometer (Lambda 1050, Perkin Elmer, Massachusets, USA) with an internal integrating sphere (Labspherer RSA-PE-20, 600 mm). Two light sources generate the relevant wavelength regions of the ultraviolet (UV, 280-380 nm, generated by a deuterium lamp), the visible region (VIS, 380-780 nm, generated by a tungsten lamp) and the near infrared (IR, 800 nm, tungsten lamp). During measurement the lamps and the related detectors change automatically. Wavelength selection is carried out by a monochromator and afterwards divided into a reference beam and a sample (plant surface or replica) beam. The detector is placed at the top of the sphere. In the reflection measurement mode, the spot of the beam goes to the adaxial surface of the sample (leaves, flowers or their replicas) sitting directly behind the sphere (Figure 4.14 A). The beam is reflected from the sample surface into the sphere. In transmission measurement mode the samples are arranged directly in front of the sphere (Figure 4.14 B). Here the beam is sent to the upper surface of the sample, crosses the sample and falls into the sphere. The inner surface of the sphere is covered with spectralon, a fluoropolymer with an extremely high diffuse reflectance in the ultraviolet, visible and near-infrared spectrum. The reflectance of this flouropolymer is $\geq 99\%$ in the spectral range from 400 to 1500 nm and $\geq 95\%$ from 250 to 2500 nm [Georgiev and Butler 2007]. After the beam is reflected from the sample, the light is reflected multiple times on the inner sphere surface until it falls into the detector. Using this sphere the total reflectance (R), which consists of the specular and diffuse reflection, could be measured. The reference beam goes to the spectralon surface and is calibrated as a 100% (R = 100%) reflective surface.

Measurements were performt exemplarily at two plant surfaces (*Calathea zebrina*, *Viola x wittrockiana*) and at the replicas of all investigated plant surfaces. Five replicas of every species were analysed ($n = 5$). Data were recorded at 1 nm intervals in the 300 to 800 nm range.

Revealing the role of the papillated cells in the colour intensification process, the surface structuring on a yellow *Viola* petal should be switched off by covering it with a liquid. Therefore an extremely colour intensive petal of *Viola x wittrockiana*, which possesses the same surface structuring as the wild pansy (*Viola tricolor*), was chosen (Figure 4.27). As the *Viola* petal is superhydrophobic (Chapter 5) a water-surfactant-mixture (1 mass%) was used as liquid. The liquid lies between the micropapillae thus forming a smooth surface, which was seen using a light microscope. Only the outermost papillae tips stuck out of the water film.

4.3 Results

For the investigation of the optical properties of plant surface structures, the micromorphology of the examined surfaces was characterized first (Section 3.4.1). The surface parameters were then compared to the reflection properties of the biological and replica surfaces (Section 3.4.2) and the angle dependent transmission patterns (Section 3.4.3).

4.3.1 Surface architecture of the biological and replica surfaces

All investigated plant leaves and petals possess convex shaped or papillated epidermal cells, which is clearly visible in the SEM pictures of the understory herbs and the colour intensive petals (Figure 4.15 to 4.18).

Four understory herbs with single structured surfaces (micropapillae), i.e. *Calathea zebrina*, *Fittonia verschaffeltii*, *Pellonia pulchra* and *Begonia geogensis* (Figure 4.15) were chosen. In addition, **three colour intensive petals** with hierarchical structuring (micropapillae with a nanofolding folding on top), i.e. *Viola tricolor*, *Cosmos atrosanguineus* and *Rosa chinensis* were examined (Figure 4.16).

Moreover **two special types of surfaces** were investigated. At first the leaves of the understory low-light plant *Maranta leuconeura*, which also possess bright green areas with dark green spots in between. In contrast to the leaves of *Calathea zebrina*, which possess also bright and dark green leaf areas (Figure 4.6 C), the bright and dark areas of the *Maranta* leaves also differ in their surface structuring. *Maranta* leaves possess slightly convex shaped cells in the bright green areas and papillose cells in the dark green areas. As an additional feature in both areas nano-incrustations on top of the cells were found (Figure 4.17). The second special case is the flower surface of *Anemone nemorosa*. In contrast to the petals mentioned above, the surface of the *Anemone* petals is characterized by a single-structuring (Figure 4.18).

For further determination of the surface architecture the lateral views on the convex shaped structures are shown in Figure 4.19 to Figure 4.21.

The cell parameters were measured at 20 cells, which were located on two different replicas (measurement of ten papillae per replica). Remarkable differences were found between the micropapillae parameters of the examined surfaces (Figure 4.22 to 4.24). The leaf micropapillae investigated vary from almost flat (*Maranta* (bright) 5.6 $\pm$1.6 μm) to a height of almost 40 $\pm$2.6 μm (*Calathea*). In flowers cells these were found to be much higher (*Cosmos* 58 $\pm$ 8 μm) than in leaves (*Calathea* 40 $\pm$ 2.6 μm), even when there are also petals with smaller cells (Rosa 24 $\pm$ 2.1 μm). Moreover, the micropapillae on all surfaces differ remarkably in there cell mid width (from 15.2$\pm$ 1.8 μm (*Rosa*) to 42$\pm$ 4.2 μm (*Pellonia*)). Because of this the structures on the examined surfaces also differ in their aspect ratios, which lie in the range from 0.17 (*Maranta* (bright)) to 2.9 (*Viola*). Further differences were found in the angles of the papillae. In leaves, relatively flat cells (*Maranta* 152 $\pm$ 6.2°) as well as sharp cells (*Calathea* 42.7 $\pm$ 1.7°) have been found. The angle of the petal micropapillae vary from 61.3 $\pm$ 4.4° (*Anemone*) to 25.5 $\pm$ 2.0° (*Viola*). Except for *Maranta* bright the other surfaces examined possess cell tip radii in a range from 2.1 $\pm$ 0.4 μm (*Viola*) to 16.9 $\pm$ 1.3 μm (*Pellonia*).

The leaves of *Maranta leuconeura* have been considered a special surface, because they possess two optically different areas. The leaves are bright green with distinct dark spots on them. These two areas differ extremely in their surface structuring. The cells of the bright green areas have only one third of the height of the cells in the dark spots (*Maranta* bright 5.63 $\pm$ 1.3 μm, dark spots 19.1 $\pm$ 2.5 μm). These differences were also recognized in the aspect ratio of the cells (bright *ar* 0.17, dark spots *ar* 0.90) and of course in the tip radius of the cells as well (bright 45.1 $\pm$ 13 μm, dark spots 6.7 $\pm$ 1.8 μm). Both areas possess a nano structuring on top of the micropapillae. In contrast to the nano structures of the petals, the *Maranta* leaves possess no folding but randomly arranged nano incrustations (Figure 4.17).
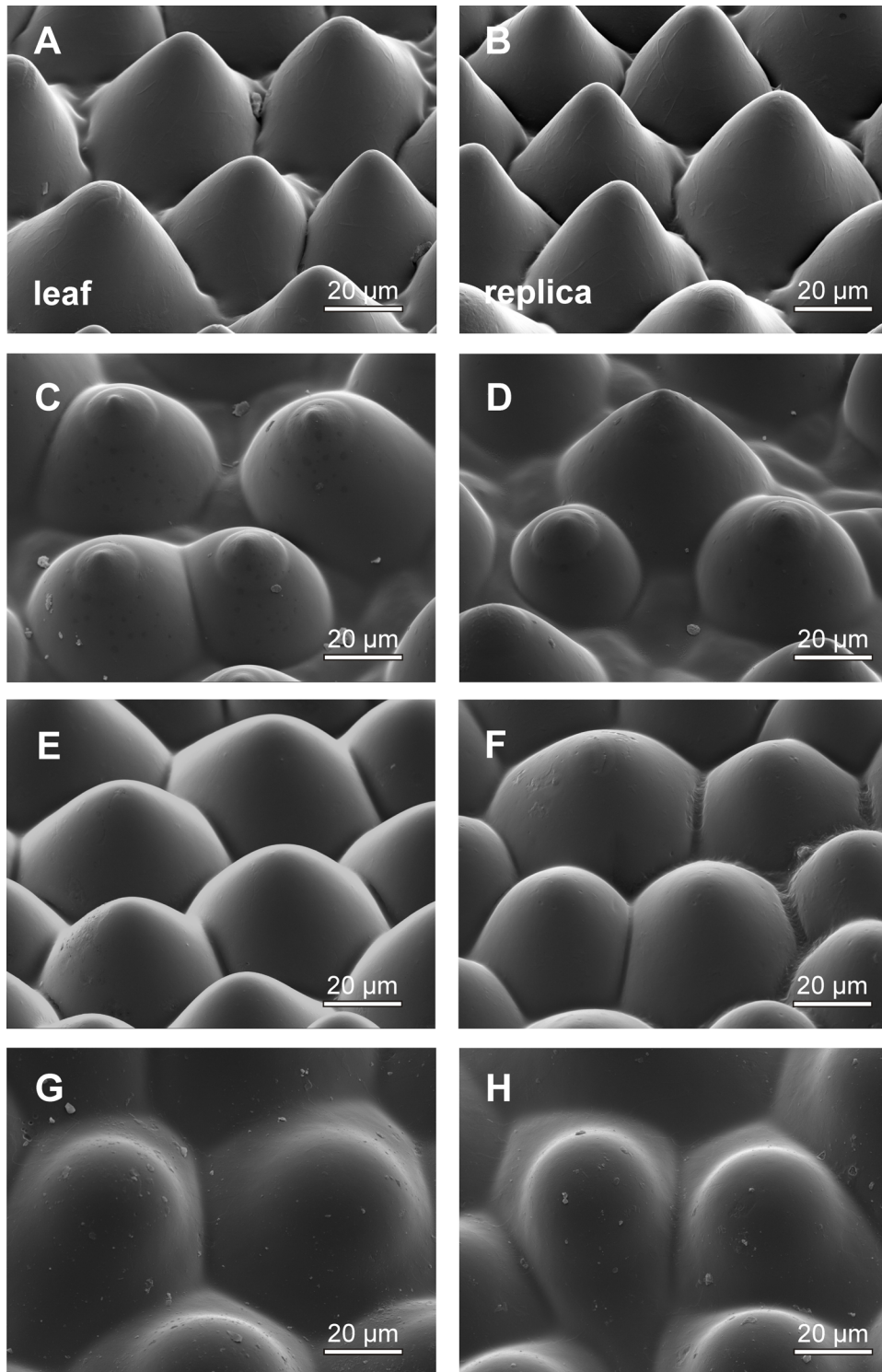
Figure 4.15: SEM micrographs of four convex shaped understory leaves (left: A,C,E,G) and their replicas (right: B,D,F,H) of *Calathea zebrina* (A,B), *Fittonia verschaffeltii* (C,D), *Begonia geogensis* (E,F) and *Pellonia pulchra* (G,H).
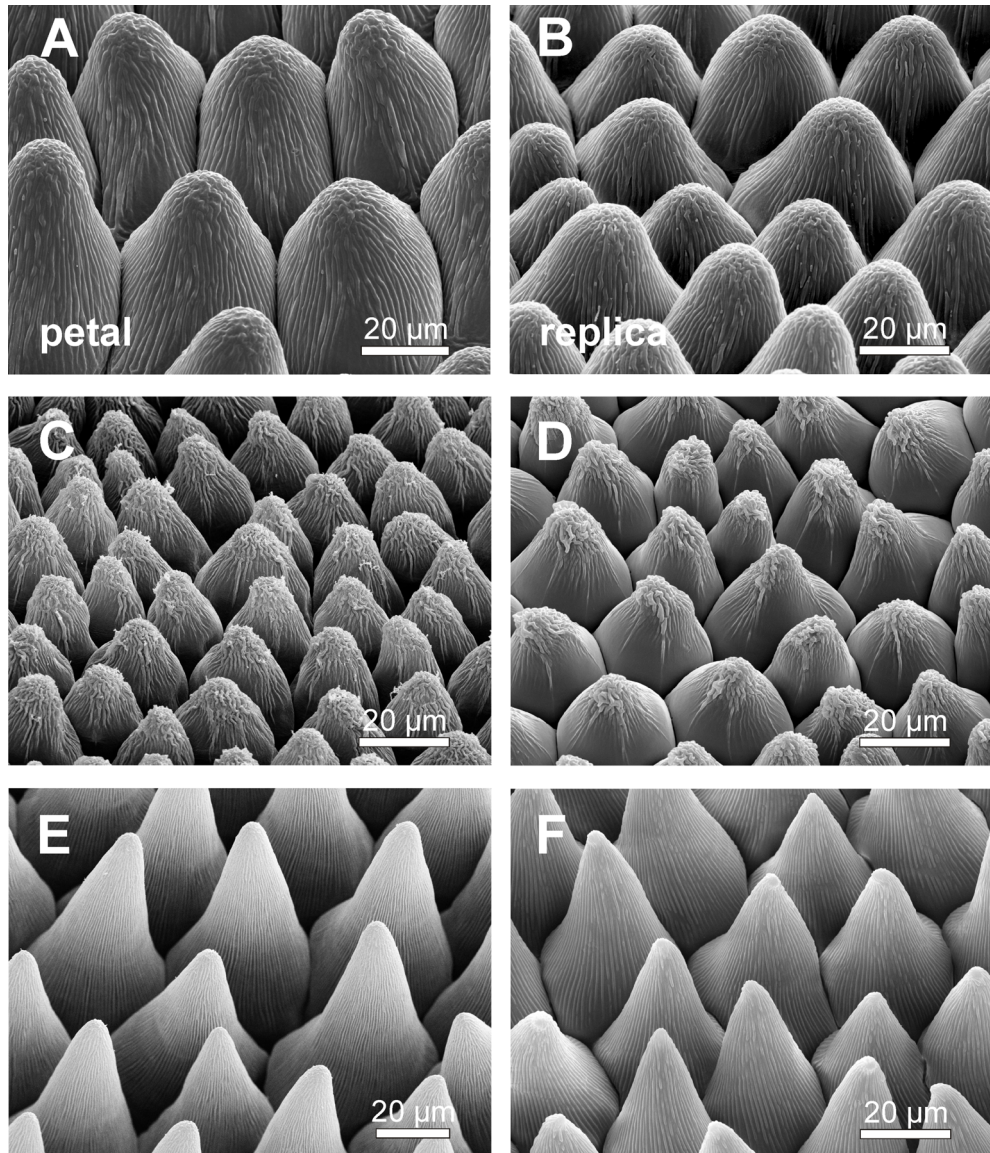
Figure 4.16: SEM micrographs of three hierarchically structured petal surfaces; convex shaped micropapillae, which are additionally covered with cuticular striations (left: A,C,E) and their replicas (right: B,D,F) of *Cosmos atrosanguineus* (A,B), *Rosa chinensis* (C,D) and *Viola tricolor* (E,F).
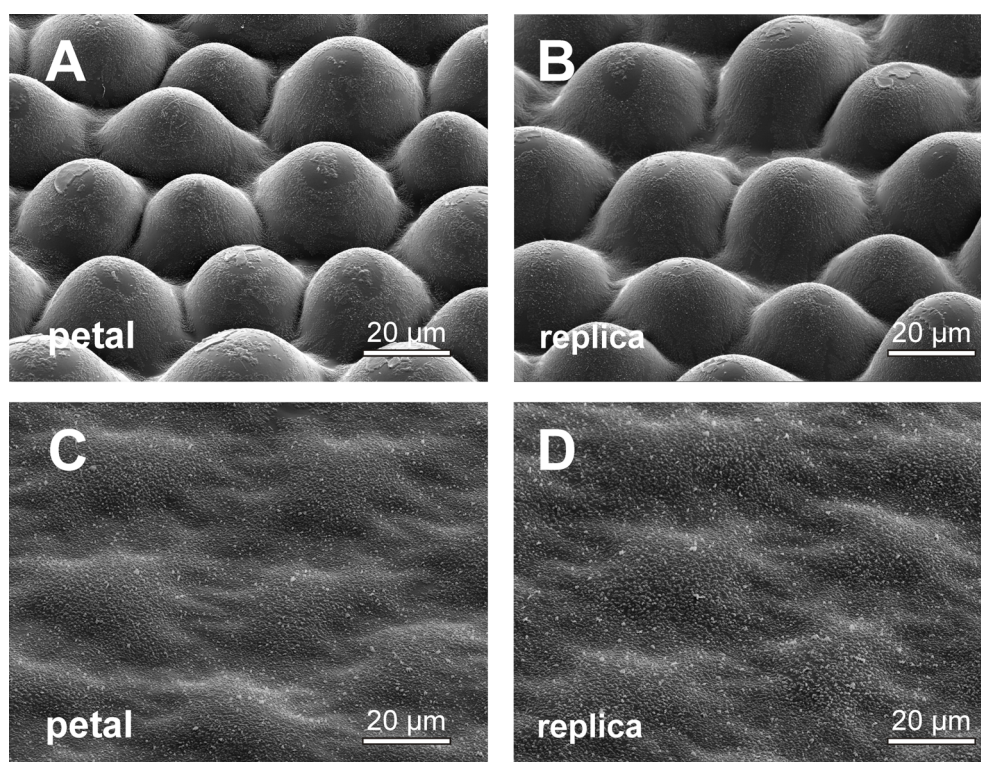
Figure 4.17: SEM micrographs of the two different areas on a leaf of *Maranta leuconeura* (left: A,C) and their replicas (right: B,D): dark green areas possess convex shaped epidermal cells (A,B), bright green areas possess almost flat epidermal cells (C,D), both areas possess nano-incrustations within the cuticle.
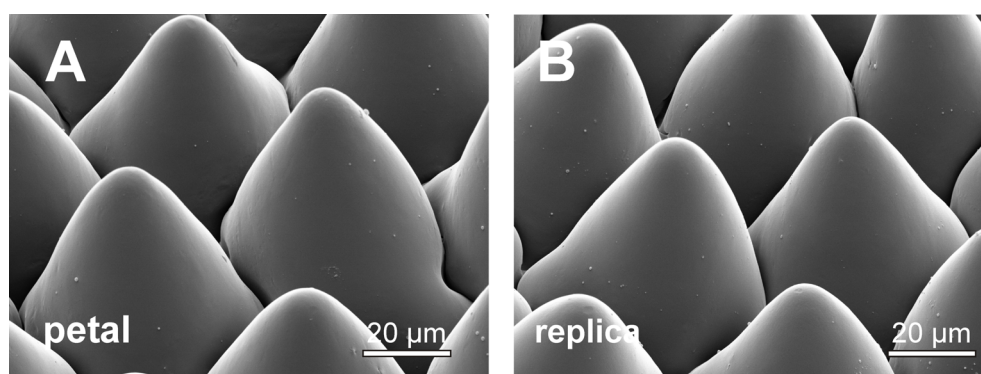
Figure 4.18: SEM micrographs of the petals of *Anemone nemorosa* (A) and its replica (B).
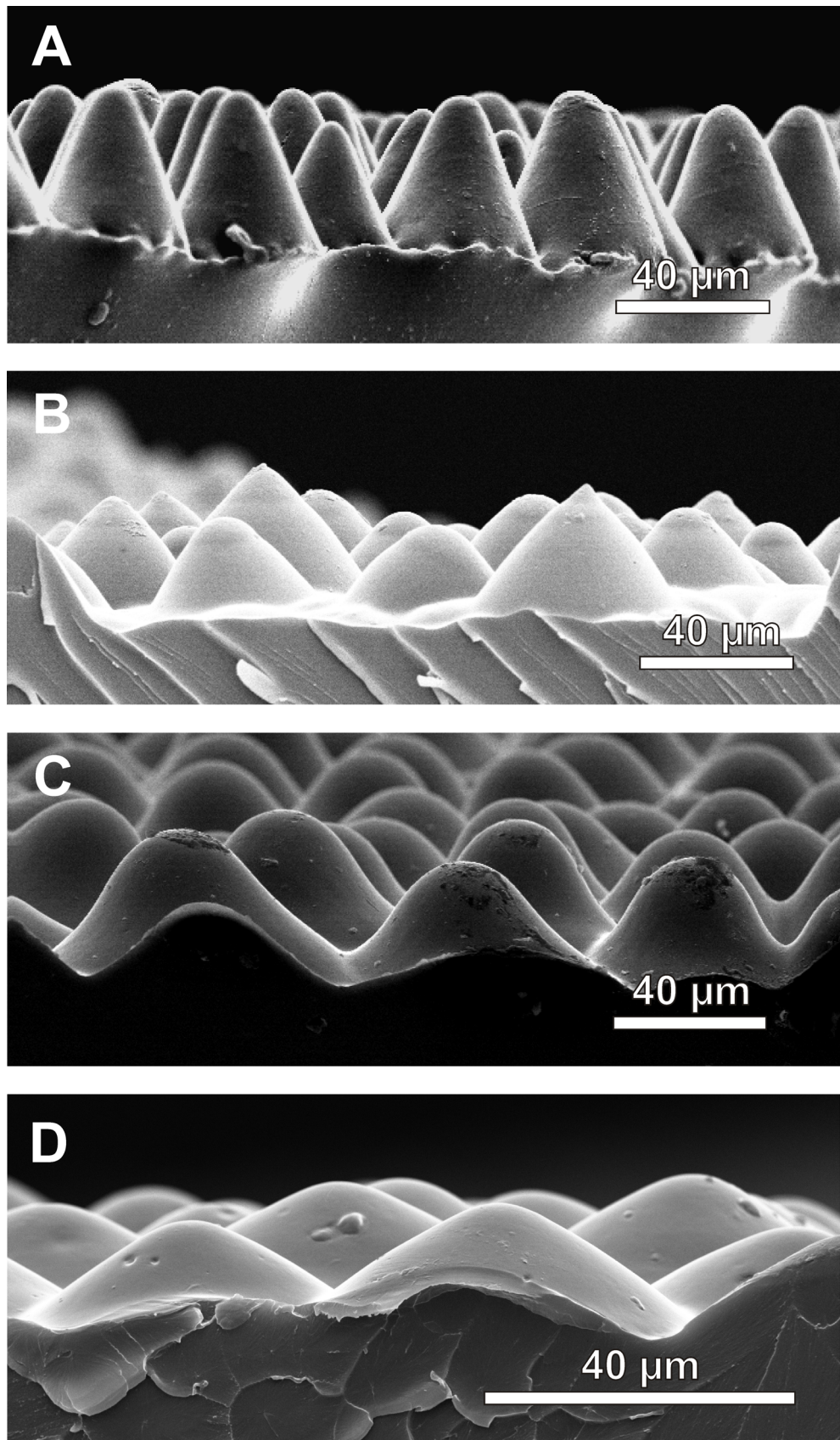
Figure 4.19: SEM micrographs of the replicas of the convex shaped understory leaves in lateral view. Replicas were prepared by freeze fracture. Presented are *Calathea zebrina* (A), *Fittonia verschaffeltii* (B), *Pellonia pulchra* (C), *Begonia geogensis* (D).
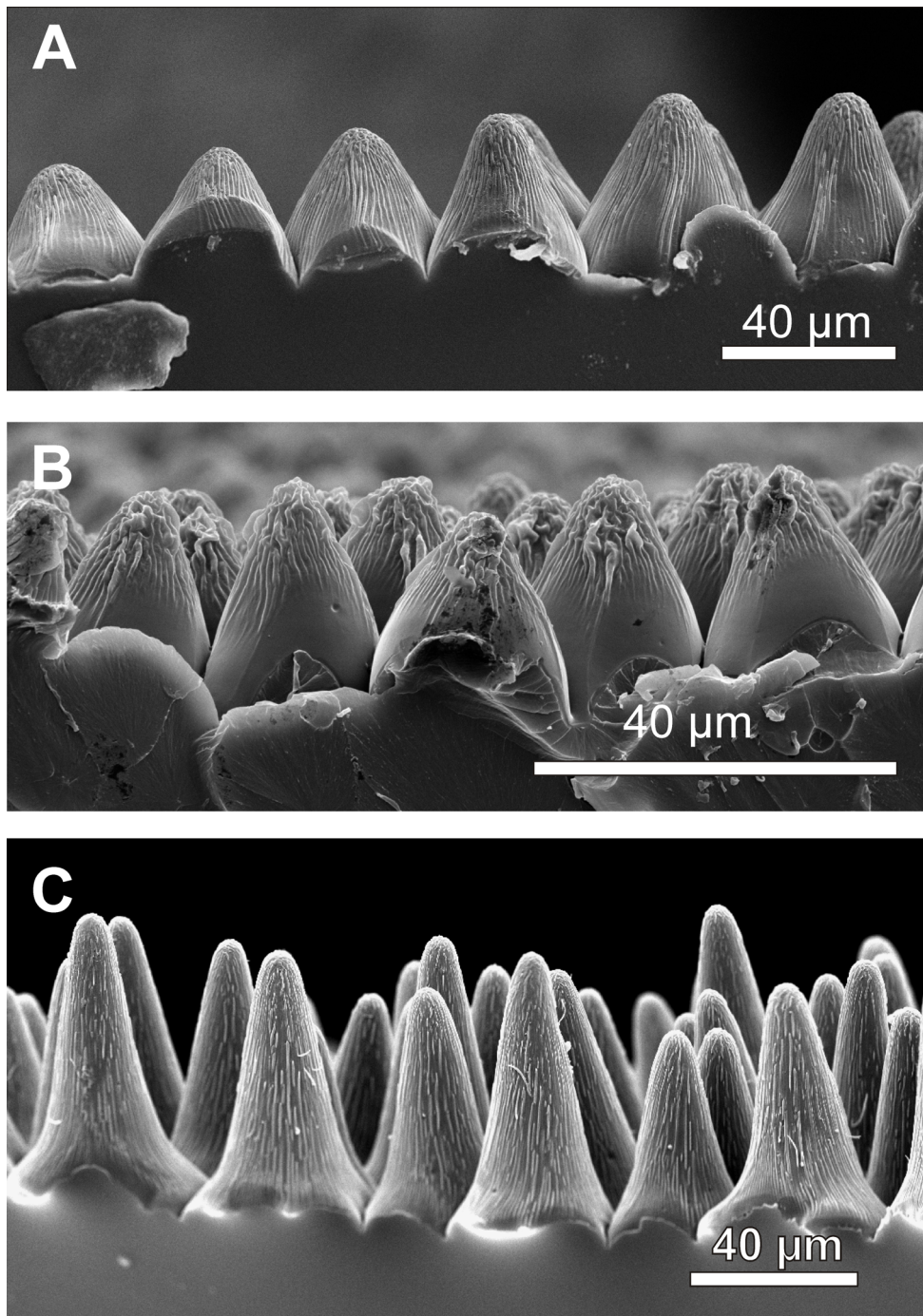
Figure 4.20: SEM micrographs of the convex shaped petal replicas in lateral view. Replicas were prepared by freeze fracture. Presented are *Cosmos atrosanguineus* (A), *Rosa chinensis* (B), *Viola tricolor* (C).
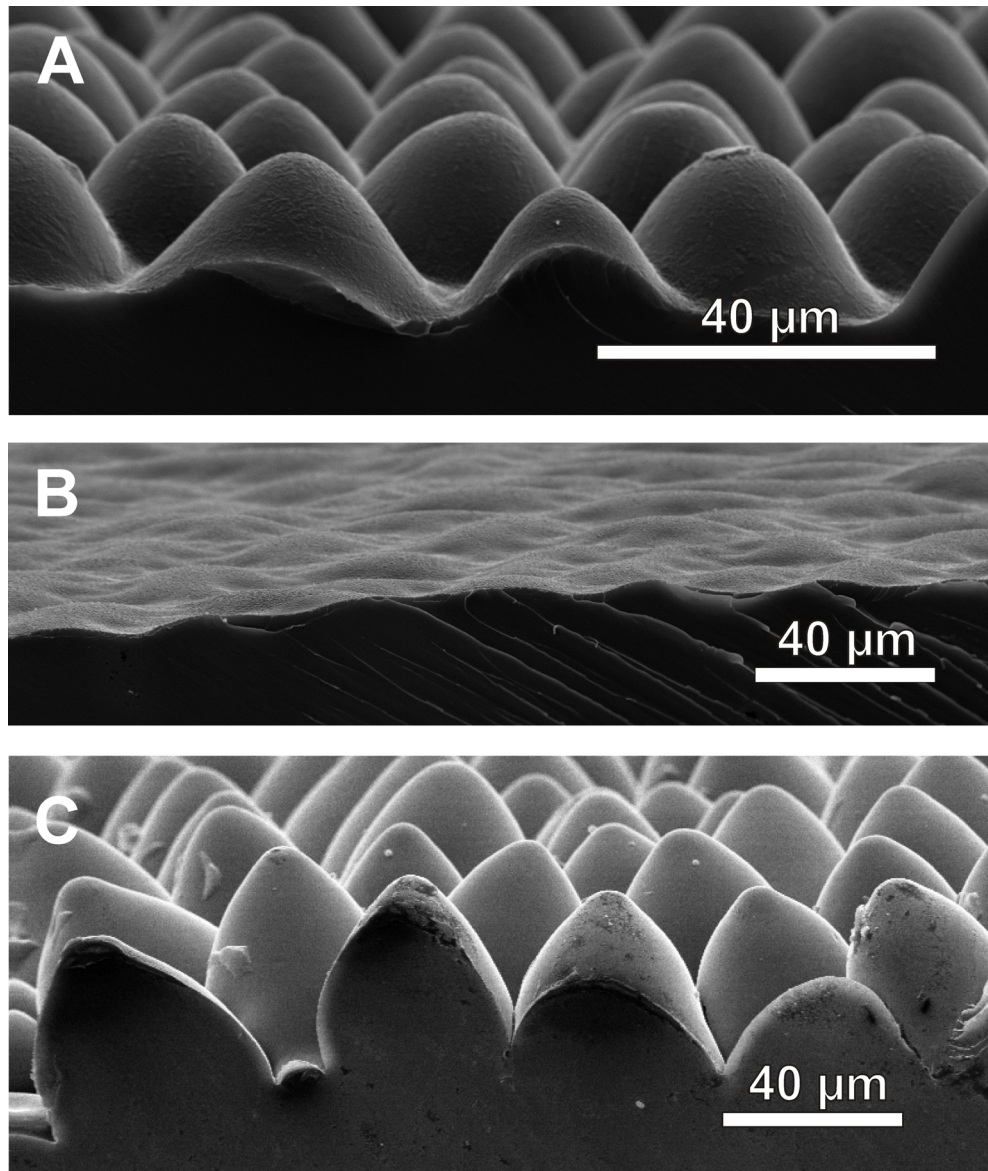
Figure 4.21: SEM micrographs of the convex shaped replicas of *Maranta leuconeura* and *Anemone nemorosa* surfaces in lateral view. Replicas were prepared by freeze fracture. Presented are the replicas of *Maranta* dark green areas (A), *Maranta* bright green areas (B) and *Anemone nemorosa* (C).
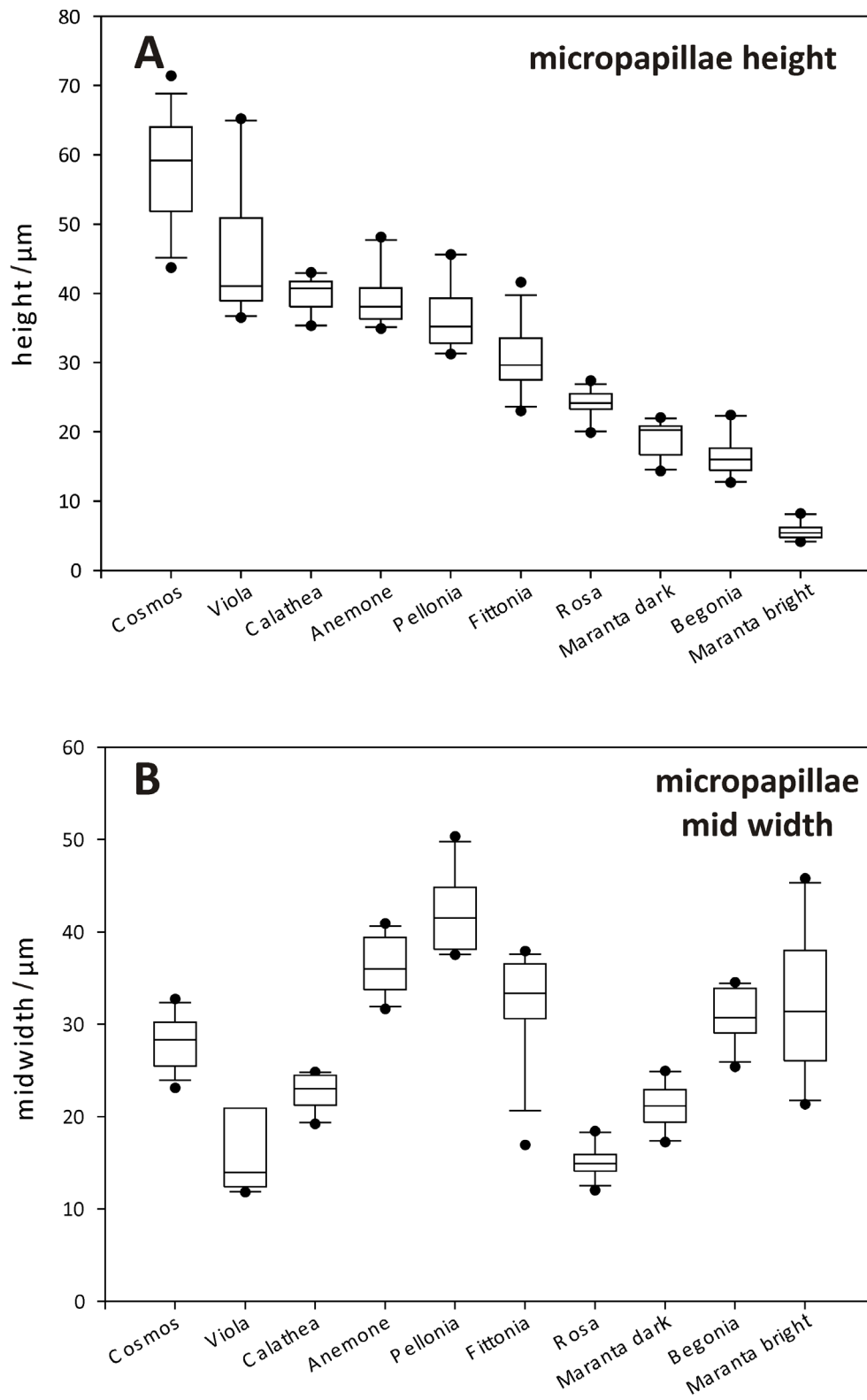
Figure 4.22: Micropapillae height (A) and width (B) of the different replicas ($n = 20$).
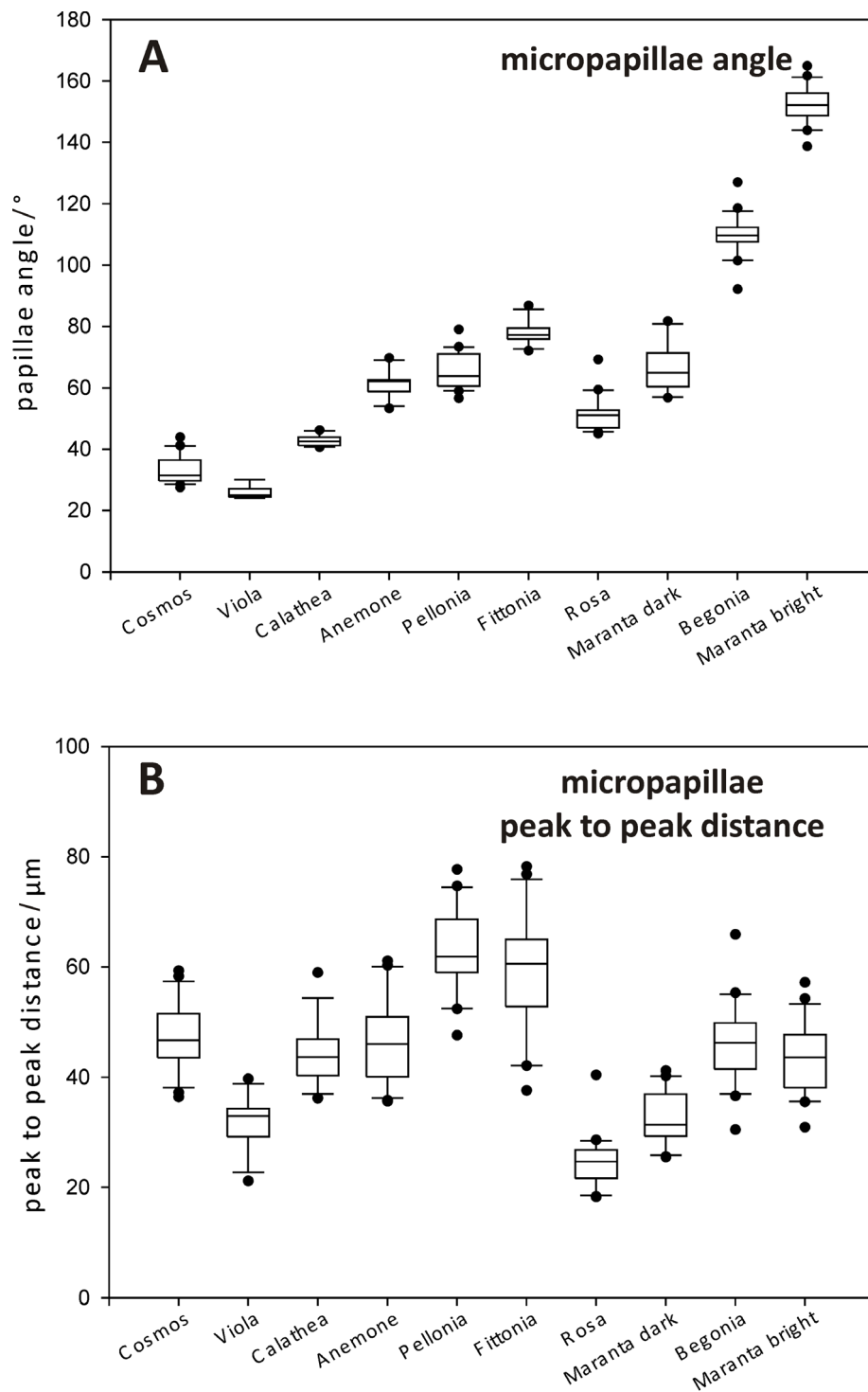
Figure 4.23: Micropapillae angle (A) and peak to peak distance (B) of the different replicas ($n = 20$).
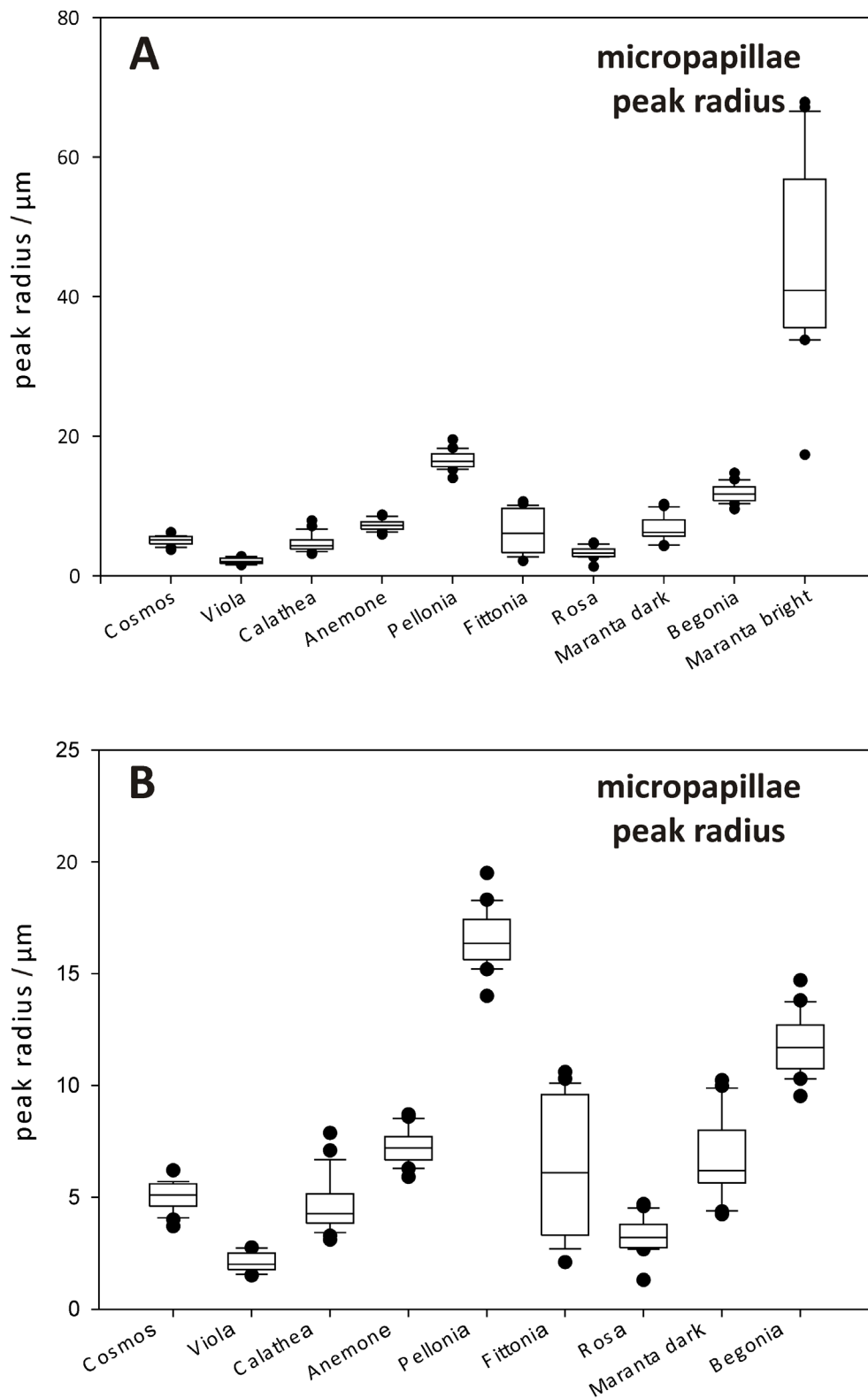
Figure 4.24: Micropapillae tip radius of all replicas (A). Graph (B) shows the same data but without *Maranta* bright ($n = 20$).
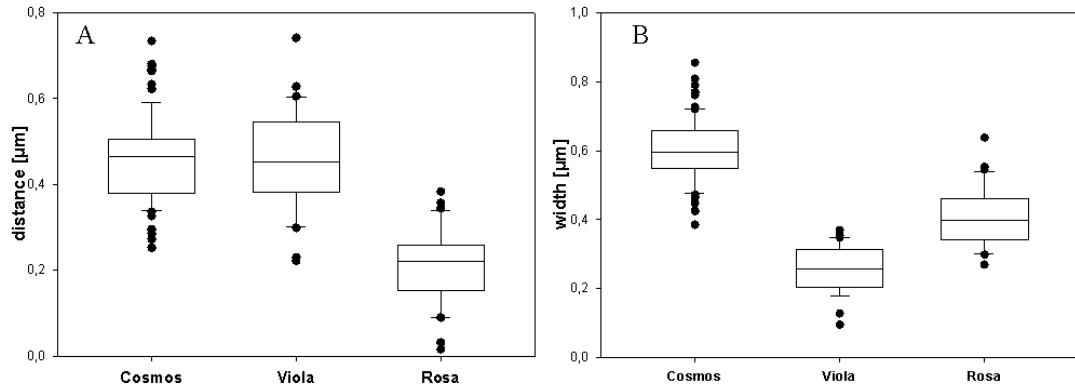
Figure 4.25: Nano-folding characteristics of the polymer replicas of *Viola*, *Cosmos* and *Rosa*: box plots with average values of the folding distance (A) and width (B) are shown ($n = 10$).

Hierarchical structured surfaces were found on the petals of 3 species (*Viola*, *Cosmos*, *Rosa*), which possess cuticular folding on top of the papillae. In contrast, the investigated leaves do not possess folding on top. Differences between the folding parameters of the three petals were found in the width and distance of the folds (Figure 4.25).

Cosmos and *Viola* possess folds with a similar distance (*Cosmos* 0.46 ± 0.1 μm, *Viola* 0.45 ± 0.12 μm) but their folds differ in width (*Cosmos* 0.6 ± 0.09 μm, *Viola* 0.26 ± 0.07 μm). The *Rosa* surfaces possess folds, which are 0.41 ± 0.09 μm in width. In contrast to the *Cosmos* and *Viola* surfaces the rose folds are arranged in a clearly smaller distance (0.21 ± 0.09 μm).

4.3.2 Reflection properties of plant surfaces

The question how much light is reflected on the surface of a plant- or replica surface was analysed using a spectrometer combined with an integrated sphere. Even though the main focus in this thesis lies on the examination of biomimetic replicas, the optical properties of two biological models have also been analysed. For instance, the reflection properties of the leaves of *Calathea zebrina* and the yellow petals of *Viola x wittrockiana* were characterized. The *Calathea* leaves possess bright green and slightly darker green areas. The reflectivity of both areas was characterized. Results are shown in Figure 4.26.

The analysed organs reveal remarkable differences in their reflection properties. The green leaves of *Calathea zebrina* possess a low reflectance in the lower spectral range (300-500 nm). The bright green areas reflect about 2.5% of the incident light in contrast to 1.3% in the dark green areas. Both areas possess a reflectivity spot at 550 nm. The reflectivities of the bright green areas are about 12% at this spot as compared to 4% of the dark green areas. In the spectral range of 600 to 680 nm the reflection is low and at around 700 nm it increases clearly; up to almost 60% at 800 nm.

The reflectance spectrum of the yellow *Voila* petal differs remarkably from the spectrum of the *Calathea* leaf. The yellow petal analysed here possesses a total reflectivity of about 1% in the spectral range from 300-480 nm. At about 500 nm there is a spontaneous increase to almost 80%. At the end of the red spectral range (at around 675 nm) the reflection decreases to about 72% and immediately increases back to 80% in the range from 700 to 800 nm.

Revealing the role of the papillated cells in the colour intensification process, the surface structuring on a yellow *Viola x wittrockiana* petal was switched off by covering it with a liquid (Figure
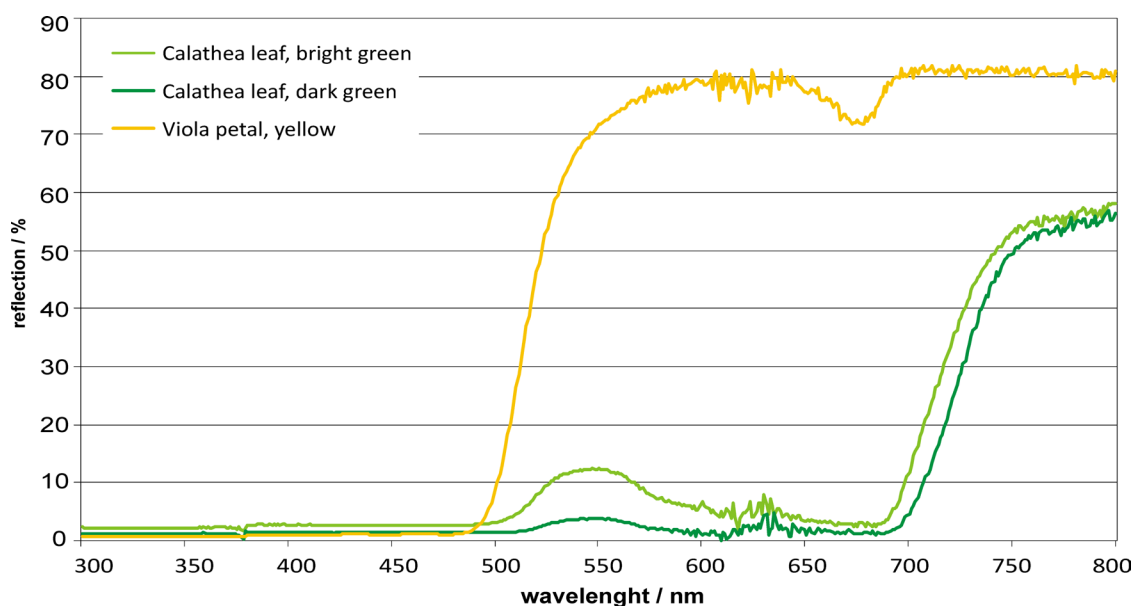
Figure 4.26: Total reflection at the upper surface of *Viola* (yellow petal) and *Calathea* (green leaf). *Calathea* possess bright green areas and slightly darker green areas. Reflection measurements of the bright and dark areas are shown.

4.27). The liquid lies between the micropapillae thus forming a smooth surface, which was seen using a light microscope. Only the outermost papillae tips stuck out of the water film.

First the untreated (structured) petal and then the liquid coated petal (smooth) was characterized in its spectral properties. After 5 minutes at ambient conditions the water film was evaporated and the petal (structured) was characterized again. This process was carried out for the intense yellow area as well as for the dark brown area (Figure 4.27). Spectral results are shown in Figure 4.28 and Figure 4.29.

Comparing the graphs of the structured petal (without water film) and the smooth petal (coated with water film) clear differences could be detected. While the structured yellow petal in the lower spectral region (300 to 500 nm) has an average reflection of 1%, the smooth petal possesses an average reflection of 3%, i.e. the reflection of the smooth petal is about 2% higher (Figure 4.29). In contrast, the reflection of the smooth petal in the upper spectral region (550 to 650 nm) is clearly lower (75%) compared to the structured petal (80%), i.e. the reflection is about 5% lower (Figure 4.28). After evaporation of the water film, the reflectance is almost the same than before liquid coating.

4.3.3 Reflection properties of biomimetic replicas

The influence of the structuring on surface reflection was examined using black replicas. The total reflectance of the structured surface was thus determined. The total reflectance of five replicas of each species were analysed ($n = 5$). All five measurements were consistent in their reflectance spectra. As an example the results of one replica of each species are shown in Figure 4.30.

The results show, that the average reflection (R) of the smooth reference between 300 and 800 nm is almost constant, i.e. the reflection is about 5%. Six of the structured replicas also possess a constant reflection, while the reflection-graphs of the other four replicas (*Fittonia*, *Pellonia*, *Begonia* and *Maranta* (bright)) possess a slight rise in the longer wavelengths starting from 700 nm. As the reflectance valus are almost contant over the howl spectral range the reflection values at 532 nm were selected and discussed later.
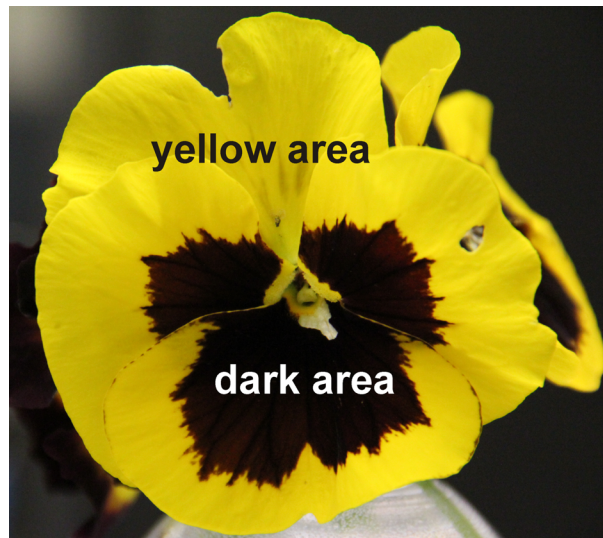
Figure 4.27: Picture of the colour intensive petals of *Viola x wittrockiana* with intense yellow and dark brown areas.
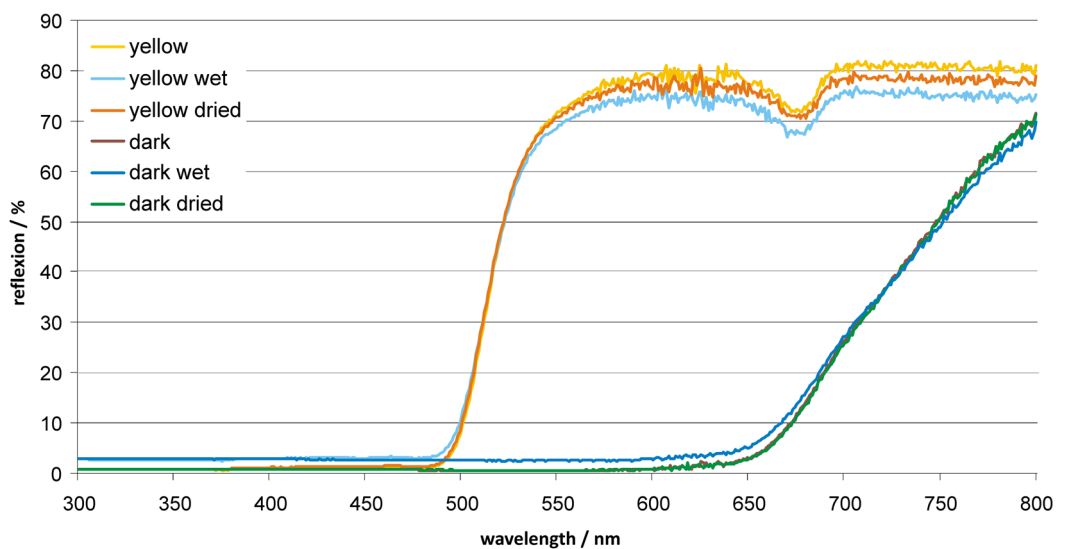
Figure 4.28: Reflection properties of the yellow and dark areas on a *Viola x wittrockiana* petal uncovered (yellow, dark), covered with a water-surfactant solution (yellow wet, dark wet) and after the water film was evaporated (yellow dried, dark dried): Reflection properties in the spectral range from 300 to 800 nm, detected in the colour intense yellow and dark brown areas.
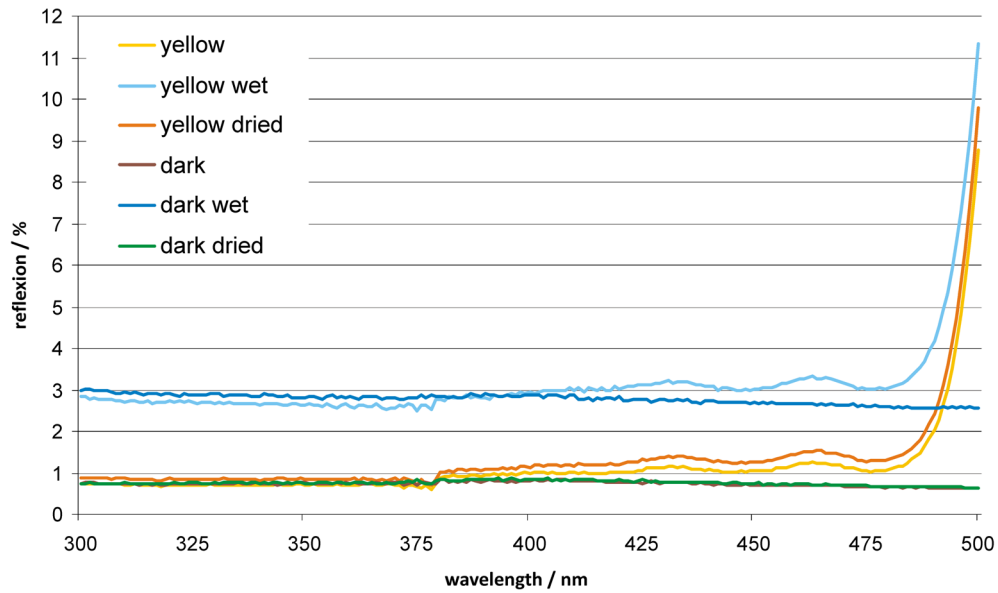
Figure 4.29: Spectral detail of Figure 4.28: Reflection properties of the *Viola x wittrockiana* petal at the yellow and dark brown areas in the range of 300 to 500 nm.
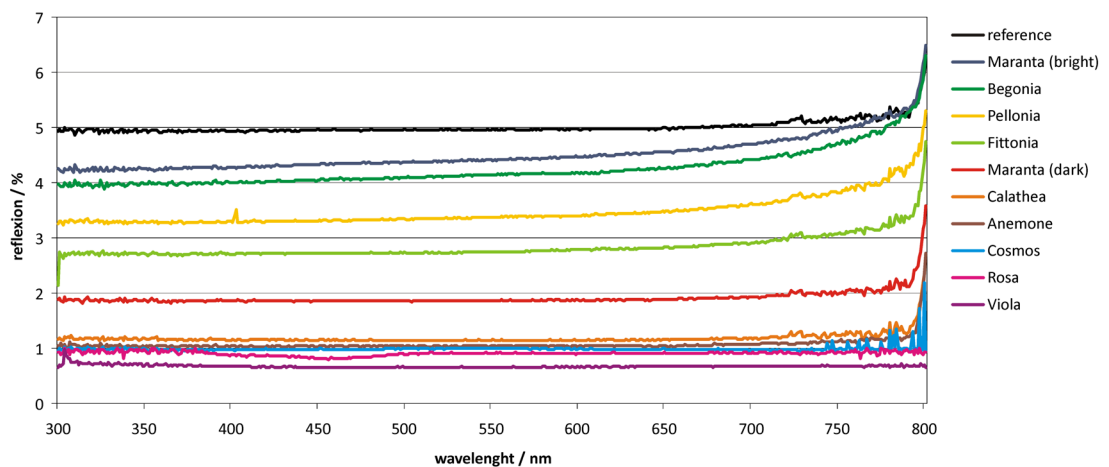
Figure 4.30: Reflectance spectra of the black pigmented leaf- and petal replicas compared to a smooth black reference - measurements were made in the range from 300 to 800 nm.
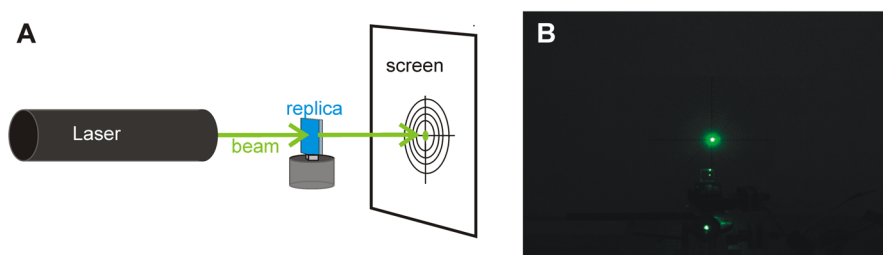
Figure 4.31: Scheme of the principal optical setup (A) and a macroscopic picture of the transmission pattern of a green beam sent at an 0° angle of incidence through a flat, unstructured polymer reference (B).

4.3.4 Angle dependent optical measurements

Angle dependent optical measurements were made to analyse the light-trapping potential of the replicas. To this end different laser beams were sent through the structured, transparent replicas and the ditribution of the beam beyond the replicas was analysed. By characterizing the beam distribution informations about the light's path within the material were captured.

Visible transmission patterns of the replicas

A red (633 nm) and a green (532 nm) laser were sent to the surface of a reference (unstructured flat polymer). The transmitted beam was projected onto a screen beyond the replica, which was provided with crosslines (Figure 4.31 A). The replica-screen distance was 31.5 cm. Visible transmission patterns were photographically documented. As an example the documented pattern of the unstructured reference produced with the green laser is shown in Figure 4.31 B.

The beam, which crosses the flat polymer, is not influenced in its direction of propagation and directly sent to the middle of the screen. A small spot could be detected (Figure 4.31 B). If a surface of a structured polymer is irradiated, the transmitted beam is changed in its direction and influenced by different effects (see Chapter 4.1.1). The resulting transmission patterns of the replicas irradiated with the red laser are shown in Figure 4.32. The transmission patterns of the replicas differ clearly in their shape, size and intensity. The smooth reference only cause a discrete spot in the optical plane in the middle of the cross line (Figure 4.31 B). The beam's direction is less changed. The transmission patterns of *Maranta* (bright) show that replicas with an almost flat surface (micropapillae ar 0.17, tip radius 45.1 μm) also produce a spot. But, in contrast to the reference, the spot of the *Maranta* bright replicas is broader.

It seems that the structures often cause ring like transmission patterns. The most prominent ring is found at the *Begonia* replicas (Figure 4.32 B). The ring patterns of the other replicas are relatively weak, as for *Calathea* (Figure 4.32, F) or *Cosmos* (Figure 4.32, H). In the extreme case of *Viola* (Figure 4.32, J), the ring pattern seems to be almost not existent. The same results were achieved by sending the green laser (532 nm) to the replica surface (Figure 4.33). In closer consideration of the green compared to the red laser irradiation of the replicas, the transmission patterns differe in size. These differences appear very strong at discrete patterns, like the pattern of *Begonia* (Figure 4.32, B). Figure 4.34 compares the size of the green and red *Begonia* transmission patterns (angle of incidence 0°).

Distribution angles of the transmitted light

For further investigation of the transmission patterns the replicas were irradiated with the IR Laser (1064 nm). The resulting transmission patterns were measured with the detector system.
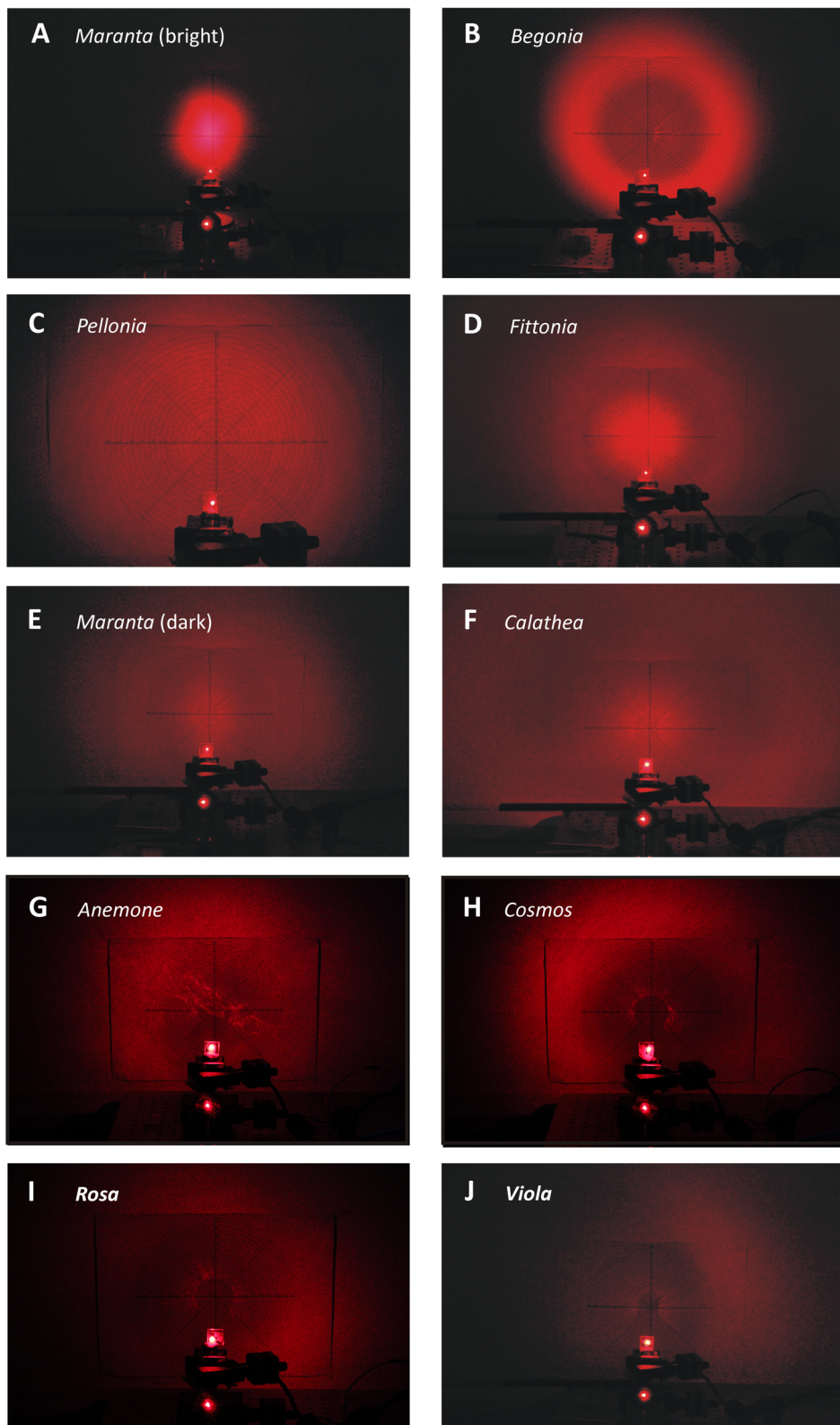
Figure 4.32: Macroscopic pictures of the transmission patterns of a red laser beam sent at an 0°
angle of incidence to the replicas of the leafs and petals.
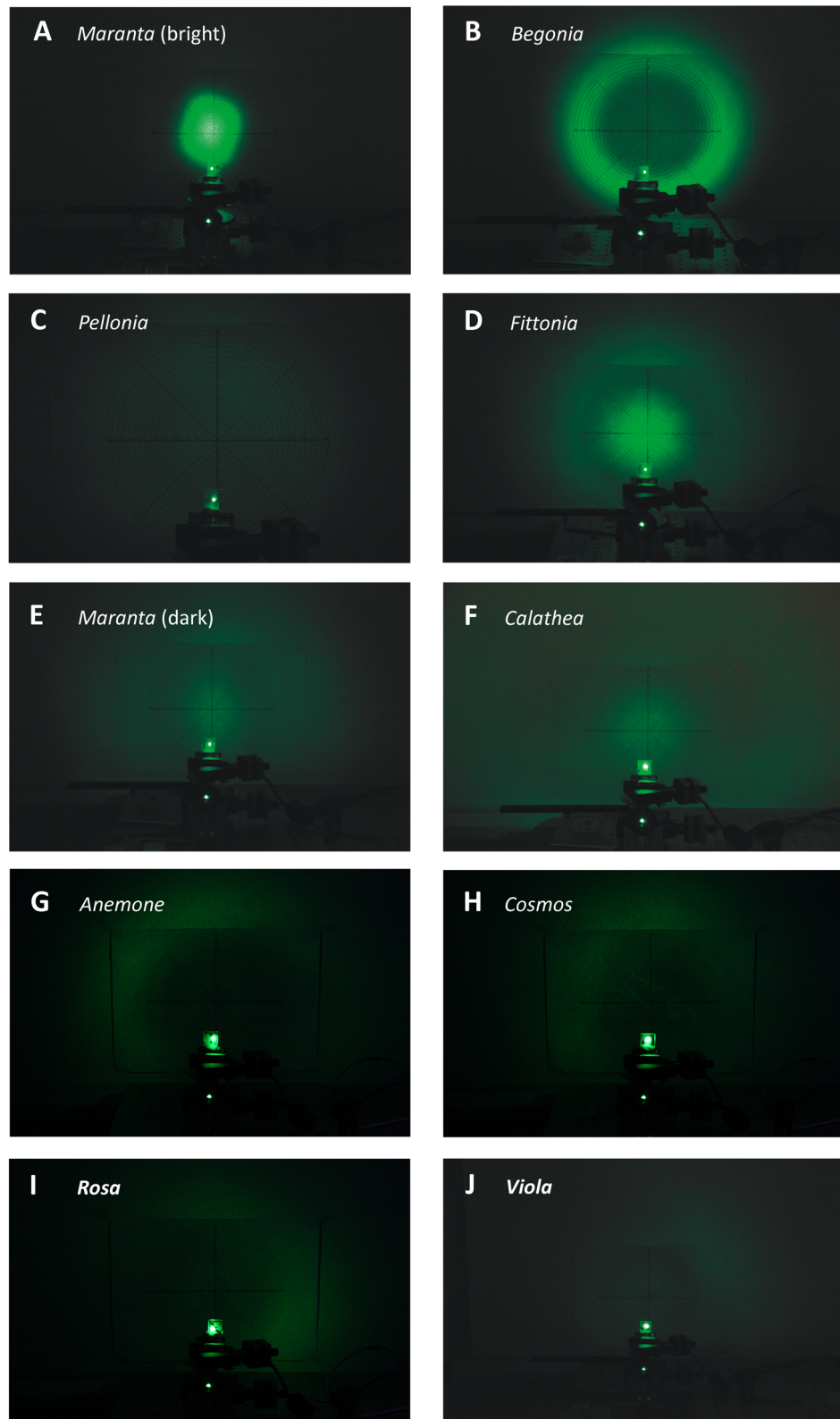
Figure 4.33: Macroscopic pictures of the transmission patterns of a green laser beam sent at an 0° angle of incidence to the replicas of the leaves and petals. The transmission patters are projected onto a screen beyond the replicas.
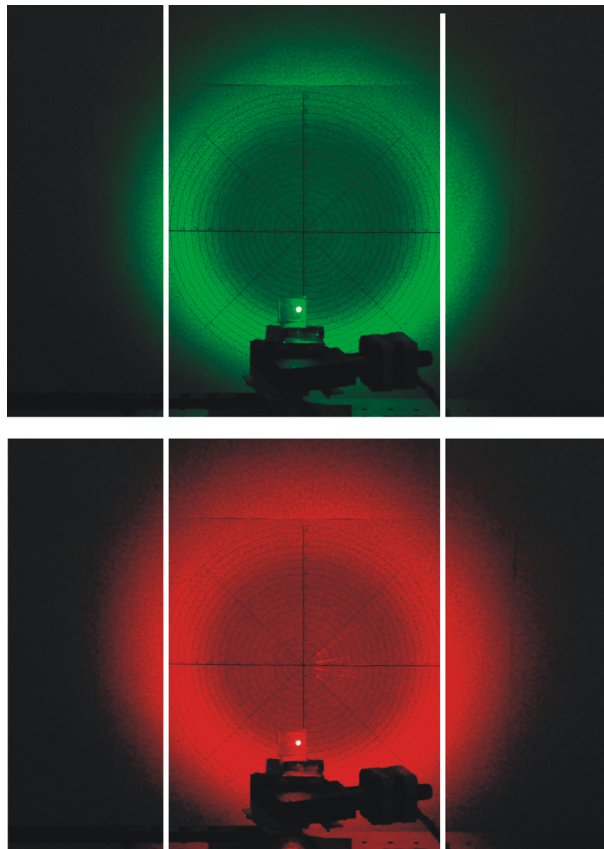
Figure 4.34: Comparison of the green and red transmission patterns (ring pattern) produced by *Begonia geogensis* replicas, angle of incidence 0°.
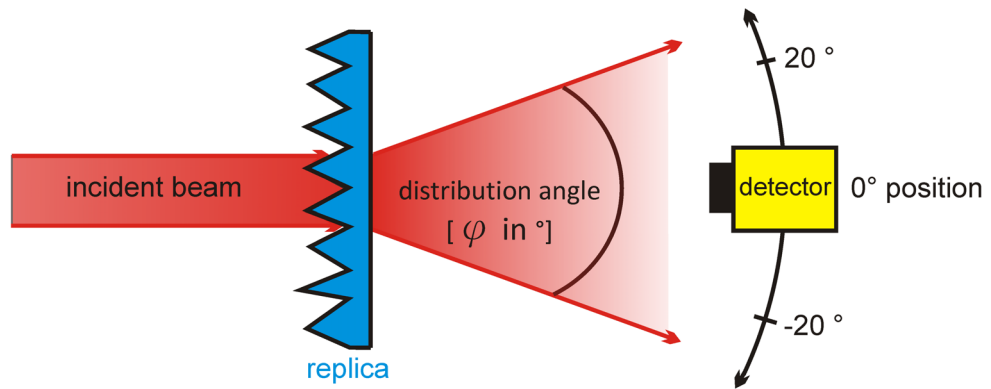
Figure 4.35: Distribution angle: Schematic of a beam sent to a structured replica surface and the resulting distribution of the transmitted beam beyond the replica (top view).

How strongly the incident beam is distributed at the different structures was determined by analysing the distribution angle (φ) (Figure 4.35).

The detector is positioned along the optical axes beyond the replica. In steps of 1° the angle dependent intensity of the transmitted light was detected. At detector position 0° the detector is arranged directly beyond the replica, in the optical path as shown in Figure 4.35. Detector position values from $\geq 0°$ to $\pm 90°$ describe the angle position of the detector. The results of these measurements are shown exemplarily with the data collected for *Maranta* (bright) replicas (Figure 4.36). Results of the other replicas are shown afterwards.

The replicas of *Maranta* (bright) leaves, which possess an almost flat surface, cause a low distribution of the beam (Figure 4.36). The detector collects signals in the range from 20° to -20° around the optical axes (0°). Thus, the total distribution angle is in 40°. As the beam is even less distributed, the detected signal spot at 0° detector position has a maximum. The height of the detected signals depends on different aspects. Particularly with regard to the characterization of replicas, which distribute the light strongly, the replica-detector distance is important. As the measurements show, some replicas distribute the beam in very strong way, thus relatively few photons reached the active area of the photodiodes (2x2 mm). The higher the distance between the replica and the detector, the less light quantum's reached the active area. Thus, for direct comparison of the results it is important to retain the distance during the measurements. Figure 4.37 shows the angel dependent transmission measurements of the different replicas.

The results show that replicas possess clearly different distribution angles. For a better distinguishing of the results the graphs are separated from each other in the Figures 4.38 and 4.39.

The distribution angles differ from 40° (*Maranta* (bright)) to almost 170° (*Viola*). The transmission graph of the *Maranta* (bright) replica possesses one intense spot at the 0° position. The graph of the *Fittonia* replica also possesses one spot in the 0° position, but in contrast to the *Maranta* replica this spot is much lower and additionally the light is more distributed (signals from -50 to $+50°$, total φ of 100°). The replicas of the *Begonia* leaves possess the inverse pattern of the *Fittonia* replicas : two relatively intense spots at the 20° and -26° positions and a low signal at the 0° position.

A graphical overview of the data collected at the biomimetic replicas is presented in table 4.1.
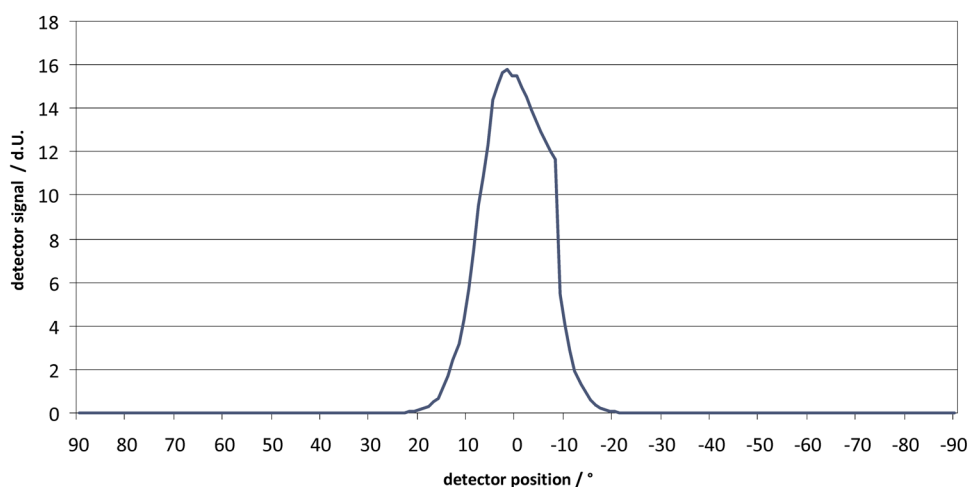
Figure 4.36: Angle dependent transmission measurement: the replica of *Maranta leuconeura* (bright) was irradiated with an IR Laser (1064 nm). The distribution of the light, caused by the surface structuring, was characterized by the detection of the light intensity beyond the replica along the optical axes; measured in $1°$ steps. Replica-detector distance 91 mm. The signal intensities are given in dimensionless units (d.U.) proportional to the voltage signal of the detector.
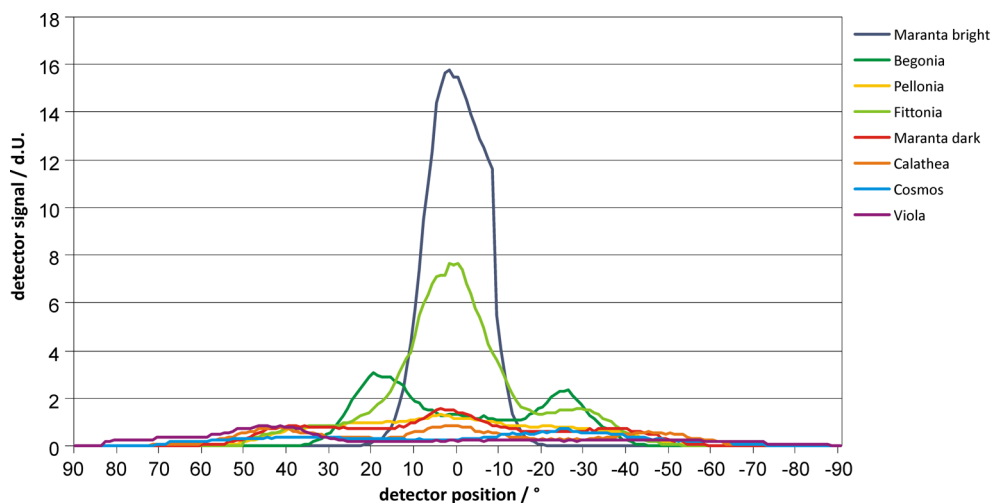
Figure 4.37: Angel dependent transmittance measurements: The different replicas were irradiated with an IR Laser beam (1064 nm) and the distribution of the beam, caused by the surface structuring, was characterized by the detector; replica-detector distance 91 mm; measurements were made in $1°$ steps in the optical plane; Signal intensities are given in dimensionless units (d.U.) proportional to the voltage signal of the detector.
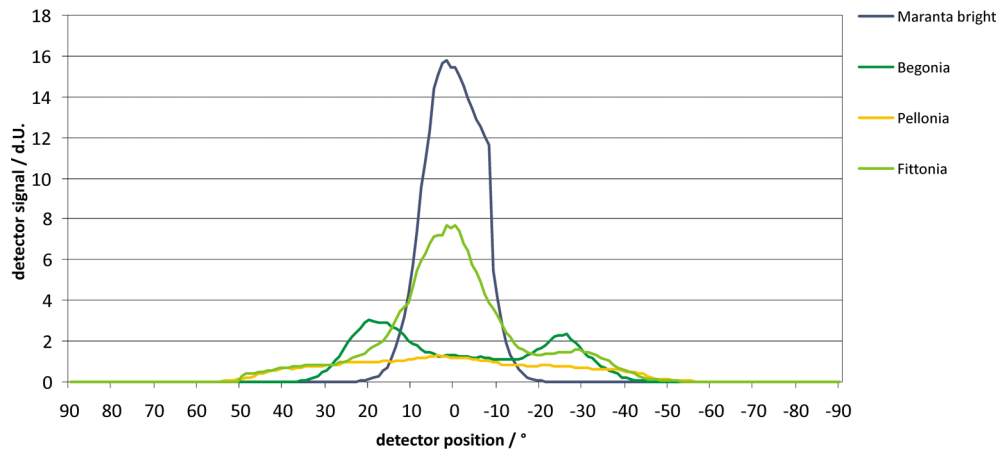
Figure 4.38: Angle dependent transmittance measurements at *Maranta* (bright), *Begonia*, *Pellonia* and *Fittonia* replicas: The different replicas were irradiated with an IR Laser beam (1064 nm) and the distribution of the beam, caused by the surface structuring, was characterized by the detector; replica-detector distance 91 mm; measurements were made in 1° steps in the optical plane; signal intensities are given in dimensionless units (d.U.) proportional to the voltage signal of the detector.
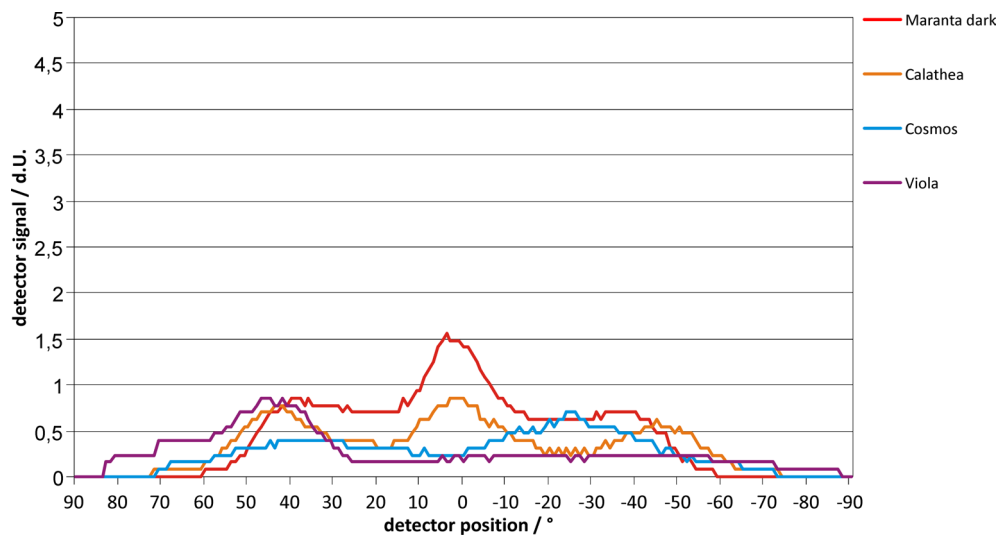
Figure 4.39: Angle dependent transmittance measurements at *Maranta* (dark), *Calathea*, *Cosmos* and *Viola* replicas: The different replicas were irradiated with an IR Laser beam (1064 nm) and the distribution of the beam, caused by the surface structuring, was characterized with the detector; replica-detector distance 91 mm; measurements were made in 1° steps in the optical plane; Signal intensities are given in dimensionless units (d.U.) proportional to the voltage signal of the detector.

Table 4.1: Graphical overview of the data collected at the biomimetic replicas: shown are SEM pictures of the surface structures, pictures of the visual transmissionpatterns (green laser), scattering angles (φ), reflection (R_{532nm}) as well as the papillae and folding parameters.

Replicas	SEM	transmissionpatterns	R [%]	papillae [µm]					folding [µm]		papillae
		VIS	φ [°]	at 532 nm	height	width	distance	tip radius	angle [°]	width	distance	**aspect ratio**
Viola			170°	0,60	45,4	15,5	32,1	2,1	26	0,26	0,45	2,93
Rosa			150°	0,90	13,8	16,5	30,7	3,29	51,3	0,41	0,21	0,84
Cosmos			140°	1,00	58,1	28,1	47,4	5,1	33,3	0,6	0,46	2,07
Anemone			140°	1,03	39,17	36,15	46,64	7,2	61	no folds		1,08
Calathea			140°	1,15	39,9	22,8	44,5	4,6	43	no folds		1,75
Maranta (d)			105°	1,87	19,1	21,16	32,63	6,65	66	no folds		0,90
Fittonia			100°	2,74	30,5	32,4	58,9	6,3	78	no folds		0,94
Pellonia			100°	3,37	36,87	41,98	62,63	14	66	no folds		0,88
Begonia			75°	4,11	16,5	31,01	46,58	11,82	109,6	no folds		0,53
Maranta (b)			40°	4,39	5,63	32,29	43,44	45,11	152	no folds		0,17
Reference			0°	4,97	/	/	/	/	/	/		/
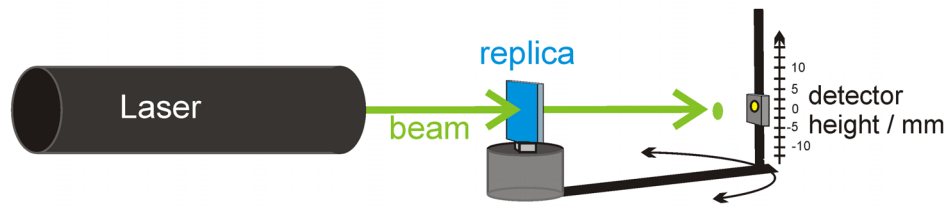
Figure 4.40: Scheme of the principal setup for the measurement of the spatial distribution of the transmission patterns. The detector moves in 1° steps around the replica and detects the transmitted light. After measuring one level beyond the replica the detector is manually moved into the next vertical level in steps of 2.5 mm.

Spatial distribution of infrared transmission patterns

For the determination of the spatial distribution of the transmission patterns the replicas were irradiated with the IR laser (1064 nm). Additionally, the detector moved beyond the replica in different vertical levels out of the optical axes and to detect the light intensity (Figure 4.40). While the horizontal movements of the detector is automatic, the vertical movements must be carried out manually. As the pure measuring time for one transmission image remains long (about 36 h) only five of the replicas were characterized in their spatial distribution, i.e. the replicas of *Calathea*, *Begonia*, *Fittonia*, *Viola* and *Cosmos*. As some replicas (e.g. *Viola*) had only a weak transmission signal, the detector had to be positioned at relatively small distance (91 mm) to the replica. This distance anticipates that the detector could move completely around the replica, as the motor unit blocks the detector's path. Even when the signals behind some replicas were relatively low, the detector could not be positioned closer to the replica as a good spatial resolution of the transmittance patterns was lost. Because of this the detector moves only from -60° (on the right side beyond the replica) to 90° (on the left side of the replica) beyond the replicas.

Moving the replicas itself in 20° steps different angles of incidence were realized and the distribution of the transmitted beam under different angles of inclination could be analysed. Transmission patterns at incidence angles of 0°, 20° and 40° were characterized. The detector measurement period at every position was 2 seconds with a sampling rate of 1024 values per second. The false-colour pictures were computed using the mean values of the collected data at every position. Using the statistical program Sigmaplot the data were computed to transmission false-colour patterns. The false-colour images are shown in Figures 4.41 to 4.42.
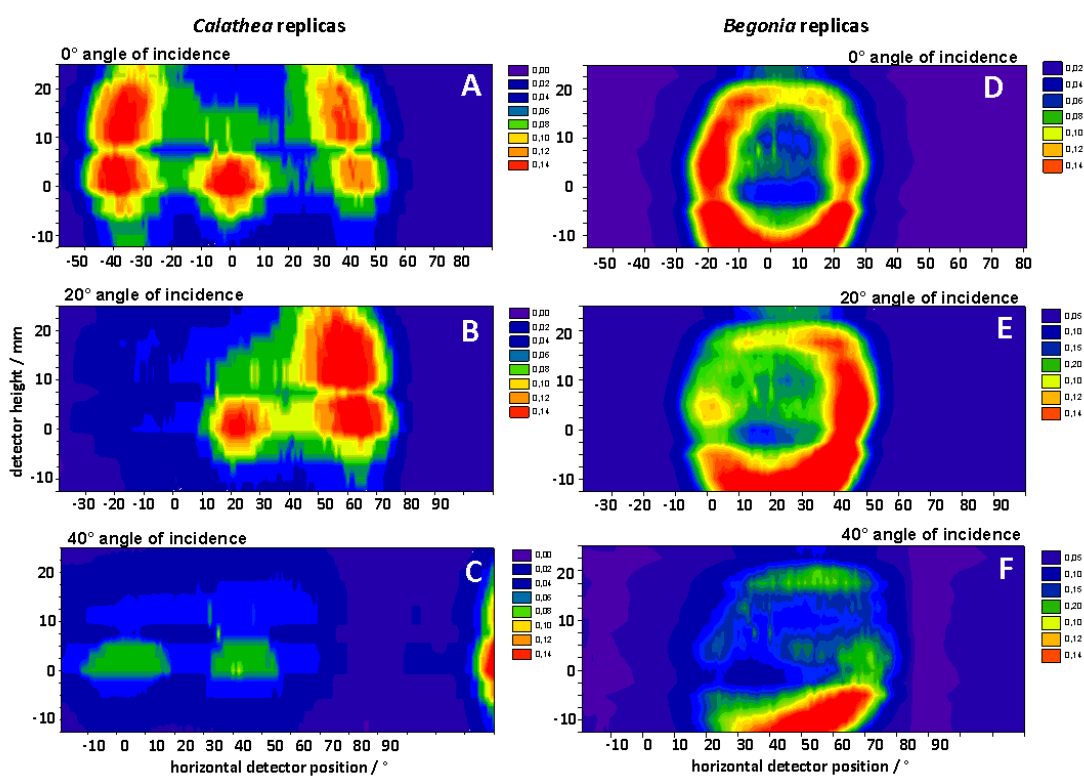
Figure 4.41: IR transmission patterns of the *Calathea* and *Begonia* replicas: an IR-Laser beam (1064 nm) was sent across the transparent structured replicas. The detector was first moved horizontally beyond the replicas and collected the light intensity in steps of 1°. The same procedure was carried out in 16 vertical levels beyond the replica. Intensities are given in dimensionless numbers proportional to the voltage signal of the detector.
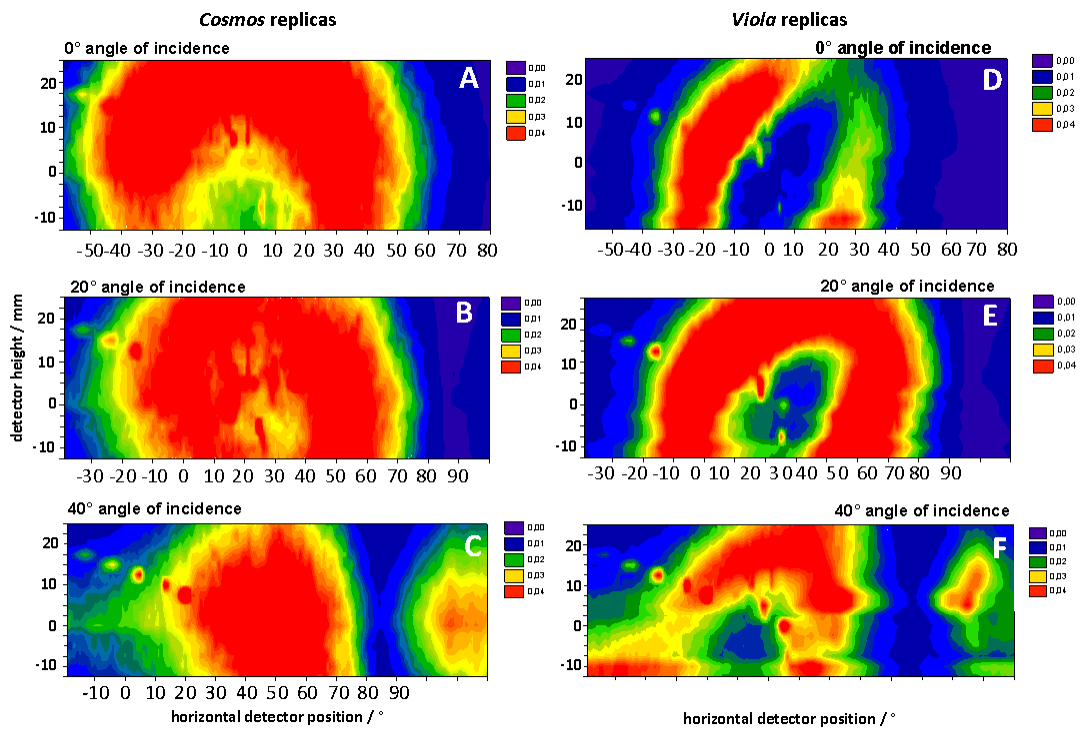
Figure 4.42: IR transmission patterns of the *Cosmos* and *Viola* replicas: an IR-Laser beam (1064 nm) was sent across the transparent structured replicas. The detector was moved horizontally beyond the replicas and collected the light intensity in steps of $1°$. The same procedure was carried out in 16 vertical levels beyond the replica. Intensities are given in dimensionless numbers proportional to the voltage signal of the detector.
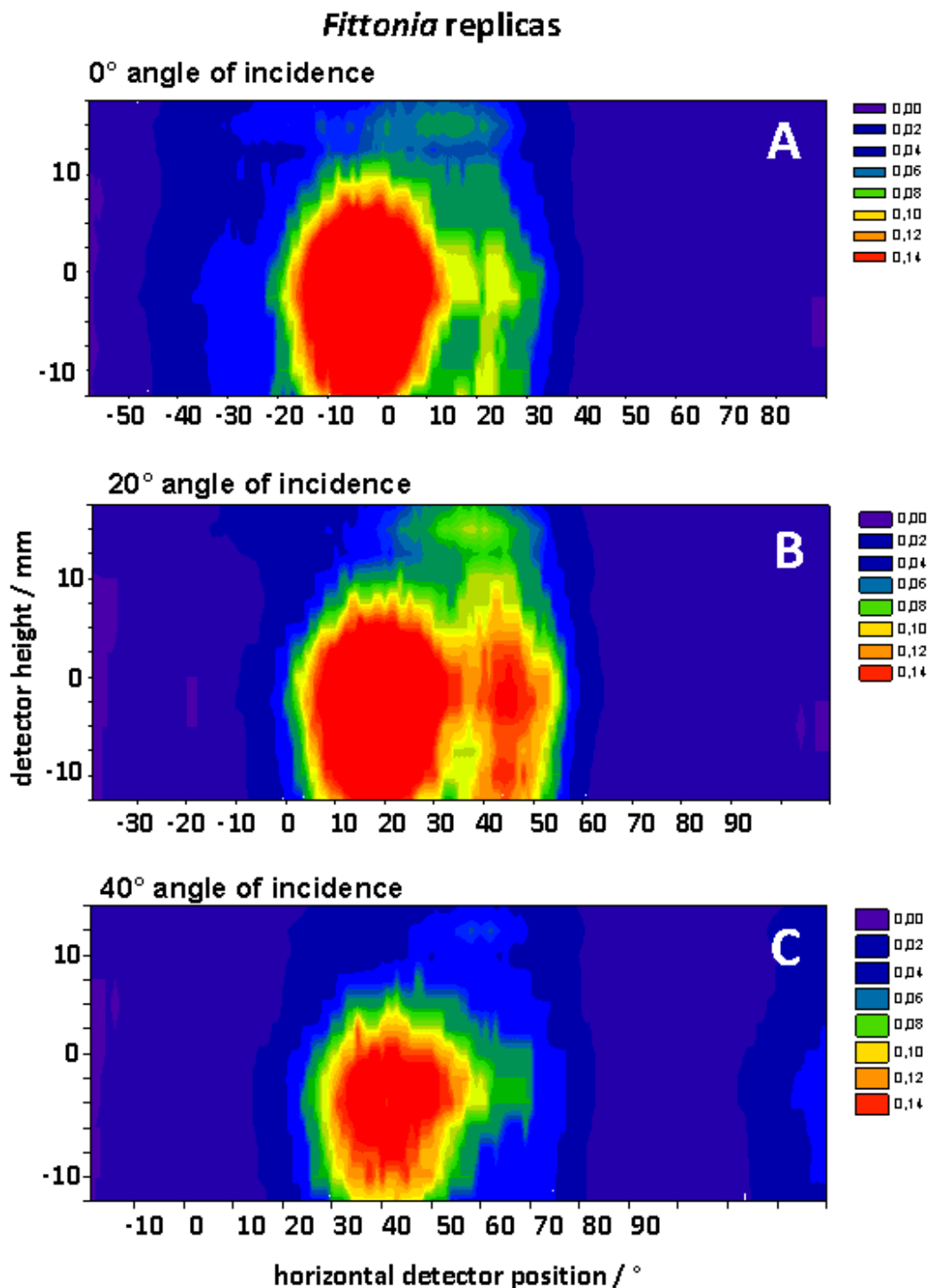
Figure 4.43: IR transmission patterns of the *Fittonia* replicas: an IR-Laser beam (1064 nm) was sent across the transparent structured replicas. The detector was moved horizontally beyond the replicas and collected the light intensity in steps of $1°$. The same procedure was carried out in 16 vertical levels beyond the replica. Intensities are given in dimensionless numbers proportional to the voltage signal of the detector.

4.4 Discussion

The micromorphology of the examined surfaces was characterized (Section 3.4.1) and compared to the reflective properties of the biological and replicated surfaces (Section 3.4.2) as well as the angle dependent transmission patterns (Section 3.4.3). For the examination of the transmission patterns a photogoniometric setup was modified. The methodical approach of this setup as well as the results of the measurements will be discussed together.

4.4.1 Surface topography of the biological and replica surfaces

All chosen biological models are characterized by conical shaped or papillated epidermal cells. This cell type was often described in terms of understory plant leaves and compared to this with special optical properties, e.g. lens effect of these cell forms [Bone et al. 1985; Vogelmann 1993]. While many studies have worked on the principal functions of these cell curvatures, little is known about the exact parameters of the microstructures and their influence on the optical properties of plant organs. Kay et al. [1981] investigated the pigment distribution in petals and the petal structure. Thereby, they analyzed the petals *via* transverse and longitudinal sections and by using the SEM. The shape of the epidermal cells was organised into classes, e.g. 'papillated', 'flat' or 'reverse-papillate'. Even when they provided principal data on whether conical or papillated cells occur on petal surfaces, data on the micropapillae are still lacking. Considerations on the optical properties of these cells were not compared to the real shape of the outer curvature of the epidermal cells.

Former investigations showed that the critical point dried biological samples possess slight preparation artifacts (shrinkage of the cells caused by the critical point drying process), while their replicas display the topography of fresh looking, turgescent cells. Because of this the characterization of the micro- and nano-structuring was made on the replicas.

The collected structure parameters will be discussed together with the optical properties of the surfaces.

4.4.2 Reflection properties of plant surfaces

The analysed organs possess remarkably differing reflection properties. These differences can mainly be attributed to differences in the pigment fraction of the organs. The green leaves of *Calathea zebrina* only reflect less light in the lower spectral range (300-500 nm). The bright green areas have an average reflection of about 2.5% in contrast to an average reflection of about 1.3% in the darkt green areas. Both areas possess a reflectivity spot at 550 nm. At this position the reflectivity of the bright green area is about 12% or 4% respectively. As differences could not be found in the shape of the micropapillae, the differences in reflectivity are likely caused by differences in the amount of chlorophyll inside the leaf. These results are in agreement with the data of Brodersen and Vogelmann [2007], which measured values from 4.2% to 17.4% at 550 nm. As plants prefer to process in the blue (400-480 nm) and yellow through red (550-700 nm) spectral ranges, the reflection in these regions is consequently low (Figure 4.26). The high reflection of wavelengths in the green spectral range (around 550 nm) is reasonable, as the solar spectrum has its maximum in the green range (500 nm) [Hecht 2001] (Figure 1.1). By reflecting these wavelengths, the plants protect themselves against damage caused by too much radiation.

The reflectance spectrum of the yellow *Voila* petal differs from the spectrum of the *Calathea* leaf, mainly due to differences in the incorporated pigments. The principal absorbing process of the pigments petals is the same as in leafs, but the pigments in petal reflect or allow other wavelengths through (Figure 4.26). A flower that is perceived as yellow contains pigments which absorb blue and green [Glover 2007]. The yellow petal analysed here possesses a total reflectivity of about 1% in the spectral range from 300-480 nm, which implies, that 99% of the incident light

is transmitted into the petal; presumably by flavonoids [Ono 2006]. This reflection value is clearly lower than the 2.3% reflectivity of papillated petals (height of the papillae 35 μm) proposed by Exner and Exner [1910] [Bernhard et al. 1968] and also lower than the reflection values measured for the dark areas of *Calathea* (1.3%). For the *Viola* petal a spontaneous reflection increase at about 500 nm to about 80% with a maximum at 600 ± 50 nm could be detected. This wavelength range concerns the yellow, orange and red spectral range send out of the petal. Compared to the green *Calathea* leaves, the petals reflect less light in lower wavelengths (300 to almost 500 nm) but much more in higher wavelengths (500 to 800 nm). Thus, the pigmentation plays an important role light-harvesting processes, the surface structuring supports the light-trapping. To analyse the structural influence on optical properties the surface structuring was eliminated by covering the *Viola* petal with a liquid resulting in a smooth surface.

Comparing the graphs of the untreated petal (without water film, structured surface) with the coated petal (with waterfilm, almost smooth surface) clear differences were detected. While the structured yellow petal in the lower spectral region (300 to 500 nm) has an average reflection of 1%, the smooth petal possesses an average reflection of 3%, i.e. the reflection is about 2% higher (Figure 4.29). In contrast the reflection of the smooth petal in the upper spectral region (550 to 650 nm) is clearly lower (75%) than that of the structured petal (80%), i.e. reflection is about 5% lower (Figure 4.28). The papillated cells in the lower region act as an anti-reflective layer, which causes a decrease in the amount of reflected light and thereby an increase of the amount of transmitted light. These results fit well with the proposed theory of multiple reflections between the surfaces of adjacent papillae [Bernhard et al. 1968]. Meaning, even if light is reflected on a papillae the reflected light then strikes another papillae and is transmitted there. However, at first sight the papillated cells in the upper spectral region seem to increase reflection. But the reduction of the surface reflection by the structuring is of course also true for the upper region and, anyhow, the colour is intensified (reflection is increased). The results suggest that the papillated cells reduce surface reflectance, allowing more light passed the surface and accordingly, allowing more light to be absorbed by the pigments inside the petal. Additionally, the surface structuring causes a path-lengthening of the light in the petal [Bernhard et al. 1968] and by this the light inside the petal strikes statistically more pigments than it would be without papillae (i.e. without papillae the paht of light within the petal is shorter). Thereby, light absorption rate is increased. Afterwards, the outgoing light is therefore more saturated, resulting in a more intense yellow, i.e. a higher reflection in the yellow spectral range. Further studies have to confirm the role played by papillated cells in the escape of the light from the petal.

In general comparison of the optical properties of different leaves and petals caused by the surface structuring requires information about the plants environment, which influence the kind and amount of pigments, leaf thickness, configuration and arrangement of the compartments as well as in their chemical composition. Because of these differences further analyses were carried out with plant surface replicas.

4.4.3 Reflection properties of biomimetic replicas

The total reflection of all structured replicas is lower than the reflection of the smooth reference (Figure 4.30). It could be observed, that the reflection at the single structured replicas (micropapillae without a folding on top) is higher than the reflection of the double structured (micropapillae with a folding on top) replicas (*Cosmos*, *Rosa*, *Viola*). In this the total reflection values of the single structured leaf replicas lie between 1.15% (*Calathea*) and 4.11% (*Begonia*). Here the total reflection values of the double structured petal replicas are between 0.6% (*Viola*) and 1.0% (*Comos*). At this point an additional folding on top of the papillae seems to support a lower reflection. A closer look to the micropapillae parameters shows a clear correlation between the reflection (selected at 532 nm) and the aspect ratio of the micropapillae (Figure 4.44).

In principal the data show that the higher the aspect ratio (ar) of the micropapillae the lower the reflection at the replica surface. The reference which has no structures (ar of 0) of course possesses the highest reflection (5%) and *Maranta* (bright) replicas with only slightly convex cell
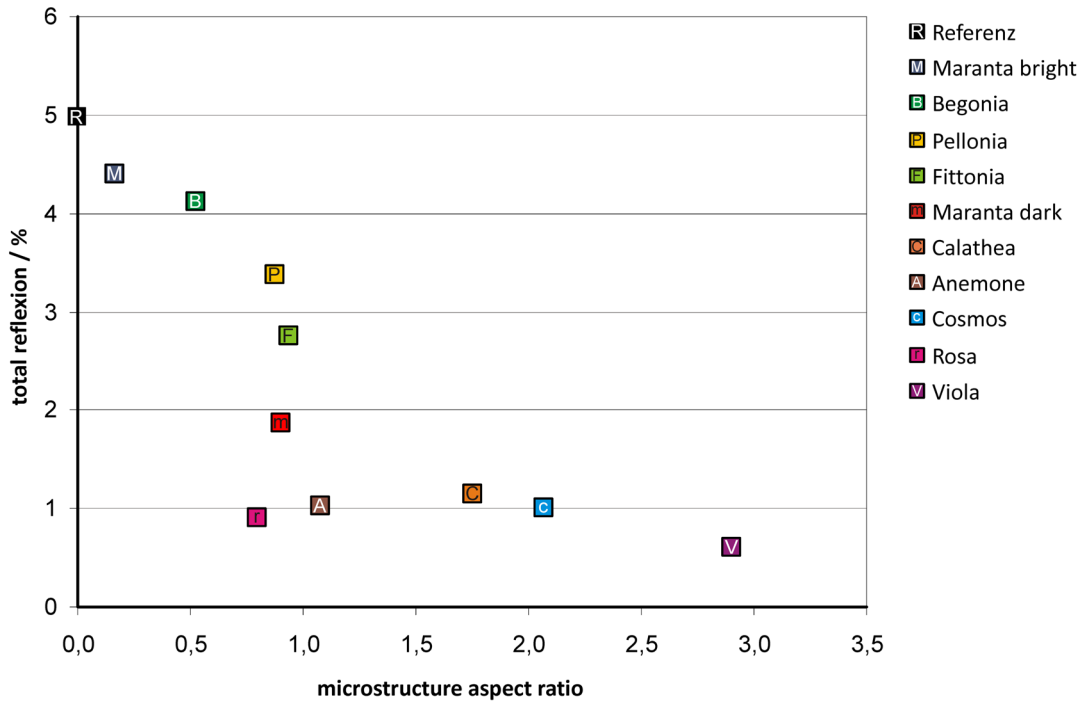
Figure 4.44: Average total reflection ($n = 5$) at 532 nm of the replicas correlated to the aspect ratio of the surface micropapillae ($n = 10$).

structures (ar 0.17) reflect about 4.4% of the incoming light. Micropapillae with an ar between 0.5 and 1 (*Begonia, Pellonia, Fittonia* and *Maranta* (dark)) reflect 4.1 to 1.9% of the incoming light. Replicas which possessing high aspect ratio structures (ar 1.0 to 3.0) reflect 1.2 to 0.6% of the incoming light (*Anemone, Calathea, Cosmos, Viola*). But there are some exceptions. The most prominent of these is found in the replicas of *Rosa*. Even though these replicas possess structures with an ar of 0.8 the reflection is about 0.9%, which is much less than for a surface with a comparable ar (*Pellonia ar* 0.88; R 3.4%). Here also the folding on top of the micropapillae, along with the other structural parameters, seems to be the reason for the low reflectance values. Thus, the reflection values were compared to the papillae angles. Figure 4.45 shows the total reflection at 532 nm compared to the average micropapillae angle.

The comparison of the reflection to the papillae angle (P_{angle}) shows, that the smaller the micropapillae angle, the lower the total reflection. The replicas with the highest papillae angle (*Maranta* (bright) and (*Begonia*) possess reflectance values higher than 4%. The smallest micropapillae possess the surfaces of *Viola* (P_{angle} 25.8°) and *Cosmos* (P_{angle} 33.3°), which reflect 0.6% or 1.0% of the incoming light respectively. Here too exceptions occur. The micropapillae of *Rosa* possess a relatively high papillae angle (P_{angle} 51.3%) and reflect only 0.9% of the incoming light. Also the micropapillae of *Anemone* replicas (P_{angle} 61°) reflect only 1% of the incoming light. Compared to the *Pellonia* replicas, which have micropapillae with a similar angle (P_{angle} 66°) but much higher reflectance values (R_{532nm} 3.4%) *Rosa* and *Anemone* possess some special features. *Rosa* has cuticular folding on top of the micropapillae. Also it is suggested here that these folds reduce the total reflectance at the replica surface. However, the replicas of *Anemone* petals possess no such folds on top of the micropapillae, but the papillae have smaller peak diameters than the *Pellonia* micropapillae and between the micropapillae small cavities could be found (Figure 4.46). Maybe the incoming light is trapped within these cavities, which results in a reduction of the total amount of light reflected. Even when the ar and papillae angle values of the *Pellonia* micropaplliae (ar 0.88; P_{angle} 66°) are similar to the values of the *Rosa* micropapillae
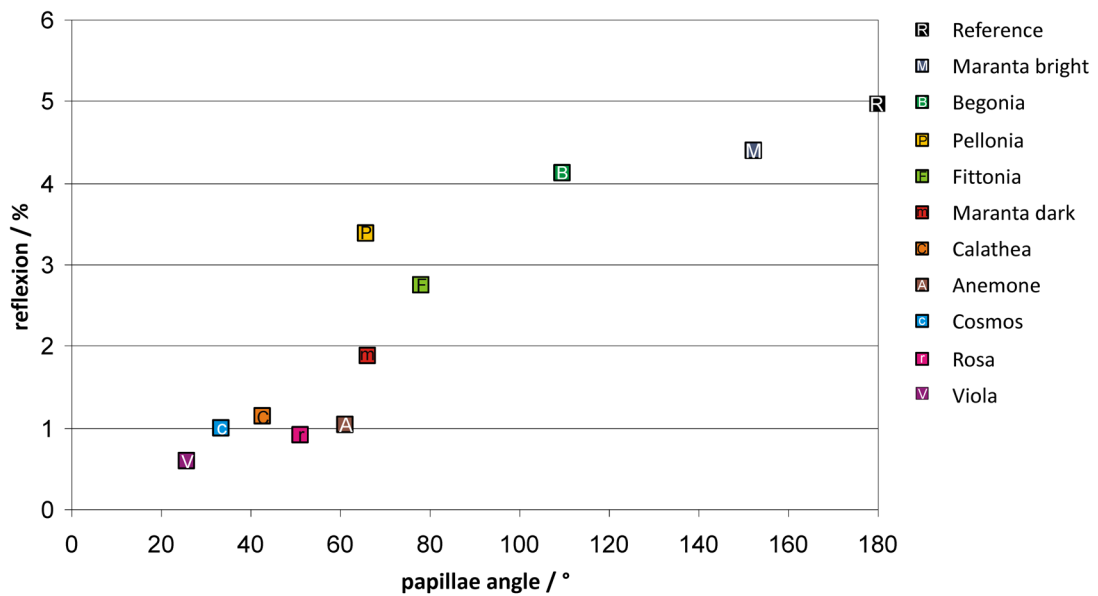
Figure 4.45: Average total reflection ($n = 5$) at 532 nm of the replicas correlated to the angle of the surface micropapillae ($n = 10$).

(ar 0.84; P_{angle} 51.3°) the reflection at the *Rosa* replica (R_{532nm} 0.9%) is much lower than the reflection at the *Pellonia* replica (R_{532nm} 3.4%). The most prominent difference is the cuticular folding on top of the micropapillae. Additionally the micropapillae of the *Rosa* replicas have very small peak radii. Figure 4.47 shows the reflection values at 532 nm compared to the tip radius of the micropaplillae.

For *Rosa* and *Pellonia* it seems that a small tip radius (tr) supports low reflectivity. But, even when a small tip radius could be detected at low reflective surfaces as on *Viola* (tr 2.1 μm) or *Cosmos* (tr 5.8 μm) they could also detected on surfaces with a higher reflectance, e.g. at *Fittonia* (tr 6.29, R 2.7%). Even when a clear trend in the data is missed, theoretical considerations suggest that a small tip radius is advantageous for the development of anti-reflective surfaces, because the big tips of the *Pellonia* micropapillae display some kind of optical plateau where much more
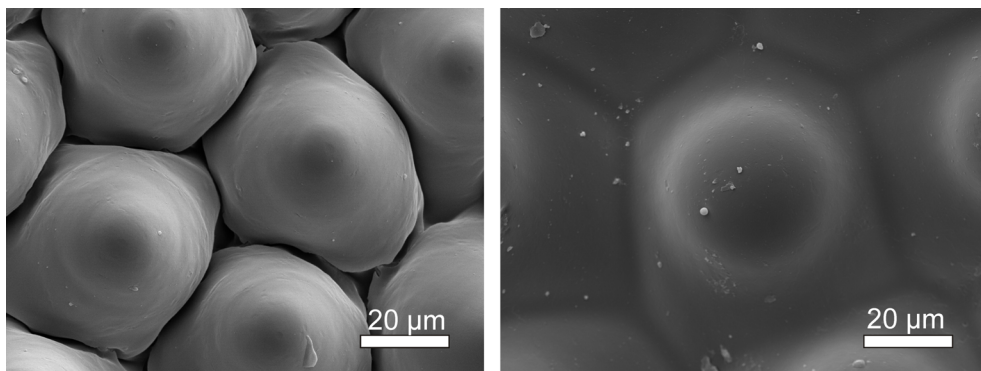
Figure 4.46: SEM pictures of the micropapillae (top view) of *Anemone nemorosa* compared to the micropapillae of *Pellonia pulchra*. The micropapillae of *Anemone* possess smaller peak diameters than *Pellonia* and small cavities between the micropapillae.
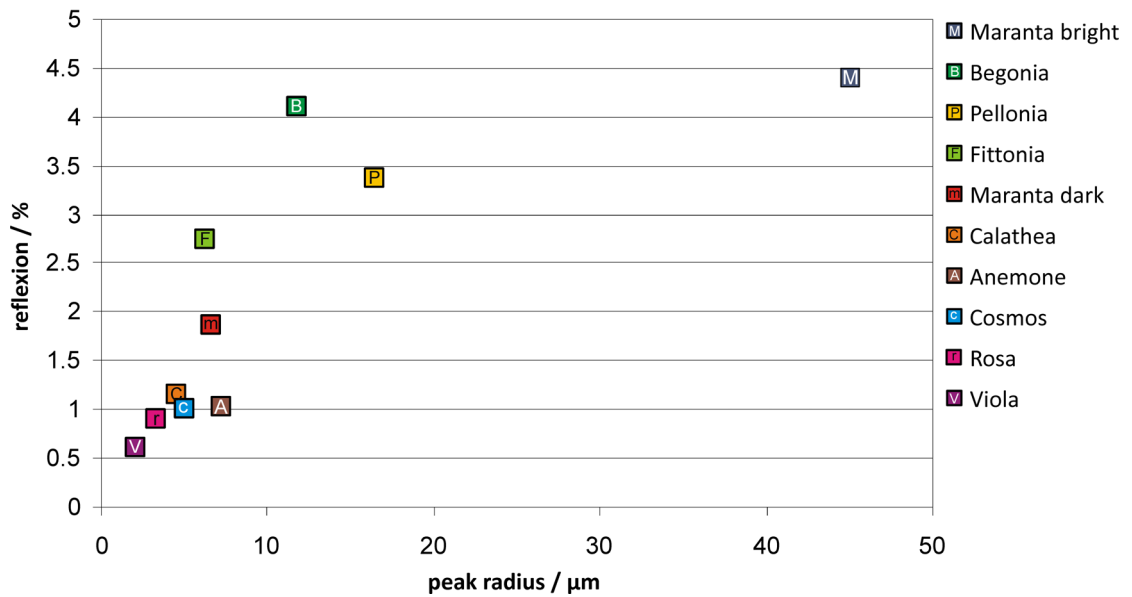
Figure 4.47: Average total reflection ($n = 5$) at 532 nm of the replicas correlated to the micropapillae tip radius ($n = 10$).

light can be reflected than at a small tip. Thus, the smaller the papillae tip the less light will be reflected.

Further the total reflection was correlated with the micropapillae peak-to-peak distance (Figure 4.48). Clear correlations between theses parameters could not be detected. But as with the tip radius we may assume that big distances between the papillae result in smooth and therefore high reflective areas as for example on *Fittonia*. So this will also be disadvantageous for a low reflective surface.

The results show that sharp micropapillae with a high aspect ratio are able to reduce the surface reflection in crucial ways. The lowest reflection (R_{532nm} 0.6%) occurs on the *Viola* petal replicas, which possess sharp P_{angle} 26°), high aspect ratio (*ar* 2.9) micropapillae. These structures reduce the reflection of the polymer used here up to 88% (compared to the unstructured polymer). In retrospect these reflection values fit very well with the measured reflection values of the *Viola* petal in the lower spectral range ($\leq$1%). So it could be assumed that the measured reflection at the *Viola* petals displays the surface reflection. Further, it could be assumed that folding on top of the micropapillae supports the anti-reflective properties of the surfaces. *Viola* replicas have the lowest reflection values (R_{532nm} 0.6%) and possess folds with a width of about 0.4 μm and a distance of about 2.2 μm. But, it is not possible to say which kind of folding causes the lowest reflection values as the micropapillae of the three double structured surfaces differ too much in their other parameters. It seems that a combination of high *ar*, small papillae angles, folding on top of the papillae and sharp tips cause the lowest reflection values (as shown for *Viola* replicas). To analyse which kind of folding on top of the micropapillae causes the lowest reflection values further analyses have to be made. For example with surfaces, which possess different kinds of folds on the same kind of micropapillae.

The lowest reflection in leaf replicas was found on *Calathea* (R_{532nm} 1.2%), which possesses micropapillae with a smaller aspect ratio (*ar* 1.8) and a papillae angle of 42.7°. Even when these surface parameters cause a low reflective surface, the double structured petal surfaces cause lower reflectivity values. The results suggest that high aspect ratio micropapillae cause a light-trapping effect at the surfaces and folds on top enhance the anti-reflective properties of the surfaces. The combination of both results in extremely low reflection values. It seems that the higher the papillae, the better the light is guided into the material. The light-trapping properties of surfaces
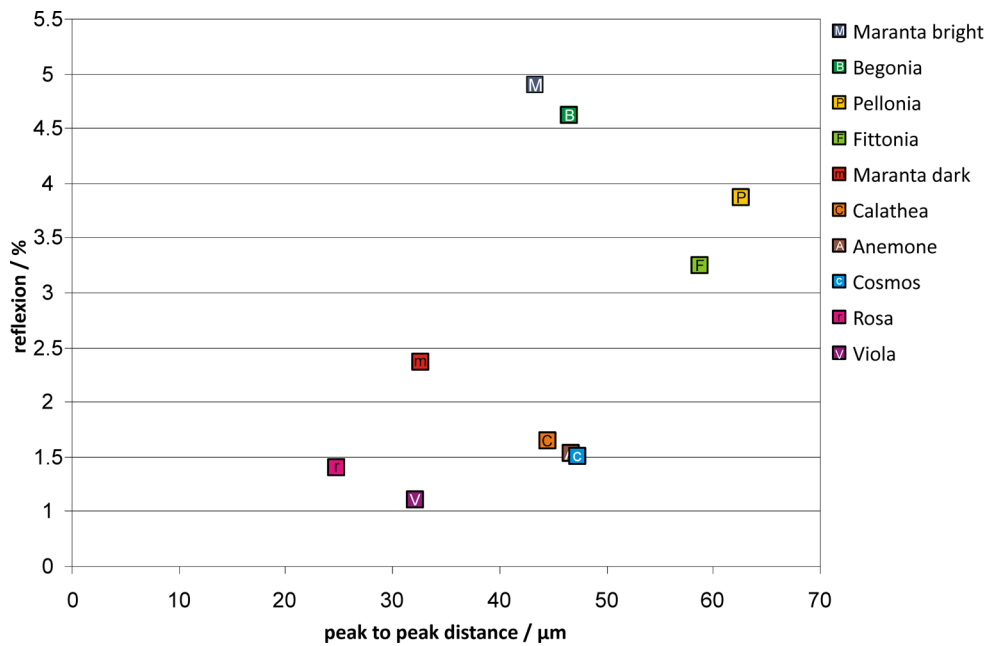
Figure 4.48: Average total reflection ($n = 5$) at 532 nm of the replicas correlated to the micropapillae distance ($n = 10$).

with low aspect ratio structures (e.g. *Begonia*) as compared to those surfaces with a high aspect ratio structures (e.g. *Viola*) are shown in Figure 4.49. The light trapping effect on a *Viola* surface is much better as the amount of multiple reflections is much higher as compared to the *Begonia* model. The other leaf replicas possess reflectance values from 2.7% (*Fittonia*) to 4.4% (*Maranta* (bright)), which are not much better than the commonly known 3% for the pyramidal structures on solar cells.

Up to now the pyramidal surface structures used on solar cells possess aspect ratios of about 1 and a typical angle of about 45°. The results suggest that a higher *ar* and a sharper structure angle will clearly reduce the reflection clearly. Furthermore, a hierarchically arranged structure in the form of striations at the structures seems to cause a further reduction of the surface reflection.

Anti-reflective, biomimetic and self-cleaning surfaces for organic solar cells were introduced by Choi and Huh [2010]. In this study the traditionally known pyramidal or grooved surface mi-
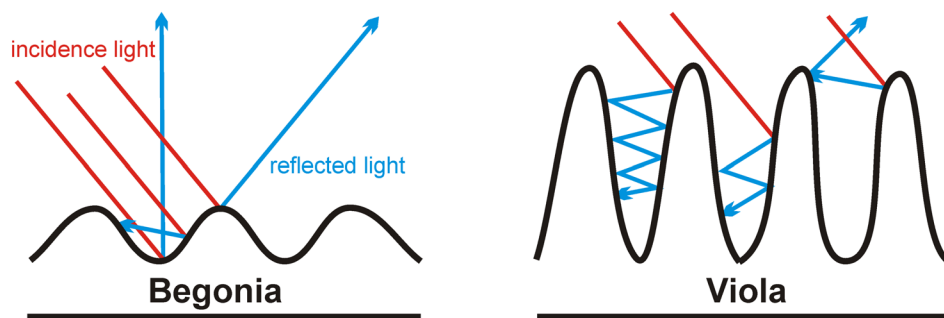
Figure 4.49: Schematic drawing of the proposed light path at low (e.g *Begonia*) and high (e.g. *Viola*) aspect ratio structures on the replicas.

crostructures are used as templates and transferred onto a glass substrate. Even when they talk about a one-step replication method there are in fact three-steps from replicating the template to the structured solar device [Choi et al. 2004, 2008a,b; Choi and Huh 2010]. Using nanoparticles (Al_2O_3) and self-assembled monolayers (SAMs) polymer micro-pyramids were prepared with a nanostructuring on top. The reflection values of these surfaces especially in the visible spectral range were heterogeneous and alternate between 3 and 12%, which are clearly higher than the reflection values found here. Additionally they worked with a polymer (transparent cured per-fluoropolyether, PEPE), which appears to have a relative low refractive index (about 1.37) and thereby increases the light transmission. It is a layer with an refractive index between air (1.0) and glass (1.52) and suppress the interfacial Fresnel's reflection [Choi and Huh 2010; Hecht 2001]. That means the lower the differences between the refractive indices involved, the lower the reflection values. The replication material used here seems to have a refractive index of about 1.5, which causes no decrease in reflectivity. However, the reflection values are much lower than at the prism structures proposed by Choi and Huh [2010]. Probably a lower refractive index material, structured with the micropapillae presented here, would cause a further decrease of reflectance.

4.4.4 Angle dependent optical measurements

Visible transmission patterns of the replicas

Figure 4.32 and 4.33 show, that the transmission patterns of the replicas clearly differ from each other in their shape, size and intensity. It seems that the replicas often cause ring patterns. From a physical point of view these ring patterns are explicable. Bone et al. [1985] referred to the lens effect of cone-shaped epidermal cells. In their work, the major point of interest was optical focal spots produced by epidermal cells when light strikes a plant surface. They postulated that chloroplasts move to these focal spots and use the intensive light there. It was supposed, that especially shadow plants use this effect to compensate for the disadvantages caused by their low-light environment. They inferred that the position of the focal spots within the papillae depend on papillae height. For example in the epidermal cells of *Medicago sativa* (cell tip radius 16 μm) the focal spots fell 30-50 μm into the underlying palisade layer [Martin et al. 1989]. It is obvious that the light focused in the spot is able to form a ring pattern in deeper regions. Light which strikes the papillae side will be concentrated over a ring. Light which strikes the papillae top is only marginally changed in it directions; it will pass the surface relatively straight. While the surface area of the papillae side is proportionately much larger than the papillae, the amount of collected light at the papillae sides is much higher than the light transmitted through the papillae tip resulting in a ring pattern. The form of the micropapillae determines the kind of ring. The higher the micropapillae the larger are the ring patterns. That means that surface structuring is crucial to determining the path of the transmitted light.

It is conspicuous that some transmission patterns are very weak in their intensity (e.g. *Viola* or *Cosmos*). It seems that they transmit almost no light or may distribute it in such a strong way that it can hardly be recognized in the pictures. Further some of the irradiated replicas themselves seem much brighter than others when irradiated with the beam. For example, the irradiated replica of *Viola* (Figure 4.32, J) seems to be much brighter than the replica of *Maranta* (dark) (Figure 4.32, E). The laser beam diameter which strikes the replica seems larger. As the laser beam diameter is constant in both cases, two other explanations are possible. First, the upper surface of the *Viola* replica reflects more light than the surface of the *Maranta* (dark) replica. Therefore the replica seems to be much brighter. This explanation has to be inconsistent, as the surface reflection of the *Viola* replicas (R_{532nm} 0.6%) is much lower than the surface reflection of the *Maranta* (dark) replicas (R_{532nm} 1.9%). The second explanation is that the bright spot at the transparent *Viola* replica is caused by reflections at the smooth backside of the replica. Reflection measurements at transparent *Viola* replicas (data not shown) reveal almost 20% reflectivity (measurements at black replicas reveal an reflectivity of about 0.6%). This means, 0.6% of the reflection comes from the upper structured surface while almost 19% come from the smooth lower surface. Measurements at transparent and black *Maranta* (dark) replicas show, that

1.9% of the reflection comes from the upper surface and almost 8% from the lower surface. As the amount of reflection depends on the angle of incidence it would seem, that the light within the *Viola* replica strikes the back side of the replica at a higher angle of incidence. Thus, the surface structuring guides the light into the material in a higher angel of incidence. The importance of this distribution angle will be discussed later in detail, as it is very important in terms of the light-trapping properties of the biomimetic structures within the material.

On closer consideration of the green compared with the red transmission patterns differences in the pattern size were recognized (Figure 4.34). The determination of the ring size reveals that the ring in the green pattern is smaller compared to the red pattern (Figure 4.34). Two physical phenomena can be the reason for this difference in size: diffraction or refraction.

Diffraction describes the situation by which light is diffracted at barriers (e.g. micropapillae). There it is imperative that the smaller the wavelength compared to the barrier size the smaller the resulting diffraction. For the actual results this means, that the green pattern (532 nm) has to be smaller than the pattern of the red light (633 nm).

On the other hand refraction could be the reason for the differences in pattern size. Electromagnetic wavelengths are typically refracted at structures, which are bigger than the wavelength of the incoming light. This effect is described by the term dispersion. In this, light composed of longer wavelengths is refracted less than with shorter wavelengths. For the actual analyses this means that the green pattern has to be bigger than the red pattern.

The results show that the green ring is smaller than the red ring (Figure 4.34), which suggests that a diffraction effect is observeable. The principal ring pattern seems to be independent from the wavelength of the light. This indicates that the structures at the leaf and petal surfaces act as a kind of diffraction grating and their structural parameters determine the grating characteristics. The plant grating constant could be defined by the mircopapillae per unit area, which would be comparable to the lines per unit area of a technical grating. The higher the grating constant, i.e. more mircopapillae per unit area, the higher the diffraction effect. This means for the plant surface, if the the number of papillae per unit area is fixed and the wavelength changes, the transmission pattern changed in size. Figure 4.34 supports this assumption as the red *Begonia* pattern is larger than the green *Begonia* pattern. If the wavelength is fixed and the number of papillae per unit area changes the diffraction effect will be also stronger and the ring patterns will be bigger in size. This effect can be observed in Figure 4.32, repectively, Figure 4.33. The results further support these suggestion as the surface of *Viola* possesses densely arranged micropapillae with a mid width of 15.5 μm and extremely high distribution angles (up to φ 170°). In constrast surfaces with broader micropapillae (less micropapillae per unit area) possess lower distribution angles, e.g. *Calathea* (mid width 22.8 μm, φ 140°)).

The nanofolding on top additionally supports the distribution of the light and causes a scattering of the light. In the extreme case of *Viola* the ring pattern is hardly to recognize. The combination of the high and sharp micropapillae with an folding on top seems most efficient for a high distribution of the light within a material.

Based on the oberserved effects it will be postulated that refraction effects are neglegtible for the replicas, as the red pattern is bigger than the green pattern. Further, especially for plants refraction seems to be neglegtible as the thickness of the cuticle and the cell wall is in micrometre dimensions [Riederer 2006] and the strenght of refraction depents on the refractive index and the thickness of the material (see dispersion in chapter 4.1.1).

Distribution angels of the transmitted light

The distribution angels differ from 40° (*Maranta* (bright)) to almost 170° (*Viola*). The transmission graph of the *Maranta* (bright) replica possesses one intense spot at the 0° position and the graph of the *Fittonia* also possesses one spot in the 0° position, but in contrast to the *Maranta* replica this spot is much lower in intensity and additionally the light is more scattered (signals
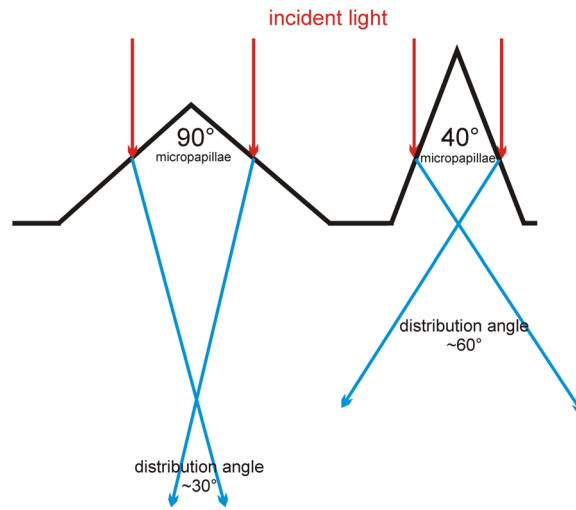
Figure 4.50: Schematic of the proposed light path irradiated in a 0° angle of inclination to the surface normal of micropapillae with an angle of 90° and 40°. The light is refracted at the papillae surface. Refraction angles are proposed using Snell's Law, with $n_1 = 1$ and $n_2 = 1.5$.

from -50 to $+50°$, total φ of 100°). These data are in agreement with the pictures made of the green and red transmission patterns. The pictures show an intense light spot in the middle of the pattern and a weak ring around the spot (Figure 4.32 D). These data correlate very well with the visible patterns as the transmission pattern is a ring. The intense spots at the 0° position are presumably caused by light, the direction of which is not changed by the surface structuring. The micropapillae of the *Fittonia* replicas are arranged with large, almost flat areas between them (Figure 4.15 C, D). If light is directed through these areas it is not changed in its path and is guided directly through the material. The replicas of the *Begonia* leaves possess the opposite pattern to the replicas of *Fittonia*: two relatively intense spots at the 20° and -26° positions and a low signal at the 0° position. In contrast to the *Fittonia* surfaces, the micropapillae of the *Begonia* replicas do not possess flat areas in between (Figure 4.15 E, F) and the incident light only strikes the papillae. Depending on the papillae angle, the light is distributed into a ring pattern. As the flat areas are missed a high spot inside the ring is missed. The slight spot results may be from the light, which passes the papillae tip where the light's direction is also not changed. In comparison to the distribution angle of *Fittonia* (φ 100°) the distribution angle of *Begonia* is slightly lower (φ 75°). This presumably is caused by the higher papillae angle of the *Begonia* micropapillae (P_{angle} 109°) as compared to the *Fittonia* micropapillae (P_{angle} 78°).

Thus, the distribution angle is presumably mainly determined by the papillae angle. A proposed light path at 90° and 40° micropapillae is shown in Figure 4.50. The drawing shows, the higher the papillae angle the lower the distribution angle. Replicas with sharp micropapillae (low papillae angles) send the transmitted light into the material at a higher angle of incidence than the micropapillae with a high papillae angle. Of course optical phenomena in a micro-papillated surface are much more complex than this. Multiple reflections obviously result in much higher distribution angles as proposed in Figure 4.50 as seen for the micropapillae of *Calathea zebrina* (P_{angle} 43°, φ 140°). Additionally, biological surfaces in general are difficult to characterize as a standard deviation often occurs. The *Viola* replicas possess the highest distribution angles (φ 170°), which are also characterized by the lowest papillae angles P_{angle} 26°). Here too the *Rosa* presents an exception as the distribution angle is about 150° and the micropapillae angle is relatively high (about 51°). This suggests that the folding plays also a role in the scattering of the incident light. The distribution angles were further compared to the total reflection (Figure 4.51).
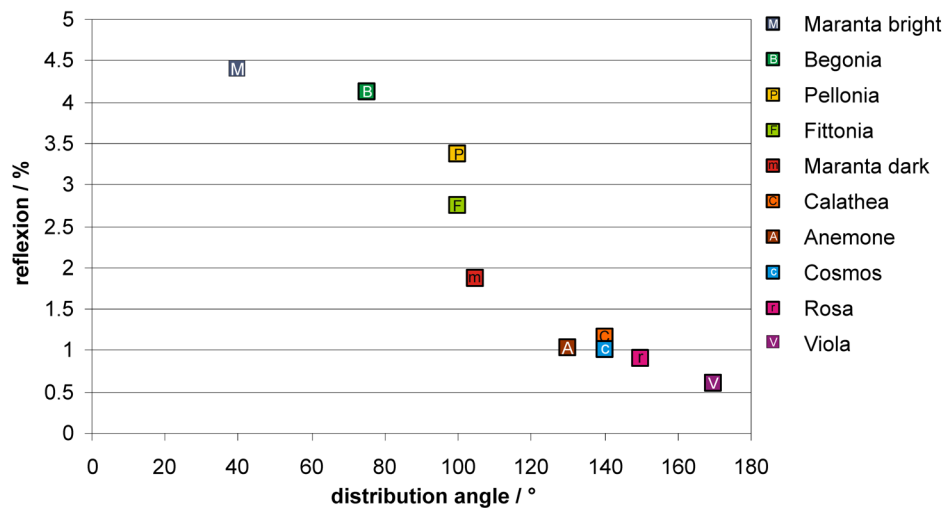
Figure 4.51: distribution angles of the light transmitted across the replicas compared to the total reflection of light at the replica surfaces.

This correlation shows that a low reflection is attended to a high distribution angle, which suggests that the anti-reflective properties at the surfaces are related to a light-trapping effect inside the material. A correlation between the surface parameters and the distribution angles was also suggested by the comparison of the reflection values of transparent compared to black replicas. In a smooth, transparent replica (polymer $n \approx 1.5$) a total average reflection of 11% was detected. In regard to the reflectivity law it could be suggested, that the reflectivity at the upper as well as at the lower surface is about 5.5%. Measurements on the black counterpart confirmed this assumption with an average reflectivity of 5.0% (reflection of the upper replica surface). Each of the surfaces makes 50% of the total reflectivity. In contrast the measurements on the transparent and black replicas does not reproduce this 50 to 50% situation shown on the smooth reference. Some surfaces had an extreme low reflectivity at the upper surface and a comparatively high reflection from the back. Extreme values were found for *Viola* (average upper side reflection almost 0.6%, average back side 19%), *Comos* (average upper side reflection 12.5%, average back side reflection 1.0%) and *Calathea* (average upper side reflection 8.7%, average back side reflection 1.3%).

The data suggest that the surface structuring defines the light's path within the material. In comparison to the smooth surface, the structures of especially *Viola*, *Cosmos* and *Calathea* 'sent' the incoming light to the back side of the replicas at a higher angle of incidence, which results in a higher back side reflection, as the reflection at a smooth surface increases as the angle of incidence is increased. This suggestion is in agreement with the high distribution angles measured here.

Spatial distribution of infrared transmission patterns

The detected IR transmission patterns at a 0° angle of incidence possess (Figure 4.41 A, D; 4.42 A, D; 4.43 A) the same principal patterns as the red and green transmission patterns (Figure 4.32 B, D, F, H, J; 4.33 B, D, F, H, J). As well as on the photographic pictures (Figure 4.32) the *Begonia* replicas posses the discrete ring pattern in the IR transmission pictures (Figure 4.41 D). Compared to the first distribution angle measurements for the *Begonia* replicas (φ 75°, Figure 4.38), the distribution angle here seems to be smaller (φ about 55°, Figure 4.41 D). It seems that only the most intensive spots are detected and the low diffuse scattering around the ring is not detected. The reason for this is probably a change in the current reaching the A/D transformer

card. The extreme differences in the replicas' scattering characteristics possess a challenge for the detection system. As the beam of the *Maranta* (bright) replicas is only less scattered, the detected signal beyond the replica is high, i.e. the current of the photodiodes is also high. The A/D transformer card should get only an input currend between 0-10 V. Thus, the incoming current has to be regulated to a maximum value of 10 V. In detecting high scattering replicas this regulation made for low scattering replicas, e.g. *Maranta* replicas, results in a lowering of the already low signals. Because of this, the weak signals next to the more intensive signals were not detected. In further studies modifications in the detection system should be made to detect a broader signal range. In the scattering measurements made first (Figure 4.37) the highest current was almost 16 V, which worked for a short period but this current was too high for long term measurements.

However, all IR transmission patterns possess the same patterns as in the green and red transmission photographs. The photodiodes did not detect the low scattering next to the spots of high intensities. For example, the IR transmission pattern of *Calathea zebrina* (0° angle of incidence) only possess a spot at the 0° detector position and a kind of ring structure around the spot, presented by four spots around the middle spot (Figure 4.41 A). The *Viola* IR transmission pattern possesses a clear oval ring pattern as was only suggested by the red and green pictures (Figure 4.32 J and Figure 4.33 J). But, the IR patterns show a lower distribution angle. As the *Viola* replicas scatter in an extreme way the detector can capture only the higher intensities and not the lower.

The intensity graduations of the more concentrated, respectively, less scattered transmission images of the *Calathea*, *Begonia* and *Fittonia* replicas range from 0.00 to 0.14. The intensity graduation of the high scattered images of the *Cosmos* and *Viola* replicas range from 0.00 to 0.04, which is much less intense. The IR images are suitable for the characterisation of the scattering of the light but not for the comparison of the total transmitted light. Future research has to work on an improved detector system, which is also able to detect the extremely low scattering for surfaces like the *Viola* replicas, even when the detector is at a greater distance from the replica.

Changing the angle of inclination results in a changing of the IR transmission patterns. The ring pattern of the *Begonia* replicas is gradually vanishing, i.e. the ring pattern gets lost. In a 40° angle of incidence only the lower part of the ring could be detected (Figure 4.41 F). The same procedure could be detected at the *Calathea* replicas, where the detected signal is clearly reduced (Figure 4.41 C). The intensity spot of the *Fittonia* replicas remains even at high angles of incidence (40°), but the size is slightly decreased (Figure 4.43 C). In contrast the ring pattern of the *Viola* transmission images with a 20° angle of incidence seem to be more complete than at 0° angles of incidence (Figure 4.42 D and E). It seems that the papillae support transmission at higher angles of incidence. Maybe not all of the papillae stand up right on the surface. Even when the ring pattern at 40° angles of incidence is slightly lost, the scattering is still high and the ring pattern could be still observed. Compared to the *Viola* pattern the *Cosmos* pattern here is much larger, i.e. the distribution angle seems bigger, but the former distribution angle measurements showed that *Cosmos* replicas had a lower distribution angle than *Viola* replicas. Indeed, the *Viola* distribution angle is higher. The intensity of the *Cosmos* pattern is higher as the scattering is lower (the detector is able to get a signal beyond the replicas). In contrast, the intensity of the *Viola* pattern is lower as the scattering is higher (at the peripheral regions of the patterns the detector is not able to detect a signal - the pattern appears to be smaller). Because of this it is important to work on an improved detector system. Regardless of this detector effect, the double structured replicas clearly cause a higher scattering of the transmitted beam even at high angles of incidence. Future research has to work on a setup to measure the angle dependent total transmittance and reflectance. Therefore one integrating sphere has to be positioned in front of the replicas and a second sphere has to be positioned beyond the replica. By varying the angle of inclination simultaneously the total transmittance and reflectance could be measured. The setup developed here is suitable to characterize the spatial distribution of the scattered light beam. Further improvements should be made in the vertical detector arm, which should be spherical to always have the same distance to the replica and an enlargement of the detection area in the

vertical direction. Up to now the detector could be moved only 15 mm down. The aim has to be the characterization of the complete sphere around the sample.

4.5 Conclusions

The surface architectures introduced here were evolved in a million-year process and are probably optimized for light-trapping processes. The combination of high, sharp micropapillae with a high aspect ratio and a fine nanofolding on top achieve extreme low reflection values (down to 0.6%). Micropapillae on top of these surfaces act as a king of diffraction grating, which determines the way of the light within the material. The biomimetic surface architectures introduced here guides the incoming light into the material at a high angle of incidence, i.e. the light is scattered into the material at a high distribution angle (up to 170°). Both aspects, low reflectance and high distribution angles, result in biomimetic light-trapping surfaces, which could be used for the opimization of high efficiency solar cells. For such surfaces an additional anti-reflective coatings (ARC), which are quite common on solar cells, are not required as the light-trapping properties are realized in a single material. This probably results in an easier and cost-efficient fabrication of high efficency solar cells.

5 Wetting of hierarchically structured petals and their replicas

Results presented in this Chapter are published in the Beilstein Journal of Nanotechnology: Schulte, A.; Droste, D.; Koch, K. and Barthlott, W. Hierarchically structured superhydrophobic flowers with low hysteresis of the wild pansy (*Viola tricolor*) – new design principles for biomimetic materials. Beilstein Journal of Nanotechnology, 2011, 2, 228-236. Further data are added and discussed.

5.1 Introduction

Plant surfaces provide a large diversity of hierarchical structures with various functions [Koch and Barthlott 2009; Bargel et al. 2006]. Different types of epidermal cells (micro-roughness) in combination with cuticular folds or epicuticular waxes (nano-roughness), or both, on top exist [Barthlott and Ehler 1977; Koch and Barthlott 2009]. Hierarchy in surface sculpture can cause water repellent and self-cleaning properties ('Lotus-Effect') [Barthlott and Neinhuis 1997; Koch and Barthlott 2009] or cause air retention under water ('Salvinia Effect') [Barthlott et al. 2010; Cerman et al. 2009]. Superhydrophobic, self-cleaning surfaces possess a static contact angle (CA) equal to or above 150°, and a low hysteresis angle, where water droplets roll-off at surface inclinations equal to or below 10° [Koch and Barthlott 2009; Roach et al. 2008]. One of the most important biological water repellent and self-cleaning surfaces is the lotus (*Nelumbo nucifera*) leaf [Barthlott and Neinhuis 1997; Neinhuis and Barthlott 1997]. Its water repellence is based on two factors: surface roughness and a hydrophobic surface chemistry. The micro-morphological characteristics of lotus leaves are papillose cells covered with a dense layer of small hydrophobic wax tubules. In plants, surface waxes occur as thin films (two-dimensional waxes) or as wax tubules, platelets, rodlets or other three-dimensional waxes [Koch et al. 2009; Barthlott and Wollenweber 1981]. In lotus leaves air remains trapped below a water droplet and the contact area between the water and the leaf surface is thereby minimized [Koch and Barthlott 2009]. This micro- and nanostructured surface, composed of low surface energy materials, leads to a high CA (163°) and a low hysteresis and tilt angle (2-3°). Additionally, lotus leaves show low adhesive properties to adhering particles. Thus contaminations by dust, pollen or even hydrophilic particles such as grime are carried away by water droplets, keeping the surface clean [Barthlott and Neinhuis 1997].

Two distinct models are proposed to explain the wetting behaviour of rough surfaces. In the Wenzel model [Wenzel 1936] roughness increases a solid surface area; this geometrically enhances its hydrophobicity. In the Cassie-Baxter model [Cassie and Baxter 1944] air remains trapped in the surface cavities below the droplets, which also leads to superhydrophobic behaviour, because the droplet is partially seated on air [Lafuma and Quéré 2003]. The Wenzel model describes homogeneous wetting by the following equation,

$$\cos\theta = r\cos\theta_0 \qquad (5.1)$$

where θ is the static contact angle for a rough surface and θ_0 is the static contact angle for a smooth surface. The surface roughness r is defined as the ratio of the actual over the apparent

surface area of the substrate. The Cassie-Baxter model describes heterogeneous wetting by the equation

$$\cos\theta = r\cos\theta_0 - f_{la}(r\cos\theta_0 + 1) \tag{5.2}$$

where f_{la} is the fraction of solid in contact with the liquid and is dimensionless.

Further important factors in surface wetting are the static contact angle hysteresis (CAH) and the tilt angle (TA). The CAH describes the difference between the advancing and receding CAs of a moving droplet, or one increasing and decreasing in volume. The CAH occurs due to surface roughness and heterogeneity [Israelachvili et al. 1994; Extrand 2002]. Low CAH results in a low TA, which describes the TA of a surface at which an applied water droplet starts to move [Extrand 2002].

Nowadays transitional states between the Wenzel and Cassie-Baxter states have been discovered. Wang and Jiang [2007] proposed five different states for superhydrophobic surfaces, where the lotus and gecko states are treated as special cases in the Cassie-Baxter model. Feng et al. [2008] proposed a sixth superhydrophobic state, called the 'Cassie impregnating wetting state' or 'petal effect'. Both describe superhydrophobic surfaces with high adhesive forces to water, and this means that the wetted surface area is smaller than in the Wenzel model but larger than in the Cassie-Baxter model. Feng et al. [2008] demonstrated this effect on rose flowers (petals). The surfaces of petals are often morphologically characterized by micro papillae with cuticular folds on top. In contrast to the lotus surface with air pocket formation between cell papilla, wax crystals and salient water droplets [Ensikat et al. 2009], the petal surface prevent air pocket formation and droplets penetrate into the cuticular folds by capillary forces. It is proposed that the sizes of both, micro- and nanostructures are larger than those found on the lotus leaves. Water droplets are expected to penetrate into the larger grooves of the petals, but not into the smaller ones and, thus, cause the Cassie impregnating wetting state [Feng et al. 2008].

The structure-based wetting characteristics of petals seem to offer a great alternative for the development of biomimetic superhydrophobic materials for micro droplet transport in micro fluidic systems, sensors or optical devices [Hong et al. 2007; Liu et al. 2010]. These hierarchically designed petal surfaces, with micropapillae and cuticular folds on the papillae top, can be reproduced precisely and are suitable for industrial production through large area foil imprinting processes. In contrast, the hierarchically organized structures of the lotus leaf are composed of micropapillae with randomly distributed tubules on top. The development of such surface architecture requires two production steps. First, the microstructures must be produced by moulding, lithography or in-print techniques. Second, the nanostructure production requires expensive lithographic techniques, or self-assembling materials, such as metal oxides [Roach et al. 2008; Bhushan and Her 2010].

Some attempts have been made to fabricate superhydrophobic surfaces with low hysteresis inspired by rose petals [Liu et al. 2010; Shi et al. 2005; Xi and Jiang 2008; Bormashenko et al. 2009; Bhushan and Her 2010]. Bhushan and Her [2010], for example, replicated dried and thereby collapsed, micropapillae, and examined the wetting behaviour of these structurally changed petals. Bormashenko et al. [2009] or Shi et al. [2005] fabricated 'petal-effect' surfaces by impregnating a polyethylene film with *Lycopodium* particles (spores) or through techniques such as electromechanical deposition of metal aggregates, which show the same wetting behaviour as rose petals, but with a different surface design than the native petals used as biological models. Xi and Jiang [2008] replicated native rose petals with a polydimetylsiloxane (PDMS), and fabricated surfaces that are topographically very similar to those of the original rose petals. However, their replicas possessed high adhesive forces to small (2 μl) water droplets, which cannot provide self-cleaning properties.

One simple and precise method to transfer petal surface structures into an artificial material is a soft lithography technique called replica moulding [Xia and Whitesides 1998]. Specifically, Koch

Figure 5.1: Macro photo of a water droplet on a flower of the wild pansy (*Viola tricolor*) [Schulte et al. 2011].

et al. [2008, 2007] introduced a cost-efficient, two-step replication technique for the replication of biological surfaces. This precise method prevents shrinking and damaging of the biological master during the replication process by avoiding a vacuum preparation step or critical temperatures, as are used in most other techniques and biological surface structures with an extremely high aspect ratio (ar) [Schulte et al. 2009].

In this study, we present the superhydrophobic surface of the wild pansy *Viola tricolor* (Figure 5.1), with a low TA and discuss the influence of papillae morphology and the dimensions of cuticular folding on the petal wetting state. To this end biomimetic replicas of four petals were generated, each differing in their surface morphology, and their wetting behaviour was examined by measuring the static CA and the TA. Finally, the contact area between a water droplet and the Viola petal surface was examined and superhydrophobic artificial petal replicas with low adhesive properties were generated.

5.2 Material and Methods

5.2.1 Plant material

The upper surface (adaxial) sides of the petals of four different plant species were investigated. Plants were cultivated in the Botanic Gardens of the Rheinische Friedrich-Wilhelms-University of Bonn (BGB). Their scientific names are given together with their registration numbers of the (BGB). Investigated species are the Chocolate Cosmos (*Cosmos atrosanguineus*; BGB 29614-8-2008), *Dahlia pinnata* (BGB 7960-9-1990), the China Rose (*Rosa chinensis*; BGB 3089-9-1979) and the Wild Pansy *Viola tricolor* (BGB 27262-4-2004).

5.2.2 Fabrication of the replicas

For the fabrication of the biomimetic polymer replicas the replication technique introduced by Koch et al. [2008] and modified in this thesis (see Chapter 2) was used. Here we briefly introduce the technique and mention the relevant modifications made. The replication technique is a two-step moulding process, in which a negative is generated first and then a positive. For generating the negative replicas, the master (biological sample) is moulded with polyvinylsiloxane dental wax (President light body Gel, ISO 4823, PLB; Coltene Whaldent, Hamburg, Germany). In the second step the negative replicas were filled with a two-component epoxy resin (RECKLI

Injektionsharz EP, RECKLI GmbH, Herne, Germany). After spilling the negative replicas, the epoxy resin had to dry for 48 h at 25° C. After hardening, the positive replicas were peeled off the negative replicas and further replicas were fabricated. In total, five petals of each species were replicated and examined afterwards.

5.2.3 Hydrophobisation of the replicas

The replicas were dip-coated (30 sec) in a fluorine polymer (Antispread, E2/50 FE 60, Dr. Tillwich GmBH Werner Stehr) and then dried for 20 min at room temperature. Antispread is a commercially available Fluorcarbon 60 for surface hydrophobization. It forms approximately 40 nm thin layers on the substrate (producer information) and causes no additional nano-structuring on the replica surfaces. A smooth surface, dip-coated with Antispread has a static contact angel of 106°.

5.2.4 Surface characterization

The surface structures of the biological samples and their replicas were investigated by scanning electron microscopy (SEM). Images were recorded using a CAMBRIDGE Stereoscan 200 SEM (Zeiss GmbH, Oberkochen, Germany), a digital image processing system (DISS 5, Version 5.4.17.0, Point electronic GmbH, Halle, Germany) was used to visualize and measure the surface structures of the petals. Fresh plant material was dehydrated with ethanol and dried in a critical point dryer (CPD 020, Balzers Union, Balzers- Pfeifer GmbH, Aßlar). On account of their stability, the replicas did not require special preparation. All samples were sputter-coated with an approximately 30 nm (at 60 mA for 30 sec), old layer (Balzers Union SCD 040, Balzers- Pfeifer GmbH, Aßlar) prior to SEM investigations. Further the surfaces were investigated using a digital optical microscope. Images were recorded using a VHX-1000 Digital Microscope (Keyence Deutschland GmbH, Neu-Isenburg, Germany). The petal could be examined without further preparations. Therefore the replicas were covered with an approximately 60 nm (at 60 mA for 60 sec) thick layer of gold.

5.2.5 Static contact angle and tilt angle measurements

The wettability of the biological samples and their replicas was characterized by CA and TA measurements using a computer-controlled goniometer OCA 30 (Dataphysics SCA 2.02, Filderstadt, Germany). Five microliters of demineralised water droplets were automatically applied to the samples via syringe and CAs were automatically determined using the Laplace-Young fitting algorithm. TAs were measured by tilting the samples (with an applied droplet on the surface) and measuring the TA at which the droplets rolled off the surface. Each measurement was repeated 10 times.

5.2.6 Cryo-SEM examinations

To display an applied droplet in contact with the petal surface, the Cryo-SEM method, developed by Ensikat et al. [2009], was used. In this method a sample-droplet (glycerol-water mixture of 1:3) complex was frozen with liquid nitrogen. A water-glycerol mixture was used as liquid to prevent crystallization patterns on the droplet surface, which occur on pure water droplets. After this the sample was separated from the droplet (5 μl) and the surface imprint of the droplet was examined under a scanning electron microscope. All examinations were performed using a CAMBRIDGE Stereoscan 200 SEM (Zeiss GmbH, Oberkochen, Germany), equipped with a digital image acquisition system (DISS 5, Point Electronic, Halle, Germany).

Table 5.1: Micropapillae characteristics of the petal polymer replicas: average values (av) and their standard deviation (σ) values are shown ($n = 30$).

	Micropapillae						
Replica	Height [µm]		Mid width [µm]		Apect ratio (ar)	Papillae peak to peak distance [µm]	
	av	σ	av	σ	av	av	σ
Cosmos	20,3	4,7	19,6	3,7	1,0	41,0	11,8
Dahlia	21,8	5,6	32,7	4,2	0,7	48,4	10,1
Rosa	13,8	3,2	16,5	3,0	0,8	31,1	8,9
Viola	40,2	13,1	18,9	3,9	2,1	24,9	3,8

5.3 Results

5.3.1 Micromorphological characteristics of the surfaces

Scanning electron microscope (SEM) investigations were made to characterize the micro- and nanostructures of the petals and their replicas. Petals of four different species were chosen, each differing in their cell shape and dimensions as well as in their wetting behaviour. Figure 5.2 illustrates the SEM micrographs of the petal surfaces and their uncoated and coated polymer replicas (in the following the uncoated replicas are marked with a subscript r (= replicas), the coated replicas with a cr (= coated replicas), the original petals are unmarked.

Petal surfaces of all four species are characterized by micropapillae with cuticular folding on top (Figure 5.2; 1a-4a). As the pictures show, the replicas possess the same surface structures as the original petals. Minor deviations between the papillae shape of the original petals and the replicas may arise from critical point preparation of the petals (Figure 5.2; 1a-4a). The replicas were made from fresh turgescent flowers and the replication material used can mould a master structure to a high precision. Because of this, one may assume that the replicas display the real shape of the fresh petal surface structures. SEM pictures also show that antispread coated replicas (Figure 5.2; 1c-4c) possess the same surface structures as the uncoated replicas (Figure 5.2; 1b-4b). Accordingly, the structure parameters were collected on the uncoated replicas. Differences between the petal structures could be found in the dimensions of papillae and folds. *Rosa$_r$* and *Viola$_r$* are characterized by relatively sharp micropapillae (Figure 5.2; 3b, 4b), while *Dahlia$_r$* and *Cosmos$_r$* possess micropapillae with rounded tops (Figure 5.2; 1b, 2b). Furthermore, the micropapillae of the four different species vary from about 14 µm (*Rosa$_r$*) to 40 µm (*Viola$_r$*) in height, from 17 µm (*Rosa$_r$*) to 33 µm (*Dahlia$_r$*) in their midwidth (papillae diameter at half the papillae height) and from 25 µm (*Viola$_r$*) to 48 µm (*Dahlia$_r$*) in their peak-to-peak distance (Table 5.1).

The average aspect ratio of the papillae shows similar values for the *Cosmos$_r$*, *Dahlia$_r$* and *Rosa$_r$* papillae (ar 1.0; 0.7; 0.8). In contrast, the average ar of the *Viola$_r$* papillae is much larger (ar 2.1). In this context it is to be noted that the standard deviation (σ) of *Viola$_r$* papillae height is also higher than the standard deviation of the other species. The micropapillae dimensions are shown schematically in Figure 5.3.

Differences between the four species were also found in the distribution and dimensions (width and distance) of the cuticular folds (Table 5.2).

While the micropapillae of *Dahlia$_r$* and *Viola$_r$* are completely covered with folds, the *Cosmos$_r$* and *Rosa$_r$* papillae only exhibit dense folding on top of the papillae and some single folds at the papillae side (Figure 5.4). Combinations of relatively thick folds separated by a small distance and thin folds separated by a large distance were found. The width of the folds varied from 260 nm (*Viola$_r$*) to 600 nm (*Cosmos$_r$*) and the distance between the single folds varied from 210 nm (*Dahlia$_r$*) to 460 nm (*Cosmos$_r$*).
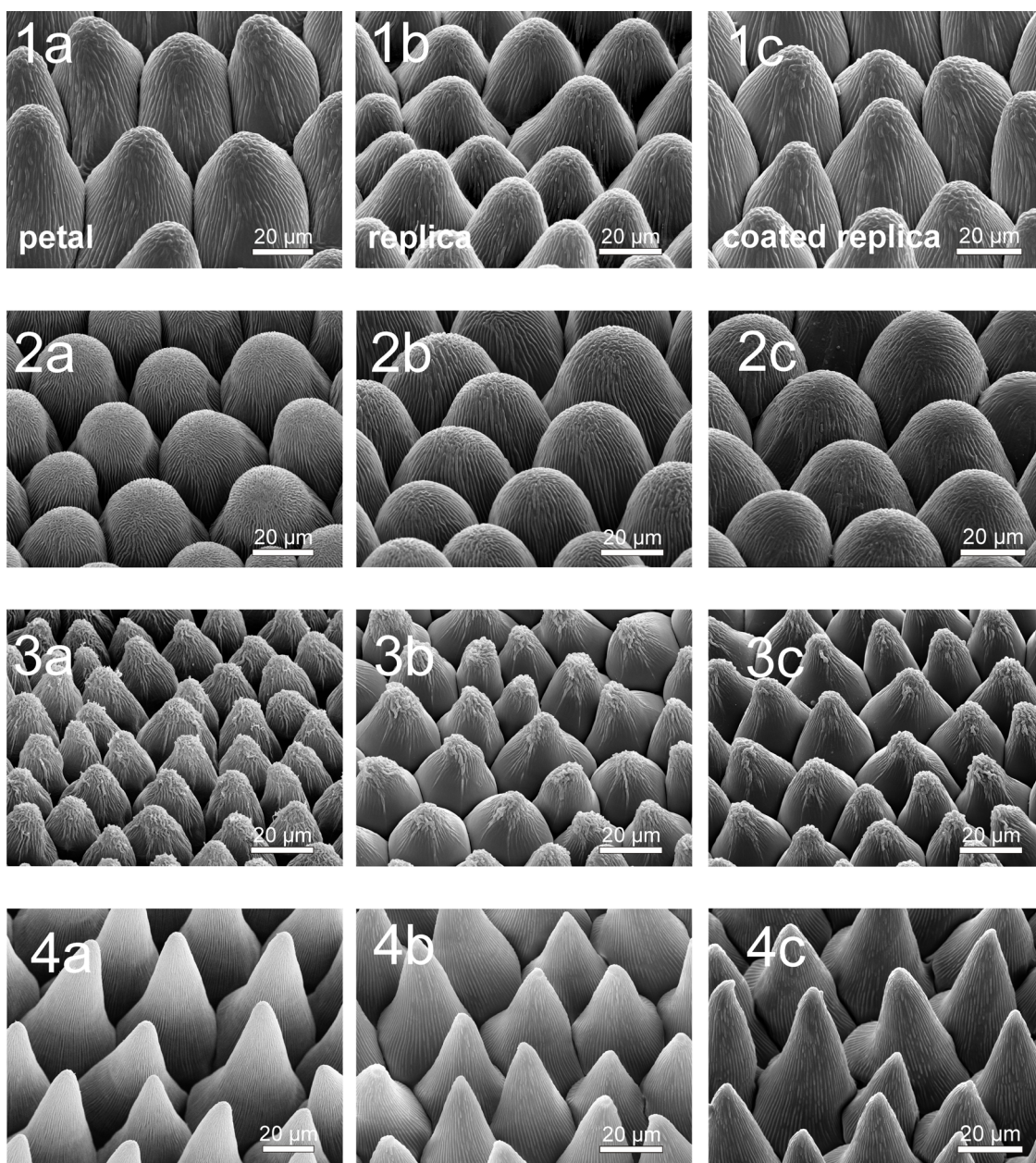
Figure 5.2: SEM micrographs of the petal surfaces (1a - 4a), the uncoated polymer replicas (1b - 4b) and the coated replicas (1c - 4c) of *Cosmos atrosanguineus* (1a - 1c), *Dahlia pinnata* (2a - 2c), *Rosa chinensis* (3a- 3c) and the wild pansy *Viola tricolor* (4a - 4c)[Schulte et al. 2011].

Table 5.2: Characteristics of cuticular folds found in the replicas of the petals: average values (av) and standard deviation (σ) values of the fold width and distance in μm ($n = 30$).

	Cuticular folds			
Replica	Width [µm]		Distance [µm]	
	av	σ	av	σ
Cosmos	0,60	0,09	0,46	0,10
Dahlia	0,39	0,08	0,21	0,06
Rosa	0,41	0,09	0,21	0,09
Viola	0,26	0,07	0,45	0,12
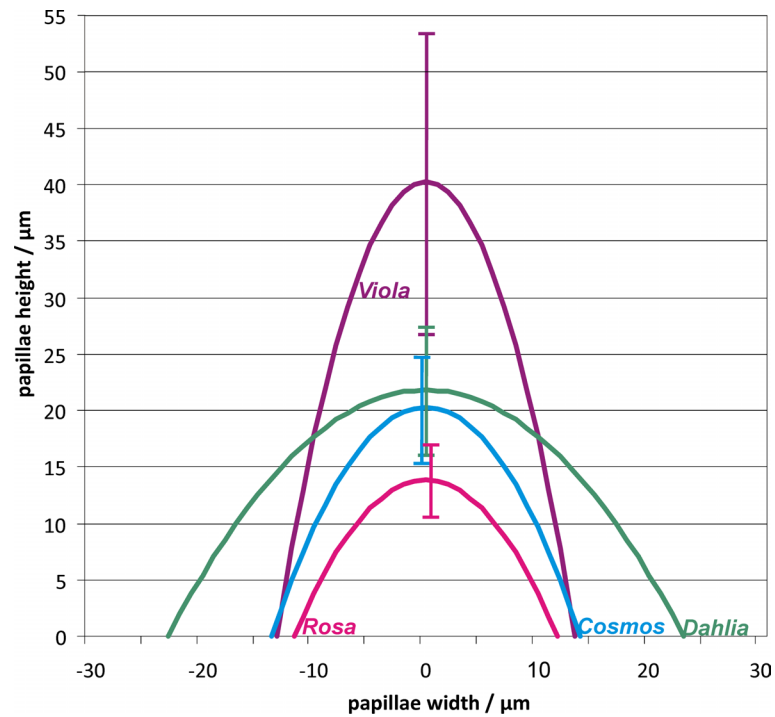
Figure 5.3: Diagram of the micropapillae dimensions of the average papilla shape on the upper surface of the *Cosmos$_r$*, *Dahlia$_r$*, *Rosa$_r$* and *Viola$_r$* petals. Also shown is the standard deviation of the papillae height (coloured bars) [Schulte et al. 2011].
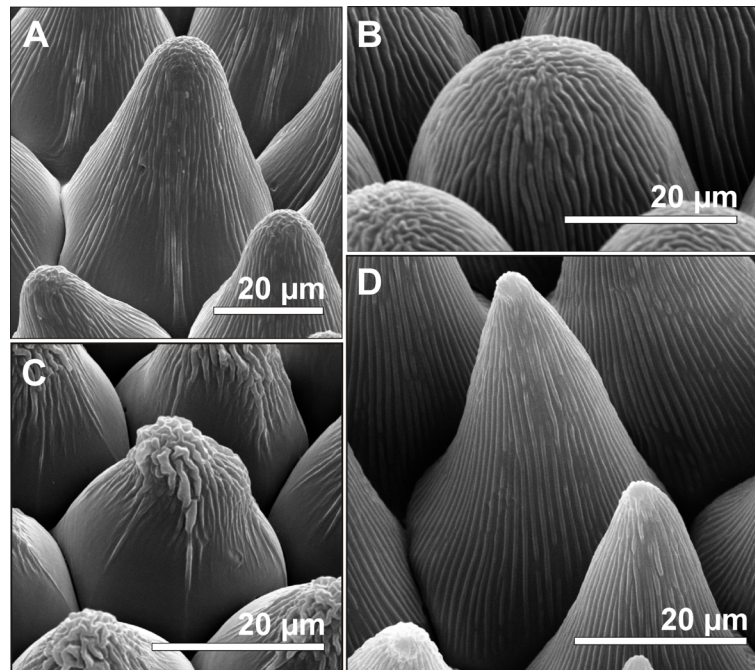
Figure 5.4: SEM micrographs of single epidermal cells and their cuticular folding on top: (a) *Cosmos*, (b) *Dahlia*, (c) *Rosa* and (d) *Viola* [Schulte et al. 2011].
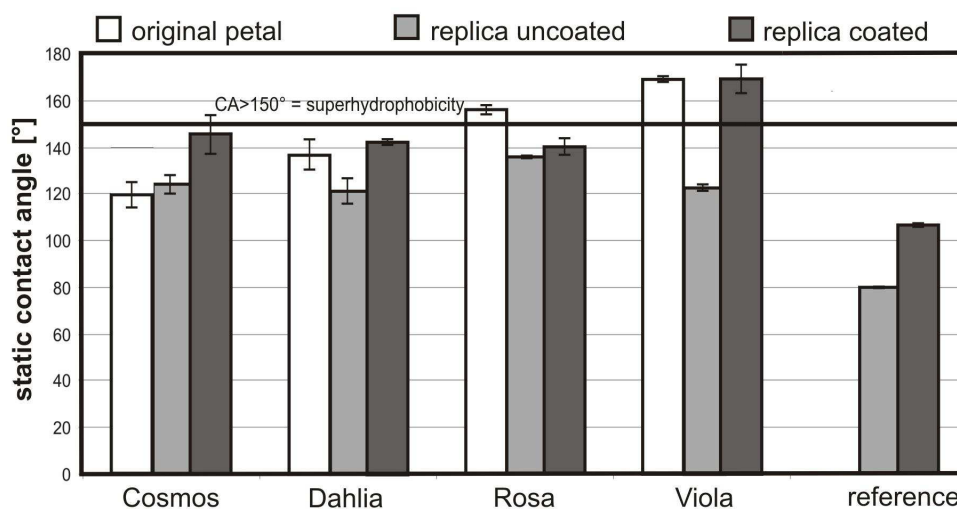
Figure 5.5: Static CAs of 5 μl water droplets on the surfaces of fresh petals, their uncoated and coated polymer replicas and the reference (uncoated and coated flat polymer) ($n = 10$) [Schulte et al. 2011].

5.3.2 Wettability of the petals and their replicas

Static CA and the TA measurements were performed to compare the wettability of different surface structures. Figure 5.5 displays the average static contac angles of the fresh petals, their uncoated and coated replicas. Two superhydrophobic petals (*Rosa* CA 155.6° and *Viola* CA 169°) and two hydrophobic petals (*Cosmos* CA 118.3° and *Dahlia* CA 136.4°) were found. Except for the case of *Cosmos$_r$* (123.8°) the polymer replicas possess lower CAs than their biological models (*Dahlia$_r$* 120.8°; *Rosa$_r$* 122.3°; *Viola$_r$* 135.6°). No uncoated polymer replicas possess superhydrophobic properties. After coating the replicas with the fluorine polymer the CAs increase clearly. By coating the hydrophilic flat uncoated reference (79.3°) the CA increases to 106.5° (increase of 34 %). The increase of the CA of the coated replicas depends on their surface structuring. Only the replicas of *Viola$_r$* reach the superhydrophobic region (168.9°) increase to the uncoated replica of about 25 %) while the others stay in the hadrophobic region (*Dahlia$_r$* 142.° (increase 18%); *Rosa$_r$* 140.0° (increase 15 %); *Cosmos$_r$* 145.2° (increase 17 %).

Figure 5.6 displays the average tilting angles of the fresh petals, their uncoated and coated replicas. Water droplets (5 μl) applied to the surface of *Cosmos*, *Dahlia* and *Rosa* stick to the surface even when it is tilted $\geq 90°$. Only water droplets applied to the *Viola* petal roll off the surface when it is tilted slightly (TA $\leq 5°$). The uncoated replicas possess al the same wetting behaviour: applied droplets stick to the surfaces even at high tilting angles ($\geq 90°$). After coating the replicas with the fluorine polymer the tilting angles changed for the coated *Rosa$_r$* (TA 44°) and *Viola$_r$* ($\leq 5°$) replicas. A remarkable standard deviation was found for the tilting angles of the *Rosa$_r$* replicas (TA $\pm 34.4°$).

5.3.3 Cryo-SEM investigations with *Viola* petals

Cryo-SEM investigations were performed to analyse a *Viola tricolor* petal in contact with a water droplet. Figure 5.7 shows a SEM picture of the micropapillae of a *Viola* petal in contact with a water-glycerol droplet. The picture shows, that some micropapillae are not in contact with the droplet, while others penetrate the droplet surface.
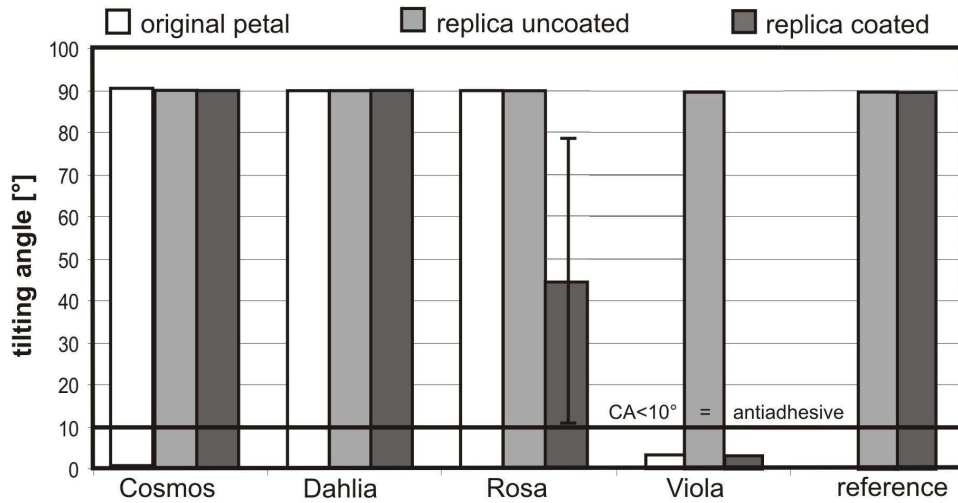
Figure 5.6: TAs of 5 μl water droplets on the surfaces of fresh *Cosmos*, *Dahlia*, *Rosa* and *Viola* flowers, their uncoated and coated polymer replicas and the TA of the reference (uncoated and coated flat polymer) ($n = 10$) [Schulte et al. 2011].
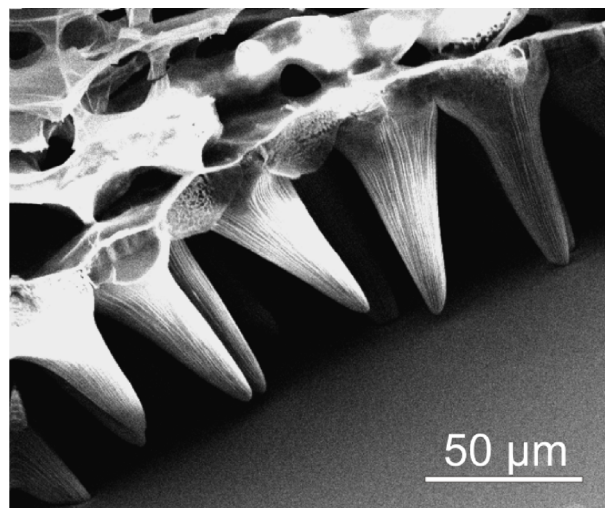
Figure 5.7: Cryo-SEM micrograph of the micropapillae of a *Viola* petal in contact with the surface of a water-glycerol droplet [Schulte et al. 2011].

5.4 Discussion

5.4.1 Micromorphological characteristics of the surfaces

The petal surfaces analysed here possess clear differences in their surface structuring. In contrast to previous studies [Feng et al. 2008; Xi and Jiang 2008; Bhushan and Her 2010], which concentrate on the surface of rose petals, the petal surfaces of different plant species where analysed and compared to each other. As some of the previous studies produced technical surfaces, which possess collapsed micropapillae, the influence of the real surface parameters on the wetting behaviour of a technical material could not be analysed [Bhushan and Her 2010]. As the SEM investigations show (Figure 5.2) the replication technique used here is able to produce exact copies of the biological models. Clear differences in the cell height, midwidth, aspect ratio and the papillae peak-to-peak distance could be found. There are many studies of the structure parameters of lotus-effect surfaces [Barthlott and Neinhuis 1997; Neinhuis and Barthlott 1997; Fürstner 2002; Koch and Barthlott 2009; Koch et al. 2010] but less is available on the structure parameters of petal surfaces combined with their wetting properties. Some studies reveal the surface parameters of petal surfaces in terms of their systematic relevance [Baagoe 1977] or their relevance for the optical properties of the petals [Whitney et al. 2011; Feng et al. 2010; Whitney et al. 2009a; Bernhard et al. 1968]. But the exact characterization of the surface architecture as compared to their wetting properties is still missed. As there are many studies on the surface parameters of *Lotus* leaves the results found here will be compared to the wetting properties and micromorphology of superhydrophobic, self-cleaning leaves of *Nelumbo nucifera* (see section 1.5.3 *Viola* petals as a model for superhydrophobic, water repellent surfaces).

In this thesis two different techniques were used for micropapillae characterization: the 3D light microscopy and SEM. The collected data for the height of the cells of *Cosmos* and *Rosa* were surprisingly much higher in SEM investigations than in 3D microscopy analyses. In comparision to the 3D microscope the replicated cells of *Cosmos* were about 20.3 ± 4.7 μm in height, while in the characterization with the freeze fracture technique in the SEM the cells of *Cosmos* are clearly higher, i.e. 58 ± 8 μm (Chapter 4). In comparable measurements made at *Viola* replicas these big differences did not occur. The heights of the *Viola* cells in the 3D microscopic measurements are about 40.2 ± 13.1 μm and in the freeze fracture measurements about 45.4 ± 10.2 μm. It has been found, that the 3D light microsope does not detect the interspaces between the closely packed micropapillae of e.g. *Cosmos* detected. The side view on the freeze fractures of the replicas reveal the actual height of the micropapillae. In the invetigation of the wetting properties of the replica surfaces the 3D microscopy technique was used for analyzing the micropapillae height and midwidth, i.e. the lower values. Especially at the hydrophobic surfaces it is assumed that the water does not penetrates into the interspaces, as they are to small.

5.4.2 Wettability of the petals and their replicas

The static CA of rose petals correlates well with the CA of roses previously measured by Feng et al. [2008] (CA 152.4°), Xi and Jiang [2008] (CA 154.3°) and Bhushan and Her [2010] (CA 155°). The CA of the *Cosmos* petal was only 118°, thus, the *Comos* surface was more hydrophilic than the other petal surfaces. Except for *Cosmos* all uncoated polymer replicas feature a lower CA than their biological model and thus did not show the same wetting behaviour. This suggests that the replica material is more hydrophobic than the cuticle of the *Cosmos* petal and more hydrophilic than the cuticles of the other species investigated. The uncoated reference polymer had a CA of 79.3°, which is by definition a hydrophilic surface [Roach et al. 2008]. These values are in line with the CA data collected in the examinations of the replication technique (Chapter 2), where the the injection resin Reckli had a CA of 77.1 ± 3.5°. With respect to the Wenzel equation (Equation 4.1) a CA decrease through structuring of the hydrophilic polymer was expected [Wenzel 1936]. In contrast to that, an increase of surface roughness has lead to an increase of the CA of the structured polymers. After covering the replicas with a hydrophobic fluorine polymer (CA of

the flat fluorine polymer: 106.5°), the CA values increased conspicuously (Figure 5.5). These results emphasize that a hydrophobic material in combination with surface roughness is the basis for the fabrication of superhydrophobic surfaces. While the CA values of the coated replicas of *Cosmos$_{cr}$*, *Dahlia$_{cr}$* and *Rosa$_{cr}$* were very similar (CA 145.2°; 141.9°; 140.0°), the CA of *Viola$_{cr}$* was much higher (CA 168.9°). A similar tendency was found for the tilting angles (TA) (Figure 5.6). The petals of *Cosmos*, *Dahlia* and *Rosa* possess high adhesion to water droplets (*Cosmos* and Dahlia TA > 90°; *Rosa*: TA 44°), thus, water droplets do not roll off the petals or the coated and uncoated replicas. These data correlate well with the reported 'petal effect'. [Feng et al. 2008] showed that *Rosa* petal surface structures impart special properties to the flowers, in that small water droplets (1-10 μl) adhere to the petals whilst larger droplets ($\geq$ 10 μl) roll-off. On *Viola* petals and their coated replicas, applied droplets rolled off at TAs of $\geq$ 5°, even when droplets with a volume smaller than 10 μl (here 5 μl) were used (Figure 5.6).

The TA of the coated *Rosa$_c$r* was very inhomogeneous. The average TA was 44° with high standard deviation ($\pm$34.4°). *Rosa* petals possess sharp micropapillae, the folds are relatively thick (410 nm $\pm$ 9 nm) and the micropapillae are only 13.8 μm $\pm$ 3.2 μm in height. With respect to wetting stages, air pocket formation on sufaces is important. In comparison of the microstructure of *Rosa* and *Viola*, larger air pocket formation was expected in *Viola*, based on the much higher micropapillae in *Viola* (40.2 μm in height). However, in roses sometimes air pocket formation might exist because some droplets rolled-off the surface at low inclination angels (TA 10°). These observations are in contrast to Feng et al. [2008]. Scanning electron microscopy studies also revealed large structural variations in petal microstructures. These surface microstructures cause optical signals [Whitney et al. 2009a; Zhang et al. 2008] or function as a tactile cue for bees [Kevan and Lane 1985]. For us the 'petal effect' or the repellence of petals seems to be a side effect and not the primary aim of the flower. A petal is a relatively short time living organ of flowers, developed for pollinator attraction, but the short duration of petal lifespan makes a self-cleaning property for pathogen defence expendable. The last point may explain why water repellence is not widespread in petals.

Several attemps were made in developing superhydrophobic (selfcleaning) solar cell surfaces. Cao et al. [2006] fabricated anti-reflective porous silicon surfaces with superhydrophobic properties, using different chemical etching techniques combined with and fluoroalkylsilane self-assembly. They reached average reflection values of about 3% over the spectral range of 300 to 800 nm and contact angles up to 161°. Even when they got good results in superhydrophpbicity the reflectance values are much higher than the values at the biomimetic surfaces developed here (down to 0.6%). Double structured surfaces were prepared, e.g. by Chang et al. [2007], who produced periodic subwavelength structures with an enhanced hydrophobic behavior by coating traditional inverted pyramid structures (Figure 1.8 B) with Teflon. At these surfaces they measured an average reflectance of 18% and contact angles of 135.9°. A superhydrophobic surface could not be prepared. Choi and Huh [2010] used conventional pyramid structures and laser grooved surfaces to fabricate double structured anti-reflective, superhydrophobic surfaces. Threrby, traditional produced expensive micro-pyramids were transferred into a perfluoropolyether (PFPE) by a complex three-step replication technique. These surfaces reflect more than 2% of the incidend light and possess contact angles of about 160° and a hysteresis about 2°. The coated biomimetic surface structures of *Viola* petals possess contact angels (CA 169°) higher than the traditional micropyramids(CA 160°), which results most likely in an improved self-cleaning of the surface.

5.4.3 *Viola* petals as a model for superhydrophobic surfaces

Viola petals do not possess the 'petal effect' and are anti-adhesive for water droplets. It is well known that hierarchical surface architecture represents optimized structures for superhydrophobic surfaces [Wenzel 1936; Callies and Quéré 2005; Sun et al. 2008; Nosonovsky and Bhushan 2007; Bhushan et al. 2009]. Based on the data presented here, we can describe two main superhydrophobic surface architectures for plant surfaces, the micropapillae with wax crystals [Koch and Barthlott 2009] and micropapillae with cuticle folds. Some remarkable differences exist between
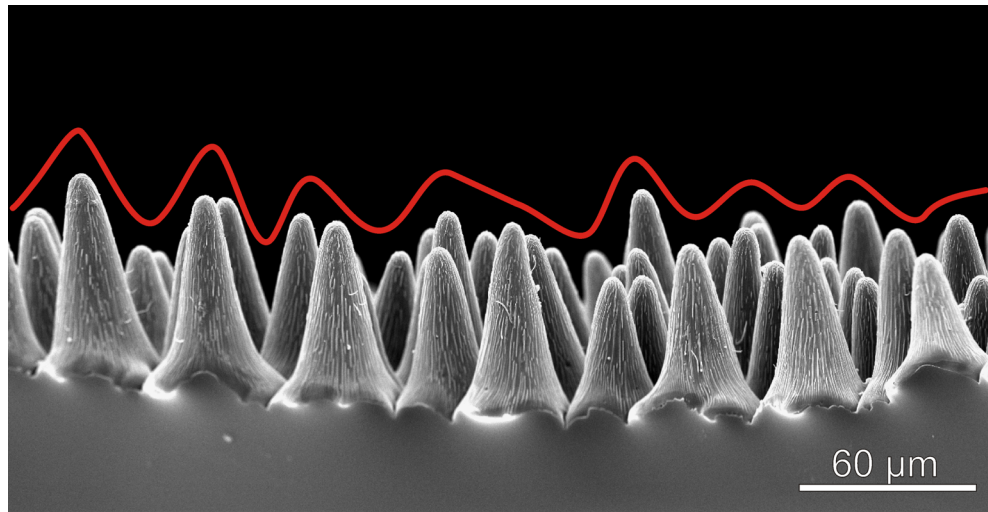
Figure 5.8: SEM micrograph of the side-face of the micropapillae of the upper surface of a *Viola* replica. Red lines indicate differences in micropapillae height.

the surface architecture of the *Lotus* leaf and *Viola* petals. In *Viola* petals microstructures are larger (average height of 40.2 μm) than in *Lotus* leaves, which have microstructures with an average height of 15 μm [Fürstner 2002]. The nanofolds in *Viola* have an average thickness of 0.26 μm, while the wax tubules of lotus are only 100 nm thick and 0.5-3 μm in length [Koch et al. 2007]. Thus the *Viola* petal does not possesses three dimensional wax crystals, but rather has a hydrophobic two dimensional wax film covering its micropapillae and nanofolds.

The distances between the structures also have an influence on the wetting stage. The average pitch value (peak-to-peak distances) of the *Lotus* micropapillae is 22.6 $\pm$ 1.9 μm [Fürstner 2002; Koch et al. 2009]. This is lower than the average pitch value of the *Rosa* micropapillae (31.1 $\pm$ 8.9 μm), but similar to the value of the *Viola* micropapillae (24.9 $\pm$ 3.8 μm). The dried rose petals investigated by Bhushan and Her [2010] showed microstructures with larger pitch values than found for the *Lotus* leaf. On such petals water droplets seem to partially penetrate into the petal microstructures leading to a 'Cassie impregnating wetting state'. The low TA found for *Viola* petals indicates a Cassie-Baxter wetting regime, in which water droplets do not penetrate into the grooves of the micropapillae. Furthermore, hysteresis can also be affected by the shape of the microstructures and adequate nano-sculpting on top. The combination of high (40.2 μm) and extremely peaked micropapillae with very fine folds (260 nm) on top apparently prevents water from penetrating into the structures by capillary force (Figure 5.4).

A high standard deviation in *Viola* micropapillae height (σ: $\pm$13.1 μm, $\approx$ 33 %, Table 5.1) demonstrates that large variations in cell heights do exist. SEM micrographs of the lateral view of several papillae support these results (Figure 5.8).

The percentage standard deviation of the micropapillae height of the other investigated species *Cosmos$_r$* (σ: $\pm$ 4.7 μm, $\approx$ 23 %), *Dahlia$_r$* (σ: $\pm$ 5.6 μm, $\approx$ 26 %) and *Rosa$_r$* (σ: $\pm$ 3.2 μm, $\approx$ 23 %)) is much smaller. The higher standard deviation of the micropapillae height is correlated to a large reduction of papilla contact to the applied water droplet. Cryo-SEM investigations (Figure 5.9) indicated that smaller micropapillae are not in contact with the applied liquid. Choi and Huh [2010] fabricated double structured optical surfaces, which also possess superhydrophobic properties (CA up to 160°) by coating them with SAMs (self assembled monolayers). They used regular structures (pyramids), which do not differ in height. Because of this droplets on top of the surfaces will get in contact with all micro-pyramids. It can be assumed, that the larger the contact area between the water droplet and a surface, the higher the adhesion of the droplet. The coated micropapillae introduced here cause static contact angles of up to 169°. The high standard deviation in the papillae height support extreme high contact angels by reducing the
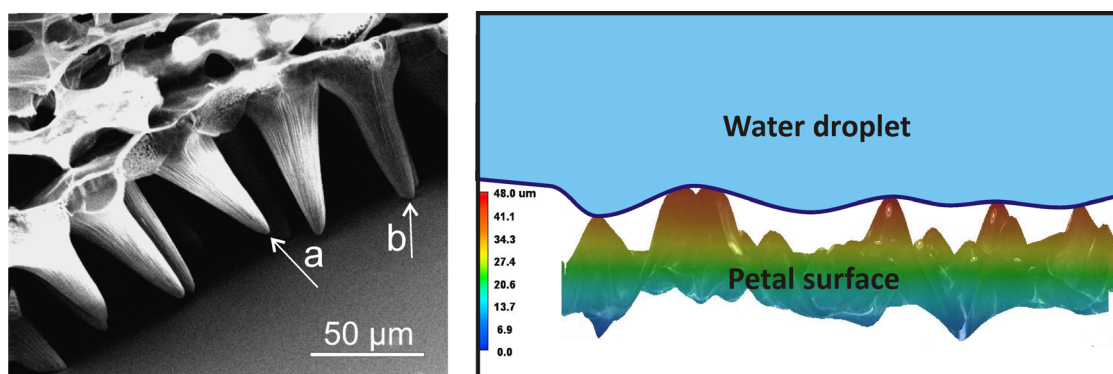
Figure 5.9: Cryo-SEM micrograph of the micropapillae of a *Viola* petal in contact with the surface of a water-glycerol droplet (A). Many micropapillae are not in contact with the droplet surface (a) while others are in contact with the droplet surface (b). Schematic of the proposed wetting state of a water droplet in a three dimensional light microscopy scan of the surface of a *Viola* petal, when a water droplet is in contact with the surface (B) [Schulte et al. 2011].

contact area between water droplet and surface. These irregularities in papillae height appear to be an advantage for the low hysteresis at these surfaces.

Thus, cell height variations further decrease the liquid-solid contact area and consequently decrease the adhesion of the liquid to the surface. Additionally, a sharp papillae tip benefits more from a lower contact area than a flat, rounded papilla tip. For the 'petal-effect' Feng et al. [2008] proposed that water droplets penetrate into the grooves between the micropapillae. *Viola* prevents water penetration into the micropapillae grooves by reducing the papillae peak-to-peak distance, which on average is 24.9 μm. Much larger peak-to-peak distances were found in $Rosa_r$ (31.1 μm), $Cosmos_r$ (41.0 μm) and $Dahlia_r$ (48.4 μm). The results presented here show that the combination of high micropapillae with high ar, sharp tips and small peak-to-peak distances is required for design of biomimetic superhydrophobic petal surfaces with low hysteresis.

The cuticular folds also have an influence on the wetting stage. On $Viola_r$ the micropapillae are completely covered with fine nano-folds (260 nm $\pm$ 70 nm), arranged at a separation of 450 $\pm$ 120 nm, whilst the micropapillae of the $Rose_r$ petals are only partially covered with broader folds (410 $\pm$ 90 nm), arranged at a separation of 210 $\pm$ 90 nm. Feng et al. [2008] note folds of 730 nm width on the micropapillae with an average diameter of 16 μm and a height of 7 μm (the differences probably result from the use of different species). Their rose petals possess a CA of 152.4° and a TA of $\geq$ 90°. By replicating the flowers, they developed a polymer film with a CA of 154.6° and a high adhesion to water droplets (TA $\geq$ 90°). Hydrophobic replicas of the *Viola* petals have a CA of 169° and a TA of $\leq$ 5°. These results show that finer folds arranged at short distances seem to prevent the penetration of water into the folds by capillary forces.

5.5 Conclusions

Flower petals provide a new design strategy for the development of superhydrophobic, light-trapping biomimetic materials. In contrast to superhydrophobic petals, where water droplets adhere, and which have been described before, a biological model (*Viola tricolor*) with a superhydrophobic, water repellent petal surface is found. Indeed, these flowers provide the typical surface architecture of petals (micropapillae with a folding on top), but a similar wetting behaviour as that described for lotus leaves. Through an easy and fast replication technique and subsequent hydrophobic coating, biomimetic replicas were fabricated. These replicas possessed the same surface structures and wettability as the biological models (Figure 5.10). The surface design of *Viola*, introduced here, seems to be easier and much more favourably to produce, e.g., by imprint
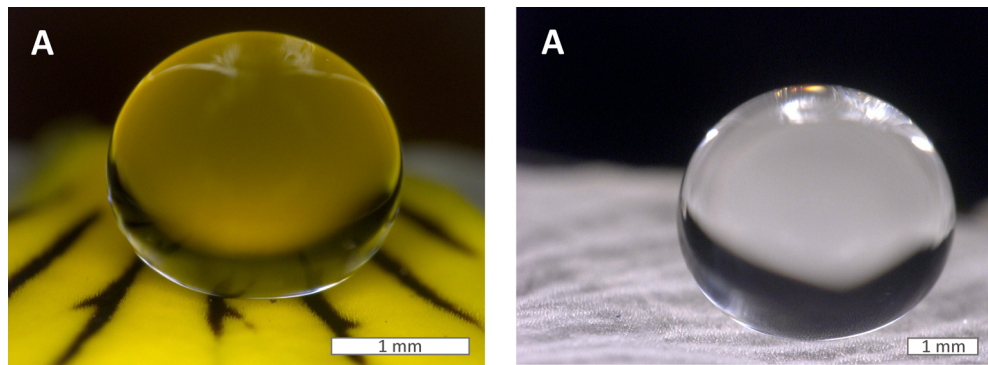
Figure 5.10: Macrographs of water droplets on hierarchically structured surfaces: Droplet on the flower of the wild pansy (*Viola tricolor*) (A) and its coated polymer replica (B) [Schulte et al. 2011].

processes, than hierarchically organized structures which could be found on the lotus leaf. In contrast to the lotus leaf with randomly distributed nanocrystals the surface structures of Viola could be qualified, for example, for large area foil imprinting processes. As these surfaces combine light-trapping and superhydrophobic properties a new surface design for the development of high efficiency, biomimetic solar cell surfaces is presented.

6 General Discussion

The utilisation of renewable energies plays a more and more important role in terms of climate change and scarce resources, e.g. oil, gas or uranium. Photovoltaics will have a central part to play in this. The AGENDA Photonik 2020, published by the German Federal Ministry of Education and Research (BMBF), proposes that around 20% of the current German demand be provided by solar energy by the year 2030. This will save about 500 million tons of carbon dioxide emissions. The European Photovoltaics Industry Association (EPIA) proposed that as much as 12% of the current European demand be provided by photovoltaics by 2020.

The preconditions for the sustainable development of this energy policy and the required growth of the solar power market are the further reduction of production costs by optimizing production techniques and the development of new technical strategies for high efficiency solar cells. New Materials with functionalized surfaces are in the focal spot of research and development and are described by the term 'Smart Photonic Components' (AGENDA Photonik 2020). In this the functionalization of surfaces is classified as one of the most important key technologies of the 21st century.

This study addresses the general question of whether plant surface structures could be used as models for the development of superhydrophobic and light trapping biomimetic surfaces for high efficiency solar cells. In this study plant surface structures were found that trap light by reducing the surface reflexion as well as by increasing the optical path length of light within the organ. Biomimetic replicas possessing these properties could be generated and used as light trapping surface prototypes for solar cells. Additionally, a biomimetic light-trapping surface with superhydrophobic, water repellent properties was generated.

Following AGENDA Photonic 2020 there is an urgent need for the optimization and development of alternative, favourable fabrication techniques, e.g. printing technologies or roll-to-roll processes. The introduced two step replication technique represents a favourable and simple technique for the fabrication of solid surface prototypes with optical effectiveness (**Chapter 3**). Building on the replication technique introduced by Koch et al. [2008], this thesis presents important modifications for the fabrication of transparent biomimetic replicas. The results show that the presented biological light-trapping structures might easily and favourably be transferred into a technical material. In contrast to former approaches [Lee et al. 2011; Bhushan and Her 2010; Feng et al. 2010], this gentle technique moulds the fragile biological surface structures in a precise way without damaging them. Soft plant surface structures can thus be prepared for optical analyses and technical implementations. Though there are already a number of works on the moulding of fragile flower surfaces [Whitney et al. 2009a], the replication performance of materials used there were not characterized. It is hardly possible to predict the precision of the structuring of replicas. Furthermore, only low-aspect ratio structures were replicated. The moulding performance of high aspect ratio structures has yet to be proved. Choi and Huh [2010] introduced a three step moulding technique for the fabrication of biomimetic, antireflective, double structured surfaces. In this commercially fabricated, stable micro-pyramids were moulded and, by the addition of nanoparticles in the second step, nanostructured surfaces were generated. In contrast to the micropapillae with nanofolding on top introduced here, Choi and Huh [2010] surfaces possess known micro pyramids with a nanoporous surface. Their replication technique proved more complex than the technique presented here as they need additional nanoparticles and three replication steps. Here the nanofolds are directly generated in the first mould. Improved stability of the nanofolds is likely. The application of the biomimetic structures introduced here onto a solar cell will be the subject of future research.

Further, AGENDA Photonik 2020 reports on the need of new surface structures for solar cells as well as improvement in the light utilization and light scattering of solar cells, e.g. nanostructures. The surface architecture introduced here, evolved in a million year process and is probably optimized for light-trapping processes (**Chapter 4**). The combination of high, sharp micropapillae with a high aspect ratio and fine nanofolding on top achieves extremely low reflexion values (down to 0.6%). An additional anti-reflective coating (ARC), quite common on solar cells, is not required. The biomimetic surface architecture proposed here guides the incoming light into the material at a flat angle, i.e. the light is scattered into the material in a high distribution angle (up to 170°). These high distribution angles are an important precondition for the light- trapping properties of solar cell materials [Hecht 2001]. Of course, the scientific search for optimized surface structures for solar cell application is already underway. Microstructures were already theoretically calculated [Ko and Yu 2011; Campbell and Green 1987] as well as experimentally fabricated [Ko and Yu 2011; Choi and Huh 2010; Chang et al. 2007; Green et al. 1992; Wenham and Green 1986]. Favoured structures are pyramids, inverse pyramids and grooved structures, which are often inroduced to the silicon (Si) wafer by expensive and extensive etching and laser structuring techniques [Chang et al. 2007]. Nanostructures are also fabricated directly on the Si-wafer[Koynov et al. 2006; Cao et al. 2006] as well as on the glass substrate [Yamada et al. 2011]. The surface architecture proposed here is a combination of micropapillae and nanostructuring on top, which combines anti-reflective and light-trapping properties. Even when Choi and Huh [2010] combine micro-pyramids with nanostructuring, the reflexion values of their surfaces are higher ($\geq$ 2%) than the values of the surfaces presented here (down to 0.6%). By replicating nanoparticles introduced into the replication material Choi and Huh [2010] generated a kind of nanoporous structure on top of the micropapillae. These nanostructures differ clearly from the nanofolding introduced here, which additionally increases the distribution of light within the mateiral (improvement of the light-trapping properties). Future research has to examine the further influence of nanofolding on the light-trapping properties of different materials.

As mentioned before, the functionalization of surfaces is considered the most important key technology of the 21$^{\text{st}}$ century. The combination of several functionalities in one material or surface promises resource and energy saving systems. With the aid of a favourable replication technique biomimetic and light trapping surfaces were generated. By coating these biomimetic replicas with a hydrophobic layer, superhydrophobic surfaces were additionally fabricated (**Chapter 5**). Static contact angles of up to 169° were detected. Best results were found in surfaces possessing, (I) high aspect ratio micropapillae ($\geq$ 2), (II) small papillae tip radii ($\approx 2\mu$m) as well as (III) fine nanofolding on top of the papillae. Especially the micropapillae of *Viola* petals possess a high standard deviation in the papillae height. Examinations of cryo droplets on the petal surface show that the droplets only lie on top of the highest papillae, while the smaller ones did not come into contact. This effect was also observed in lotus leaves [Barthlott and Neinhuis 1997; Neinhuis and Barthlott 1997]. The coated micropapillae introduced here cause static contact angles of up to 169°. The high standard deviation in the papillae height seems to support extremely high contact angles by reducing the contact area between the water droplet and the surface. These irregularities in papillae height seem to be an advantage for the wetting properties of surfaces, as they result in a extreme low hysteresis and by this self-cleaning surfaces could be generated. As dust can significantly deteriorate the performance of photovoltaic cells the development of self-cleaning properties of solar cell surfaces is of great economic interest [El-Shobokshy and Hussein 1993]. The biomimetic structures introduced here combine light-trapping with superhydrophobic properties in a single surface and promise a resouce and energy saving system.

The results presented give important suggestions for the fabrication of 'new' functional technical surfaces following the example of 'old' functional biological surfaces. Especially in the fabrication of high efficiency solar cells these biological surfaces are an important source of inspiration in developing new materials for 'Smart Photonic Component'.

7 Summary

Schulte, Anna Julia (2012). Light-trapping and superhydrophobic Plant Surfaces – Optimized Multifunctional Biomimetic Surfaces for Solar Cells. Doctoral thesis, Mathematisch-Naturwissenschaftliche Fakultät, Rheinische Friedrich - Wilhelms-Universität Bonn.

This study analyses the optical and wetting properties of structured leaf and flower surfaces as well as their replicas. The aim of this work is the development of new light trapping biomimetic surface architectures for the optimization of high efficiency solar cells with superhydrophobic (self-cleaning) properties.

For the development of light-trapping biomimetic surfaces the leaves of 5 low-light plants as well as 4 colour intensive petals were chosen. All plant surfaces are characterized by micropapillated epidermal cells (single structured). Three petals additionally possess a cuticular folding on top of the micropapillae (hierarchical structured).

By separating the plant surface structures from the biological template, the optical properties of the structuring could be analysed. For this purpose biomimetic replicas were generated using a modified replication technique. By developing a vacuum chamber for the application of the moulding material, artifacts caused by air inclusions in the replication process could be avoided. A new transparent replication resin was found, which replicates to the high precision of a few nanometres. The low viscosity material positively affects the replication of petals as it flows more easily between the hierarchically structured petal micro-architecture. High precision plant surface replicas were generated.

The reflexion of light in the surfaces of biomimetic polymer replicas of low-light plant leaves (e.g. *Calathea zebrina*) as well as of colour intensive petals (e.g. *Viola tricolor*, *Cosmos atrosanguineus*) is more than 80% lower as compared to a smooth polymer surface. In contrast to the surface reflection of a smooth reference surface (5%), single structured surfaces (*Calathea zebrina* reflect about 1% and double structured surfaces (e.g. *Viola tricolor*, *Rosa*) reflected only about 0.6% of the incident light. Thus, these surfaces reflect less light than commonly used types of textured solar cell surfaces with an anti-reflective coating (reflexion about 3%). At the biomimetic surfaces the light is trapped between the micropapillae through multiple reflexions, which increase the amount of light transmitted. Even under high angles of inclinations the reflexion is reduced and optical losses could be reduced.

Angle dependent transmittance measurements reveal the light-trapping potential of plant surface structures *via* path lengthening of the light within the leaves and petals. It was found that high aspect ratio micropapillae ($ar \geq 2.0$) with small papillae angles (26°) allow entrance angles of the transmitted light into the material of up to 170°. The extreme low angels of light entrance cause the path lengthening of the incoming light within the replicas. This fact is an important condition for the optical optimization of solar cell surfaces.

The combination of light trapping and superhydrophobic properties in a single surface structure is of great interest for the development of new multifunctional surfaces, especially in high efficiency solar cells. The replicas of *Viola tricolor* petals (coated with a hydrophobic layer) possess these multifunctional properties. Their surfaces are characterized by high aspect ratio micropapillae ($ar \geq 2.0$) combined with dense cuticular folding (folding width 260 nm, distance 450 nm) on top. Additionally, features such as extremely small papillae tips (radii about 2.1μm) and small papillae angles (26°) result in a light-trapping and superhydrophobic surface. Thus, replicas

were generated, which provide ideal surface designs for the optimization of new biomimetic light-trapping and superhydrophobic (self-cleaning) solar cell surfaces.

8 Zusammenfassung

**Schulte, Anna Julia (2012). Light-trapping and Superhydrophobic Plant Surfaces –
Optimized Multifunctional Biomimetic Surfaces for Solar Cells. Dissertation, Mathe-
matisch-Naturwissenschaftliche Fakultät, Rheinische Friedrich - Wilhelms-Universität
Bonn.**

In dieser Studie wurden die optischen Eigenschaften sowie die Benetzungseigenschaften pflanz-
licher Oberflächen und deren Repliken untersucht. Diese funktionalen Oberflächen wurden als
potentielle Vorbilder für die Optimierung von hoch effizienten Solarzellen untersucht. Ziel die-
ser Arbeit war es, die strukturbedingten optischen Eigenschaften pflanzlicher Oberflächen ("light-
trapping") wie auch ihre Benetzungseigenschaften (Superhydrophobie) in ein technisches Substrat
zu übertragen.

Dazu wurden zunächst die Blätter von fünf Schwachlichtpflanzen und vier farbintensiven Blüten
als biologische Vorbilder ausgewählt. Alle neun ausgewählten Pflanzenoberflächen wiesen konvex
geformte bis papillöse Mikrostrukturen (Einfachstrukturierung) auf. Drei der neun Oberflächen
wiesen zusätzlich eine übergelagerte Nanofaltung auf (Doppelstrukturierung).

Im nächsten Schritt wurde mit Hilfe der Replikation die Oberflächenstrukturierung der biologi-
schen Vorbilder abgeformt und somit in ein technisches Substrat übertragen - biomimetische Ober-
flächenrepliken resultieren. Im Rahmen dieser Arbeit wurde die von Koch et al. [2008] vorgestellte
Replikationsmethode modifiziert um optisch transparente, artefaktfreie Repliken herzustellen. Da-
bei wurde ein neues, transparentes Replikationsharz herausgestellt, das mit hoher Präzision bis in
den Nanometerbereich abformt. Durch seine Fließeigenschaften eignete es sich hervorragend zur
Herstellung präziser Abformungen. Mit Hilfe einer zusätzlich entwickelten Vakuumkammer kann
nun die Applikation der Abformungsmaterialen im Vakuum erfolgen: Replikationsartefakte, he-
vorgerufen durch Lufteinschlüsse, werden vermieden. Präzise biomimetische Repliken für optische
Analysen wurden hergestellt.

Anschließend wurden die Reflexionseigenschaften dieser biomimetischen Repliken untersucht. Wäh-
rend glatte Referenz-Polymeroberflächen bis zu 5% des einfallenden Lichts reflektierten, wurden
an den besten strukturierten Repliken (*Viola tricolor*) lediglich 0,6% reflektiert, d.h. eine Re-
duktion der Oberflächenreflexion um mehr als 80% konnte erreicht werden. Einfachstrukturierte
Repliken zeigten ebenfalls hervorragende Reflexionswerte von nur 1%. Damit reflektieren diese
biomimetischen Oberflächen weniger Licht, als die derzeit üblicherweise eingesetzten, texturierten
und beschichteten Solarzellen (Reflexion um 3%). Dies bedeutet, dass biomimetische Oberflächen-
strukturen das eingestrahlte Licht besonders effizient einfangen; selbst unter schrägem Lichtein-
fall.

Winkelabhängige Transmissionsmessungen zeigten zusätzlich das große Potential dieser Oberflä-
chen, Licht innerhalb der Repliken einzufangen (light-trapping). Es konnte gezeigt werden, dass
gerade papillöse Strukturen mit hohen Aspektverhältnissen ($ar \geq 2.0$) und geringen Papillenwin-
keln (26°), das Licht extrem breit in das Material streuen und somit verteilen. Beste Ergebnisse
zeigten auch hier die Strukturen von *Viola tricolor* mit Streuwinkeln von bis zu 170°. Durch diese
hohen Streuwinkel verlängert sich der Weg des Lichts im Material und eine Absorption des Lichts
wird wahrscheinlicher. Diese Eigenschaft ist eine sehr wichtige Voraussetzung für die Optimierung
von hoch effizienten Solarzellen.

Die Kombination dieser Licht einfangenden mit wasserabweisenden Eigenschaften war Ziel des
letzten Kapitels dieser Arbeit und ist besonders für die Enwicklung multifunktionaler Solarzellen
von Bedeutung. Hydrophobierte Repliken von *Viola tricolor* Blüten wiesen beide gewünschten

Eigenschaften auf. Es zeigte sich, dass Mikrostrukturen mit hohen Aspektverhältnissen ($ar \geq 2.0$), geringen Papillenwinkeln (26°), extrem kleinen Papillenspitzen (Radii um 2.1 μm) und einer aufliegenden dichten Nanofaltung (Faltenbreite 260 nm, -abstand 450 nm) in einer lichtfangenden und wasserabweisenden technischen Oberfläche resultieren. Diese Oberflächen eignen sich damit als Prototypen zur Optimierung von hoch effizienten, selbstreinigenden Solarzellen.

Erklärung

Hiermit versichere ich, dass ich die vorliegende Dissertation selbständig angefertigt und die benutzten Quellen vollständig angegeben habe. Sie wurde an keiner anderen Hochschule als Dissertation eingereicht und wurde auch nicht an einer anderen Stelle veröffentlicht. Für die Erstellung der vorgelegten Arbeit wurde keine Hilfe von Vermittlungs- bzw. Beratungsdiensten in Anspruch genommen.

Bonn,   Mai 2012

Anna Julia Schulte

List of Figures

List of Tables

Bibliography

Baagoe, J. (1977). Microcharacters in the ligules of the Compositae. In Heywood, V. H., Harborne, J. B., and Turner, B. L., editors, *The biology and chemistry of the Compositae*, volume 1, pages 119–139.

Bargel, H., Koch, K., Cerman, Z., and Neinhuis, C. (2006). Evans Review No. 3: Structure-function relationships of the plant cuticle and cuticular waxes - a smart material? *Functional Plant Biology*, 33:893–910.

Barthlott, W. (1991). Raster-Elektronenmikroskopie pflanzlicher Oberflächen: Ökologische und stammesgeschichtliche Aspekte der Mikrostrukturen. *Rheinische Friedrich-Wilhelms-Universität Bonn (Hrsg.) Forschungsbericht 1987-1989, S. 126-137*, pages 126–137.

Barthlott, W. and Ehler, N. (1977). Raster-Elektronenmikroskopie der Epidermis-Oberflächen von Spermatophyten. In Mainz, A. d. W. u. d. L., editor, *Tropische und Subtropische Pflanzenwelt*, volume 19, pages 367–467. Steiner, Wiesbaden.

Barthlott, W. and Neinhuis, C. (1997). Purity of the sacred lotus, or escape from contamination in biological surfaces. *Planta*, 202:1–8.

Barthlott, W., Schimmel, T., Wiersch, S., Koch, K., Brede, M., Barczewski, M., Walheim, S., Weis, A., Kaltenmaier, A., Lederer, A., and Bohn, H. (2010). The Salvinia Paradox: super-hydrophobic surfaces with hydrophilic pins for air retention under water. *Advanced Materials*, 22:1–4.

Barthlott, W. and Wollenweber, E. (1981). Zur Feinstruktur, Chemie und taxonomischen Signifikanz epicuticularer Wachse und ähnlicher Sekrete. *Tropische und subtropische Pflanzenwelt*, 32:7–67.

Bay, M. (2010). *Konstruktuion und Entwicklung eines Messaufbaus zur Bestimmung der optischen Eigenschaften von Zahnhart- und Weichgewebe bei Anwendung eines Nd:YVO4 Lasers*. PhD thesis, Zentrum für Zahn-, Mund- und Kieferheilkunde der Rheinischen Friedrich-Wilhelms-Universität Bonn.

Bernhard, C., Gemne, G., and MØller, A. (1968). Modification of specular reflexion and light transmission by biological surface structures. *Quarterly Reviews of Biophysics*, 1:89–105.

Bhushan, B. and Her, E. (2010). Fabrication of superhydrophobic surfaces with high and low adhesion inspired from rose petals. *Langmuir*, 26(11):8207–8217.

Bhushan, B., Jung, Y. C., and Koch, K. (2009). Micro-, nano- and hierarchical structures for superhydrophobicity, self-cleaning and low adhesion. *Philosophical Transactions of the Royal Society A: Mathematical, Physical and Engineering Sciences*, 367(1894):1631–1672.

Bone, R., Lee, D., and J.M., N. (1985). Epidermal cells functioning as lenses in leaves of tropical rain-forest shade plants. *Applied Optics*, 24(10):1408–1412.

Bormashenko, E., Stein, T., Pogreb, R., and Aurbach, D. (2009). ´Petal Effect´ on surfaces based on lycopodium: high-stick surfaces demonstrating high apparent contact angles. *The Journal of Physical Chemistry C*, 113:5568–5572.

Brodersen, C. and Vogelmann, T. (2007). Do epidermal lens cells facilitate the absorptance of diffuse light? *American Journal of Botany*, 94(7):1061–1066.

Callies, M. and Quéré, D. (2005). On water repellency. *Soft Matter*, 1:55–61.

Campbell, P. and Green, M. (1987). Light trapping properties of pyramidally textured surfaces. *Journal of Applied Physics*, 62(1):243–249.

Cao, M., Song, X., Zhai, J., Wang, J., and Wang, Y. (2006). Fabrication of highly antireflective silicon surfaces with superhydrophobicity. *J. Phys.Chem. B*, 110:13072–13075.

Cassie, A. and Baxter, S. (1944). Wettability of porous surfaces. *Transactions of the Faraday Society*, 40:546–551.

Cerman, Z., Striffler, B. F., and Barthlott, W. (2009). Dry in the water: the superhydrophobic water fern Salvinia - a model for biomimetic surfaces. In Gorb, S. N., editor, *Functional Surfaces in Biology: little structures*, volume 1. Springer, Berlin, Heidelberg.

Chang, Y., Mei, G., Chang, T., Wang, T., Lin, T., and Lee, C. (2007). Design and fabrication of a nanostructured surface combining antireflective and enhanced-hydrophobic effects. *Nanotechnology*, 18:6.

Chattopadhyay, S., Chen, L.-C., and Chen, K.-H. (2006). Nanotips: growth, model, and application. *Critical Reviews in Solid State and Material Science*, 31:15–53.

Chazdon, R. and Pearcy, R. (1991). The importance of sunflecks for forest understory plants. *BioScience*, 41(11):760–766.

Chen, Q., Hubbard, G., Shields, P., Liu, C., Allsopp, D., Wang, W., and Abbott, S. (2009). Broadband moth-eye antireflection coatings fabricated by low-cost nanoimprinting. *Applied Physics Letters*, 94(26):3pp.

Choi, S.-J. and Huh, S.-Y. (2010). Direct structuring of a biomimetic anti-reflective,self-cleaning surface of light harvesting in organic solar cells. *Macromolecular Rapid Communications*, 31(6):539–544.

Choi, S.-J., Suh, K., and Lee, H. (2008a). Direct UV-replica molding of biomimetic hierarchical structure for selective wetting. *Journal of the American Chemical Society*, 130:6312–6313.

Choi, S.-J., Suh, K., and Lee, H. (2008b). A geometry controllable approach for the fabrication of biomimetic hierarchical structure and its superhydrophobicity with near-zero sliding angle. *Nanotechnology*, doi:10.1088/0957-4484/19/27/275305:5.

Choi, S.-J., Yoo, P., Beaek, S., Kim, T., and Lee, H. (2004). An ultraviolet-curable mold for surb-100-nm lithography. *Journal of the A*, 126:7744–7745.

Christensen, K. and Hansen, H. (1998). SEM-studies of epidermal patterns of petals in the angiosperms. *Opera botanica*, 135:91.

Clapham, P. and Hutley, M. (1973). Reduction of lens reflexion by the "moth eye" principle. *Nature*, 244:281–282.

Comba, L., Corbet, S., Hunt, H., Outram, S., Parker, J., and Glover, B. (2000). The role of genes influencing the corolla in pollination of Antirrhinum majus. *Plant, Cell and Environment*, 23(6):639–647.

Combes, D., Bousquet, L., Jacquemoud, S., Sinoquet, H., Varlet-Grancher, C., and Moya, I. (2007). A new spectrogoniophotometer to measure leaf spectral and directional optical properties. *Remote Sensing of Environment*, 109:107–117.

Crisp, D. and Thorpe, W. (1950). A simple replica technique suitable for the study of surface structure. *Nature*, 4190:273.

Deniz, H., Khudiyev, T., Buyukserin, F., and Bayindir, M. (2011). Room temperature large-area nanoimprinting for broadband biomimetic antireflection surfaces. *Applied Physics Letters*, 99:3pp.

Ehler, N. (1975). *Beitrag zur Kenntnis der Mikromorphologie der Coroll-Epidermen von Stapelien und ihre taxonomische Verwertbarkeit*. Trop. u.subtrop. Pflanzenwelt. Akad.Wiss.u.Lit., Mainz.

El-Shobokshy, M. S. and Hussein, F. (1993). Effect on dust with different physical properties on the performance of photovoltaic cells. *Solar Energy*, 51:505–511.

Endler, J. (1993). Teh color of light in forests and its implications. *Ecological Monographs*, 63:27.

Ensikat, H. J., Schulte, A. J., Koch, K., and Barthlott, W. (2009). Droplets on Superhydrophobic Surfaces: Visualization of the Contact Area by Cryo-Scanning Electron Microscopy. *Langmuir*, 25(22):13077–13083. doi: 10.1021/la9017536.

Exner, F. and Exner, S. (1910). Die physikalischen Grundlagen der Blütenfärbungen. *Sitzungsber. Kais. Akad. Wiss. Wien, Math.-nat. Kl. I*, 119:191–245.

Extrand, C. (2002). Model for contact angles and hysteresis on rough and ultraphobic surfaces. *Langmuir*, 18:7991–7999.

Faustini, M., Nicole, L., Boissiére, C., Innocenzi, P., Sanchez, C., and Grosso, D. (2010). Hydrophobic, antireflective, self-cleaning, and antifoging sol-gel coatings: an eample of multifunctional nanostructured materials for photovoltaic cells. *Chemistry of Materials*, 22:4406–4413.

Feng, L., Zhang, Y., Li, M., Zheng, Y., Shen, W., and Jiang, L. (2010). The structural color of red rose petals and their duplicas. *Langmuir*, 26(18).

Feng, L., Zhang, Y., Xi, J., Zhu, Y., Wang, N., Xia, F., and Jiang, L. (2008). Petal effect: a superhydrophobic state with high adhesive force. *Langmuir*, 24:4114–4119.

Fürstner, R. (2002). *Untersuchungen zum Einfluss von Struktur und Chemie auf die Benetzbarkeit und die Selbstreinigung superhydrophober Oberflächen*, volume 5 of *Schriftenreihe Mechanische Verfahrenstechnik*. Shaker-Verlag, Aachen.

Gao, J., Liu, Y., Xu, H., Wang, Z., and Zhang, X. (2009). Mimicking biological structured surfaces by phase-separation micromolding. *Langmuir*, 25:4365–4369.

Gates, D. and Tantraporn, W. (1952). The reflectivity of decidous trees and herbaceous plants in the infrared to 25 microns. *Science*, 115(2997):613–316.

Gausmann, H., Allen, W., and D.E., E. (1974). Refractive index of plant cell walls. *Applied Optics*, 13:109–111.

Georgiev, G. and Butler, F. (2007). Long-term calibration monitoring of Spectralon diffusers BRDF in the air-ultraviolet. *Applied Optics*, 46(32).

Glover, B. (2007). *Flowers & Flowering*. Oxford University Press, Oxford, New York.

Glover, B. and Martin, C. (1998). The role of petal cell shape and pigmentation in pollination success in Antirrhinum majus. *Heredity*, 80:778–784.

Gorb, S. (2007). Visualization of native surfaces by two-step molding. *Microscopy today*, 15:44–46.

Gorton, H. and Vogelmann, T. (1996). Effects of epidermal cell shape pigmentation on optical properties of Antirrhinum petals at visible and ultraviolet wavelengths. *Plant Physiology*, 112:10.

Gosh, N., Bajoria, A., and Vaidya, A. (2009). Surface chemical modification of poly(dimetylsiloxane)-based biomimetic materails: oil-repellent surfaces. *Applied Materials and Interfaces*, 1:2636–2644.

Green, M., Wenham, S. R., and Srinivasamohan, N. (1992). Sculpted solar cell surfaces.

Green, P. and Linstead, P. (1990). A procedure for SEM of complex shoot structures applied to the inflorescence of snapdragon (Antirrhinum). *Protoplasma*, 158:33–38.

Haberlandt, G. (1914). In *Physiological Plant Anatomy*, page 777. Macmillian, London, 4 edition.

Han, X. and Wang, J. (2011). A Novel Method for Fabrication of the Biomimetic Shark-Skin Coating. *Advanced Materials Research*, 239:3014–3017.

Hebant, C. and Lee, D. (1984). Ultrastructural basis and developmental control of blue iridescence in selaginella leaves. *American Journal of Botany*, 71(2):216–219.

Hecht, E. (2001). *Optik*. Oldenbourg Wissenschaftsverlag GmbH, München, Wien, Oldenbourg.

Holdermann, K. (2002). Method for the wet chemical pyramidal texture etching of silicon surfaces.

Hong, X., Gao, X., and Jiang, L. (2007). Application of superhydrophobic surface with high adhesive force in no lost transport of superparamagnetic microdroplet. *Journal of the American Chemical Society*, 129:1478–1479.

Hozumi, A. and Takai, O. (1997). Preparation of ultra water-reppellent films by microwave plasma-enhanced CVD. *Thin solid films*, 303:222–225.

Israelachvili, J. N., Chen, Y.-L., and Yoshizawa, H. (1994). Relationship between adhesion and friction forces. In Rimai, D., DeMejo, L., and Mittal, K., editors, *Fundamentals of adhesion and interfaces*, pages 261–279. VSP, Utrecht.

Jacquemoud, S. and Ustin, S. (2001). Leaf optical properties: A state of the art. In *Proc. 8th Int. Symp. Physical Measurements and Signatures in Remote Sensing*, pages 223–232.

Kang, S.-H., Tai, T.-Y., and Fang, T.-H. (2010). Replication of butterfly wing microstructures using molding lithography. *Current Applied Physics*, 10:625–630.

Kay, Q., Daoud, H., and Stirton, C. (1981). Pigment distribution,light reflection and cell structure in petals. *Botanical Journal of the Linnean Society*, 83b:57–84.

Kevan, P. and Lane, M. (1985). Flower petal microtexture is a tactile cue for bees. *PNAS*, 82(14):4750–52.

King-Smith, R. and Vanderbilt, D. (1993). Theory of polarization of crystalline solids. *Local Environment*, 4:5.

Knapp, A. and Carter, G. (1998). Variability in leaf optical properties among 26 species from a broad range of habitats. *American Journal of Botany*, 85(7):940–946.

Knoll, F. (1938). Über den Samtglanz der Blumenblätter. *Photografie und Forschung*, 2:137–148.

Ko, Y. and Yu, J. (2011). Highly transparent sapphire micro-grating structures with large diffuse light scattering. *Optics express*, 19(16):15574–15583.

Koch, K. and Barthlott, W. (2009). Superhydrophobic and superhydrophilic plant surfaces: an inspiration for biomimetic materials. *Philosophical Transactions of the Royal Society A: Mathematical, Physical and Engineering Sciences*, 367(1893):1487–1509.

Koch, K., Bhushan, B., and Barthlott, W. (2009). Multifunctional surface structures of plants: An inspiration for biomimetics. *Progress in Materials Science*, 54(2):137–178. doi: DOI: 10.1016/j.pmatsci.2008.07.003.

Koch, K., Bhushan, B., and Barthlott, W. (2010). Multifunctional Plant Surfaces and Smart Materials. In Bhushan, B., editor, *Springer Handbook of Nanotechnology*, pages 1399–1436. Springer, Berlin, Heidelberg, New York, 3 edition.

Koch, K., Dommisse, A., Barthlott, W., and Gorb, S. (2007). The use of plant waxes as templates for micro- and nanopatterning of surfaces. *Acta Biomaterialia*, 3:905–909.

Koch, K., Schulte, A., Fischer, A., Gorb, S., and Barthlott, W. (2008). A fast, precise and low-cost replication technique for nano- and high-aspect-ratio structures of biological and artificial surfaces. *Bioinspiration & Biomimetics*, 3(046002):10pp.

Koynov, S., Brandt, M., and Stutzmann, M. (2006). Black nonreflecting silicon surfaces for solar cells. *Applied Physics Letters*, 88:203107–203109.

Lafuma, A. and Quéré, D. (2003). Superhydrophobic states. *Nature Materials*, 2:457–460.

Lakhtakia, A., Martín-Palma, R., Motyka, M., and Pantano, C. (2009). Fabrication of free-standing replicas of fragile, laminar, chitinous biotemplates. *Bioinspiration & Biomimetics*, 4:4pp.

Lee, D., Bone, R., Tarsis, S., and Storch, D. (1990). Correlates of leaf optical properties in tropical forest sun and extreme-shade plants. *American Journal of Botany*, 77(3):370–380.

Lee, D. and Graham, R. (1986). Leaf optical properties of rainforest sund and extreme shade plants. *American Journal of Botany*, 73(8):1100–1108.

Lee, S.-M., Üpping, J., Bielawny, A., and Knez, M. (2011). Structure-based color of natural petals discriminated by polymer replication. *Applied Materials and Interfaces*, 3(1):30–34.

Lee, Y., Ju, K., and Lee, J. (2010). Stable biomimetic superhydrophobic surfaces fabricated by polymer replication method from hierarchically structured surfaces of Al templates. *Langmuir*, 26:14103–14110.

Liu, M., Zheng, Y., Zhai, J., and Jiang, L. (2010). Bioinspired super-antiwetting interfaces with special liquid-solid adhesion. *Accounts of Chemical Research*, 43(3):368–377.

Martin, G., Myres, D., and Vogelmann, T. (1991). Characterization of plant epidermal lens effects by a surface replica technique. *Journal of experimental botany*, 42:581–587.

Martin, G., Sedley, A., Josserand, A., Bornmann, J., and Vogelmann, T. (1989). Epidermal focussing and the light microenvironment within leaves of Medicago sativa. *Physiologia Plantarum*, 76:485–492.

Martin, J. and Juniper, B. (1970). The cuticles of plants. *The cuticles of plants*, page 347 pp.

McClendon, J. and Fukshansky, L. (1990). On the interpretation of absorption spectra of leaves.I.Introduction and the correction of leaf spectra for surface reflection. *Photochem. Photobiol.*, 51:203–210.

Mlcak, R. and Tuller, H. (1994). Electrochemical etching process. 5,338,416.

Myers, D., Vogelmann, T., and Bornmann, J. (1994). Epidermal focussing and effects on light utilization in Oxalis acetosella. *Physiologia Plantarum*, 91:651–656.

Neinhuis, C. and Barthlott, W. (1997). Characterization and distribution of water-repellent, self-cleaning plant surfaces. *Annals of Botany*, 79:667–677.

Noda, K.-I., Glover, B., Linstead, P., and Martin, C. (1994). Flower color intensity depends on specialized cell shape controlled by Myb-related transcription factor. *Nature*, 369:661–664.

Nosonovsky, M. and Bhushan, B. (2007). Hierarchical roughness optimization for biomimetic superhydrophobic surfaces. *Ultramicroscopy*, 107(10-11):969–979. doi: DOI: 10.1016/j.ultramic.2007.04.011.

Parker, A. (2004). A vision for natural photonics. *Philosophical transactions of the Royal Society A*, 362:2709–2720.

Parker, A. R. (2009). Natural photonics for industrial inspiration. *Philosophical Transactions of the Royal Society A: Mathematical, Physical and Engineering Sciences*, 367(1894):1759–1782.

Pfündel, E., Agati, G., and Cerovic, Z. (2006). Optical properties of plant surfaces. In Riederer, M. and Müller, C., editors, *Biology of the plant cuticle*. Blackwell Publishing, Oxford.

Poulson, M. and Vogelmann, T. (1990). Epidermal focussing and effects upon photosythetic light-harvesting in leaves of Oxalis. *Plant, Cell and Environment*, 13:803–811.

Prüm, B., Seidel, R., Bohn, H., and Speck, T. (2012a). Impact of cell shape in hierarchical structured plant surfaces on the attachment of male Colorado potato beetles (Leptinotarsa decemlineata). *Beilsteiln Journal of Nanotechnology*, 3:57–64.

Prüm, B., Seidel, R., Bohn, H., and Speck, T. (2012b). Plant surfaces with cuticular folds are slippery for beetles. *Journal of the Royal Society Interface*, 9:127–135.

Quake, S. and Scherer, A. (2000). From micro-to nanofabrication with soft materials. *Science*, 290(5496):1536–1540.

Riederer, M. Müller, C. (2006). *Biology of the plant cuticle.* Blackwell Publishing.

Roach, P., Shirtcliffe, N. J., and Newton, M. I. (2008). Progress in superhydrophobic surface development. *Soft Matter*, 4(2):224–240. 10.1039/b712575p.

Saison, T., Peroz, C., Chauveau, V., Berthier, S., Sondergard, E., and Arribart, H. (2008). Replication of butterfly wing and natural lotus leaf structures by nanoimprint on silica sol-gel films. *Bioinspiration & Biomimetics*, 3:5pp.

Schmid, H. and Michel, B. (2000). Siloxane polymers for high-resolution, high-accuracy soft lithography. *Macromolecules*, 33:3042–3049.

Schulte, A., Droste, D., Koch, K., and Barthlott, W. (2011). Hierarchically structured superhydrophobic flowers with low hysteresis of the wild pansy (Viola tricolor)–new design principles for biomimetic materials. *Beilstein Journal of Nanotechnology*, 2:228–236.

Schulte, A., Koch, K., Spaeth, M., and Barthlott, W. (2009). Biomimetic replicas: Transfer of complex architectures with different optical properties from plant surfaces onto technical materials. *Acta Biomaterialia*, 5:1848–1854.

Shi, F., Chen, X., Wang, L., Niu, J., Yu, J., Wang, Z., and Zhang, X. (2005). Roselike microstructures formed by direct in situ hydrothermal synthesis: from superhydrophilicity to superhydrophobicity. *Chemistry of Materials*, 17:6177–6180.

Shin, T.-K., Ho, J.-R., and Cheng, J.-W. J. (2004). A new approach to polymeric microlens array fabrication using soft replica molding. *IEEE Photonics Technology Letters*, 16(9):2078–2080.

Sims, D. and Gamon, J. (2002). Relationships between leaf pigment content and spectral reflectance across a wide range of species, leaf structures and developmental stages. *Remote Sensing of Environment*, 81:337–354.

Singh, A., Jayaram, J., Madou, M., and Akbar, S. (2002). Pyrolysis of negative photoresists to fabricate carbon structures for microelectromechanical systems and electrochemical applications. *Journal of the electrochemical society*, 149:E78.

Sitte, P., Weiler, E., Kadereit, J., Neuhaus, G., and Sonnewald, U. (2008). *Strasburger - Lehrbuch der Botanik.* Spektrum Akademischer Verlag.

Smith, W., Vogelmann, T., DeLucia, E., Bell, D., and Shepherd, K. (1997). Leaf form and photosynthesis.Do leaf structure and orientation interact to regulate internal light and carbon dioxide? *Bioscience*, 47(785-793):785–793.

Stavenga, D., Foletti, S., Palasantzas, G., and Arikawa, K. (2006). Light on the moth-eye corneal nipple array butterflies. *Proceedings of the Royal Society B*, 273:661–667.

Stirton, C. (1980). Petal sculpturing. In Pulhill, R. and Raven, P., editors, *Advances in legume systematics.* HMSO, London, London.

Sun, C.-H., Gonzalez, A., Linn, N. C., Jiang, P., and Jiang, B. (2008). Templated biomimetic multifunctional coatings. *Applied Physics Letters*, 92(5):0511071–3.

Sun, T., Feng, L., Gao, X., and Jiang, L. (2005). Bioinspired surfaces with special wettability. *Accounts of chemical research.*, 38:644–652.

Toda, Y. (1918). Physiological Studies on Schistostega osmundacea (Dicks.) Mohr. *The Journal of the College of Science*, 40:1–30.

Vogelmann, T. (1993). Plant tissue optics. *Annual Review of Plant Physiology and Plant Molecular Biology*, 44:231–251.

Vukusic, P., Hallam, B., and Noyes, J. (2007). Brilliant whiteness in ultrathin beetle scales. *Science*, 315:348.

Vukusic, P. and Sambles, J. (2003). Photonic structures in biology. *Nature*, 424:852–855.

Vukusic, P., Sambles, J. R., Lawrence, C. R., and Wootton, R. J. (2001a). Structural colour Now you see it now you don't. *Nature*, 410(6824):36. TY - JOUR 10.1038/35065161.

Vukusic, P., Sambles, R., Lawrence, C., and Wakely, G. (2001b). Sculpted-mulitlayer optical effects in two species of papilio butterfly. *Applied Optics*, 40(7):1116–1125.

Wagemann, H.-G. and Eschrich, H. (2010). *Photovoltaik - Solarstrahlung und Halbleitereigenschaften,Solarzellenkonzepte und Aufgaben*. Vieweg+Teubner, Wiesbaden.

Wagner, P., Fürstner, R., Barthlott, W., and Neinhuis, C. (2003). Quantitative assessment to the structural basis of water repellency in natural and technical surfaces. *Journal of Experimental Botany*, 54(385):1295–1303.

Wang, S. and Jiang, L. (2007). Definition of Superhydrophobic States. *Advanced Materials*, 19(21):3423–3424. 10.1002/adma.200700934.

Wenham, S. and Green, M. (1986). Laser grooved solar cell.

Wenzel, R. (1936). Resistance of solid surfaces to wetting by water. *Industrial and Engineering Chemistry*, 28(8):988–994.

Whitesides, G., Ostuni, E., Takayama, S., Jiang, X., and Ingber, D. (2001). Soft lithography in biology and biochemistry. *Annual review of biomedical engineering*, 3:335–373.

Whitney, H., Bennett, K., Dorling, M., Sandbach, L., Prince, D., Chittka, L., and Glover, B. (2011). Why do so many petals have conical epidermal cells? *Annals of Botany*, 108:609–616.

Whitney, H., Dyer, A., Chittka, L., Rands, S., and Glover, B. (2008). The interaction of temperature and sucrose concentration on foraging preferences in bumblebees. *Naturwissenschaften*, 95:845–850.

Whitney, H., Kolle, M., Alvarez-Fernandez, R., Steiner, U., and Glover, B. (2009a). Contributions of iridescence to floral patterning. *Communicative & Integrative Biology*, 2(3):230–232.

Whitney, H.M.and Kolle, M., Andrew, P., Chittka, L., Steiner, U., and Glover, B. (2009b). Floral iridescence, produced by diffractive optics, acts as cue for animal pollinators. *Science*, 323:130–133.

Woolley, J. (1971). Reflectance and transmittance of light by leaves. *Plant Physiology*, 47:656–662.

Xi, J. and Jiang, L. (2008). Biomimic superhydrophobic surface with high adhesive forces. *Industrial & Engineering Chemistry Research*, 47:6354–6357.

Xia, Y. and Whitesides, G. M. (1998). Soft Lithography. *Angewandte Chemie International Edition*, 37(5):550–575. 10.1002/(SICI)1521-3773(19980316)37:5<550::AID-ANIE550>3.0.CO;2-G.

Yamada, N., Ijiro, T., Okamoto, E., Hayashi, K., and Masuda, H. (2011). Characterization pf antireflection moth-eye film on crystalline silicon photovoltaic module. *Progress in Photovoltaics: Research and Applications*, 19(2):134–140.

Youngblood, J. and McCarthy, T. (1999). Ultrahydrophobic polymer surfaces prepared by simultaneous ablation of polypropylen and sputtering of poly(tetrafluoroethylen) using radio frequency plasma. *Macromulecules*, 32:6800–6806.

Zhang, Y., Hayashi, T., Inoue, M., Oyama, Y., Hosokawa, M., and Yazawa, S. (2008). Flower Color Diversity and Its Optical Mechanism. *Acta Hort. (ISHS)*, 766:469–476.

Appendix

See attached the publication of Schulte et al. [2011].

Hierarchically structured superhydrophobic flowers with low hysteresis of the wild pansy (*Viola tricolor*) – new design principles for biomimetic materials

Anna J. Schulte[*1], Damian M. Droste[1], Kerstin Koch[2] and Wilhelm Barthlott[1]

Abstract

Hierarchically structured flower leaves (petals) of many plants are superhydrophobic, but water droplets do not roll-off when the surfaces are tilted. On such surfaces water droplets are in the "Cassie impregnating wetting state", which is also known as the "petal effect". By analyzing the petal surfaces of different species, we discovered interesting new wetting characteristics of the surface of the flower of the wild pansy (*Viola tricolor*). This surface is superhydrophobic with a static contact angle of 169° and very low hysteresis, i.e., the petal effect does not exist and water droplets roll-off as from a lotus (*Nelumbo nucifera*) leaf. However, the surface of the wild pansy petal does not possess the wax crystals of the lotus leaf. Its petals exhibit high cone-shaped cells (average size 40 µm) with a high aspect ratio (2.1) and a very fine cuticular folding (width 260 nm) on top. The applied water droplets are in the Cassie–Baxter wetting state and roll-off at inclination angles below 5°. Fabricated hydrophobic polymer replicas of the wild pansy were prepared in an easy two-step moulding process and possess the same wetting characteristics as the original flowers. In this work we present a technical surface with a new superhydrophobic, low adhesive surface design, which combines the hierarchical structuring of petals with a wetting behavior similar to that of the lotus leaf.

Introduction

Plant surfaces provide a large diversity of hierarchically designed structures with various functions [1,2]. Different types of epidermal cells (micro-roughness) exist in combination with cuticular folds or epicuticular waxes (nano-roughness), or both, on top [1,3]. Hierarchy in surface sculpture can cause water repellent and self-cleaning properties ("Lotus effect") [4-6] or cause air retention under water ("Salvinia effect") [7,8]. Superhydrophobic, self-cleaning surfaces possess a static contact angle (CA) equal to or above 150°, and a low hysteresis angle, where water droplets roll-off at surface inclinations equal to or below 10° [6,9]. One of the most important biological water repellent and self-cleaning surfaces is the lotus

(*Nelumbo nucifera)* leaf [4,5]. Its water repellence is based on two factors: Surface roughness and a hydrophobic surface chemistry. The micro-morphological characteristics of lotus leaves are papillose cells covered with a dense layer of small hydrophobic wax tubules. In plants, surface waxes occur as thin films (two-dimensional waxes) or as wax tubules, platelets, rodlets or other three-dimensional waxes [1,10]. In lotus leaves, air remains trapped below a water droplet and the contact area between the water and the leaf surface is thereby minimized [1]. This micro- and nanostructured surface, composed of low surface energy materials, leads to a high CA (163°) and a low hysteresis and tilt angle (2–3°). Additionally, lotus leaves show low adhesive properties to adhering particles. Thus, contamination by dust, pollen or even hydrophilic particles such as grime are carried away by water droplets which results in a clean surface [4].

Two distinct models are proposed to explain the wetting behavior of rough surfaces. In the Wenzel model [11] roughness increases a solid surface area; this geometrically enhances its hydrophobicity. In the Cassie–Baxter model [12] air remains trapped below the droplet in the surface cavities, which also leads to a superhydrophobic behavior, because the droplet sits partially on air [13].

The Wenzel model describes homogeneous wetting by the following equation,

$$\cos\theta = r\cos\theta_0 \qquad (1)$$

where θ is the static CA for a rough surface and θ_0 is the static CA for a smooth surface. The surface roughness r is defined as the ratio of the actual over the apparent surface area of the substrate. The Cassie–Baxter model describes heterogeneous wetting by the equation,

$$\cos\theta = r\cos\theta_0 - f_{la}(r\cos\theta_0 + 1) \qquad (2)$$

where f_{la} is the fraction of solid in contact with the liquid and is dimensionless.

Further important factors in surface wetting are the static contact angle hysteresis (CAH) and the tilt angle (TA). The CAH describes the difference between the advancing and receding CAs of a moving droplet, or of one increasing and decreasing in volume. The CAH occurs due to surface roughness and heterogeneity [14,15]. Low CAH results in a low TA, which describes the TA of a surface at which an applied water droplet starts to move [15].

Nowadays, transitional states between the Wenzel and Cassie–Baxter states have been discovered. Wang and Jiang [16] proposed five different states for superhydrophobic surfaces, where the lotus and gecko states are treated as special cases in the Cassie–Baxter model. Feng et al. [17] proposed a sixth superhydrophobic state, called the "Cassie impregnating wetting state" or "petal effect". Both describe superhydrophobic surfaces with high adhesive forces to water, and this means that the wetted surface area is smaller than in the Wenzel model but larger than in the Cassie–Baxter model. Feng et al. [17] demonstrated this effect on rose flowers (petals). The surfaces of petals are often morphologically characterized by micro papillae with cuticular folds on top. In contrast to the lotus surface with air pocket formation between cell papilla, wax crystals and salient water droplets [18], the petal surface seems to prevent air pocket formation and droplets penetrate into the cuticular folds by capillary forces. It is proposed that the sizes of both micro- and nanostructures are larger than those found on the lotus leaves. Water droplets are expected to penetrate into the larger grooves of the petals, but not into the smaller ones and, thus, cause the Cassie impregnating wetting state [17].

The structure-based wetting characteristics of petals seem to offer a great alternative for the development of biomimetic superhydrophobic materials for micro droplet transport in micro fluidic systems, sensors or optical devices [19,20]. These hierarchically designed petal surfaces, with micropapillae and cuticular folds on the papillae top, can be precisely reproduced and are suitable for the industrial production in large area foil imprinting processes. In contrast, the hierarchically organized structures of the lotus leaf are composed of micropapillae with randomly distributed tubules on top. The development of such a surface architecture requires two production steps. Firstly, the microstructures must be produced by moulding, lithography or in-print-techniques. Secondly, the nanostructure production requires expensive lithographic techniques, or self-assembling materials, such as metal oxides [9,21].

Some attempts have been made to fabricate superhydrophobic surfaces with high adhesion properties inspired by rose petals [20,22-25]. Bhushan and Her [25], for example, replicated dried and thereby collapsed, micropapillae, and examined the wetting behavior of these structurally changed petals. Bormasheko et al. [24] or Shi et al. [22] fabricated "petal effect" surfaces by impregnating a polyethylene film with *Lycopodium* particles (spores) or with techniques such as electromechanical deposition of metal aggregates, which show the same wetting behavior as rose petals, but showed a different surface design than the native petals used as biological models. Xi and Jiang [23] replicated native rose petals with polydimethylsiloxane (PDMS),

and fabricated surfaces that are topographically very similar to those of the original rose petals. However, their replicas possessed high adhesive forces to small (2 µl) water droplets, which cannot provide self-cleaning properties.

One simple and precise method to transfer petal surface structures into an artificial material is a soft lithography technique called replica moulding [26]. Specifically, for the replication of biological surfaces Koch et al. [27,28] introduced a cost-efficient, two-step replication technique. This precise method prevents shrinking and damaging of the biological master during the replication process by avoiding a vacuum preparation step or critical temperatures as are used in most other techniques, and biological surface structures with an extremely high aspect ratio (ar) can be replicated [29].

In this study, we present the superhydrophobic surface of the wild pansy *Viola tricolor* (Figure 1), with a low TA and discuss the influence of papillae morphology and the dimensions of cuticular folding on the petal wetting state. To this end biomimetic replicas of four petals, differing in their surface morphology, were generated and their wetting behavior was examined by measuring the static CA and the TA. Finally, the contact area between a water droplet and the *Viola* petal surface was examined and superhydrophobic artificial petal replicas with low adhesive properties were generated.

Results and Discussion
Micromorphological characteristics of the surfaces

Scanning electron microscope (SEM) investigations were made to characterize the micro- and nanostructures of the petals and their replicas. Petals of four different species which differ in their cell shape and dimension as well as in their wetting behavior were chosen. Figure 2 illustrates the SEM micrographs of the petal surfaces and their uncoated and coated polymer replicas [in the following the uncoated replicas are marked with a subscript *r* (= *replicas*), the coated replicas with a *cr* (= *coated replicas*) and the original petals are unmarked].
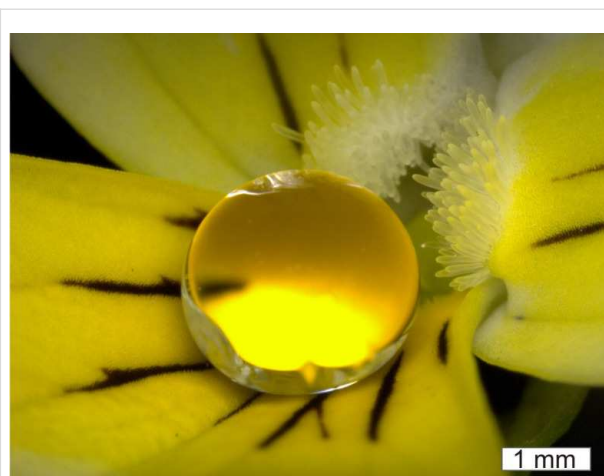
Figure 1: Macro photo of a water droplet on a flower of the wild pansy *(Viola tricolor).*

Petal surfaces of all four species are characterized by micropapillae with a cuticular folding on top (Figure 2; 1a–4a). As the pictures show, the replicas possess the same surface structures as the original petals. Minor deviations between the papillae shape of the original petals and the replicas may arise from critical point preparation of the petals (Figure 2; 1a–4a). The replicas were made from fresh turgescent flowers and the replication material used can mould a master structure to a high precision (replica deviations <2 nm from a master structure; Supporting Information File 1, Figure S1). Because of this, one may assume that the replicas display the real shape of the fresh petal surface structures. SEM pictures also show that antispread coated replicas (Figure 2; 1c–4c) possess the same surface structures as the uncoated replicas (Figure 2; 1b–4b). Accordingly, the structural parameters were collected on the uncoated replicas. Differences between the petal structures could be found in the dimensions of papillae and folds. *Rosa_r* and *Viola_r* are characterized by relatively sharp micropapillae (Figure 2; 3b, 4b), while *Dahlia_r* and *Cosmos_r* possess micropapillae with rounded tops (Figure 2; 1b, 2b). Furthermore, the micropapillae of the four different species vary from about 14 µm (*Rosa_r*) to 40 µm (*Viola_r*) in height, from 17 µm (*Rosa_r*) to 33 µm

Table 1: Micropapillae characteristics of the petal polymer replicas: average values (av) and their standard deviation (σ) values are shown (*n* = 30).

Replica	Micropapillae						
	Height [µm]		Midwidth [µm]		Aspect ratio (ar)	Papillae peak to peak distance [µm]	
	av	σ	av	σ	av	av	σ
Cosmos_r	20.3	4.7	19.6	3.7	**1.0**	41.0	11.8
Dahlia_r	21.8	5.6	32.7	4.2	**0.7**	48.4	10.1
Rosa_r	13.8	3.2	16.5	3.0	**0.8**	31.1	8.9
Viola_r	40.2	13.1	18.9	3.9	**2.1**	24.9	3.8
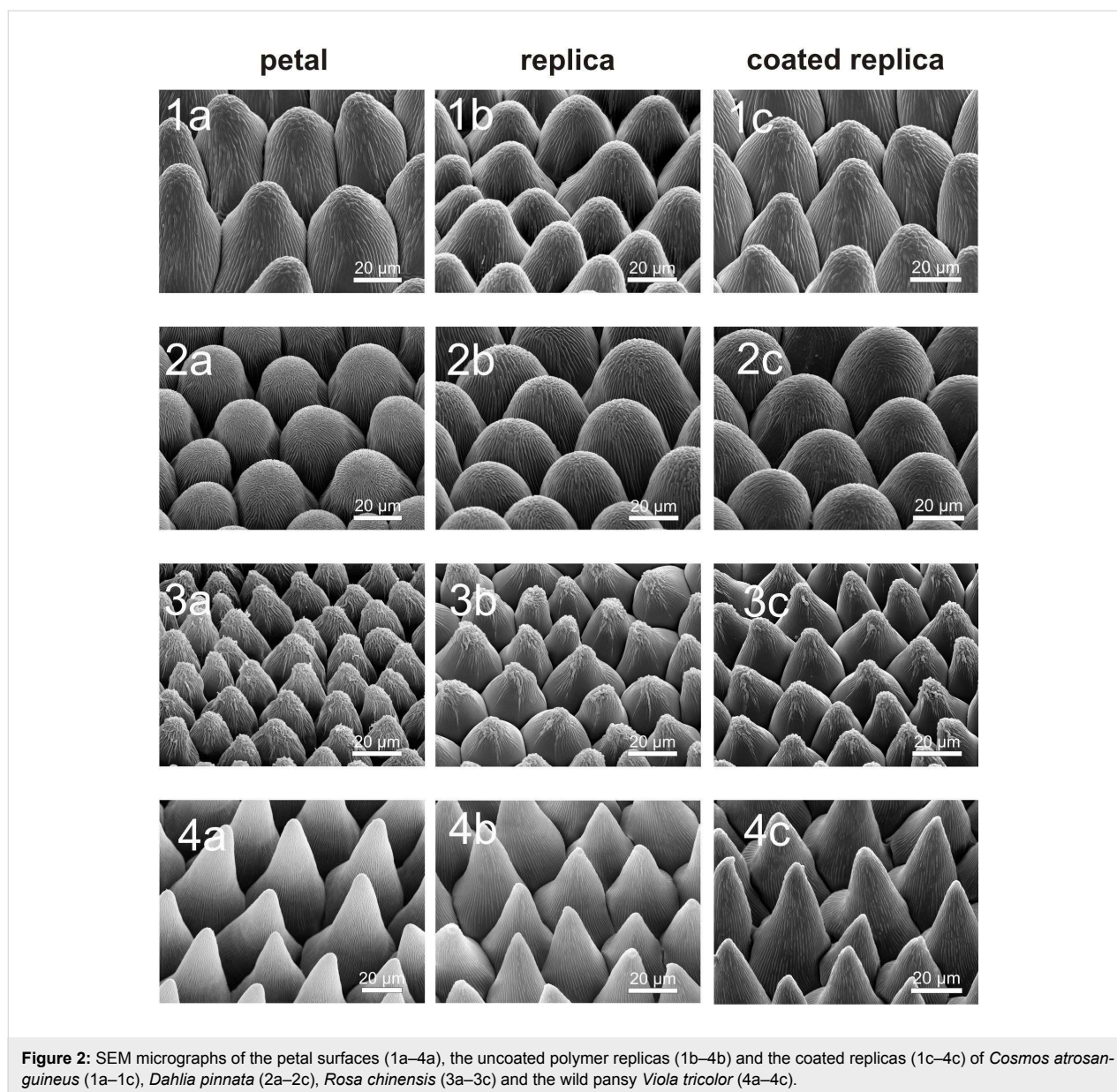
Figure 2: SEM micrographs of the petal surfaces (1a–4a), the uncoated polymer replicas (1b–4b) and the coated replicas (1c–4c) of *Cosmos atrosanguineus* (1a–1c), *Dahlia pinnata* (2a–2c), *Rosa chinensis* (3a–3c) and the wild pansy *Viola tricolor* (4a–4c).

(*Dahlia$_r$*) in their midwidth (papillae diameter at half of the papillae height) and from 25 μm (*Viola$_r$*) to 48 μm (*Dahlia$_r$*) in their peak-to-peak distance (Table 1).

The average aspect ratio (ar) of the papillae shows similar values for the *Cosmos$_r$*, *Dahlia$_r$* and *Rosa$_r$* papillae (ar 1.0; 0.7; 0.8). In contrast, the average ar of the *Viola$_r$* papillae is much larger (ar 2.1). In this context it is noted that the standard deviation (σ) of *Viola$_r$* papillae height is also higher than the standard deviation of the other species. The micropapillae dimensions are shown schematically in Figure 3.

Differences between the four species were also found in the distribution and dimensions (width and distance) of the cuticular folds (Table 2). While the micropapillae of *Dahlia$_r$* and *Viola$_r$* are completely covered with folds, the *Cosmos$_r$* and *Rosa$_r$* papillae only exhibit dense folding on top of the papillae and some single folds at the papillae side (Supporting Information File 1, Figure S2). Combinations of relatively thick folds separated by a small distance and thin folds separated by a large distance were found. The width of the folds varied from 260 nm (*Viola$_r$*) to 600 nm (*Cosmos$_r$*) and the distance between the single folds varied from 210 nm (*Dahlia$_r$*) to 460 nm (*Cosmos$_r$*).

Wettability of the petals and their replicas

Static CA and the TA measurements were performed to compare the surface structures with the wettability. Two super-

Figure 3: Diagram of the micropapillae dimensions of the average papilla shape on the upper surface of the *Cosmos_r*, *Dahlia_r*, *Rosa_r* and *Viola_r* petals. Also shown is the standard deviation of the papillae height (colored bars).

Table 2: Characteristics of cuticular folds found in the replicas of the petals: average values (av) and standard deviation (σ) values of the fold width and distance in µm (*n* = 30).

| | Cuticular folds | | | |
| Replica | Width [µm] | | Distance [µm] | |
	av	σ	av	σ
Cosmos_r	0.60	0.09	0.46	0.10
Dahlia_r	0.39	0.08	0.21	0.06
Rosa_r	0.41	0.09	0.21	0.09
Viola_r	0.26	0.07	0.45	0.12

hydrophobic petals (*Rosa* CA 155.6° and *Viola* CA 169°) and two hydrophobic petals (*Cosmos* CA 118.3° and *Dahlia* CA 136.4°) were found (Figure 4).

The static CA of the rose petals correlates well with the CA of roses previously measured by Feng et al. [17] (CA 152.4°), Xi at al. [23] (CA 154.3°) and Bhushan et al. [25] (CA 155°). The CA of the *Cosmos* petal was only 118°, thus, the *Cosmos* surface was more hydrophilic than the other petal surfaces. Except for *Cosmos*, all uncoated polymer replicas feature a lower CA than their biological model and thus did not show the same wetting behavior. This suggests that the replica material is more hydrophobic than the cuticle of the *Cosmos* petal and more hydrophilic than the cuticles of the other species investigated. The flat uncoated polymer had a CA of 79.3°, which is by definition a hydrophilic surface [9]. With respect to the Wenzel equation (Equation 1) a CA decrease through structuring of the hydrophilic polymer was expected [11]. In contrast to that, an increase of surface roughness has led to an increase of the CA of the structured polymers. After covering the replicas with a hydrophobic fluorine polymer (CA of the flat fluorine polymer: 106.5°), the CA values increased conspicuously (Figure 4). These results emphasize that a hydrophobic material in combination with surface roughness is the basis for the fabrication of superhydrophobic surfaces.

While the CA values of the coated replicas of *Cosmos_cr*, *Dahlia_cr* and *Rosa_cr* were very similar (CA 145.2°; 141.9°; 140.0°), the CA of *Viola_cr* was much higher (CA 168.9°). A similar tendency was found for the TAs (Figure 5). The petals of *Cosmos, Dahlia* and *Rosa* possess high adhesion to water droplets (*Cosmo*s and *Dahlia* TA >90°; *Rosa*: TA 44°), thus, water droplets do not roll-off from the petals or the coated and
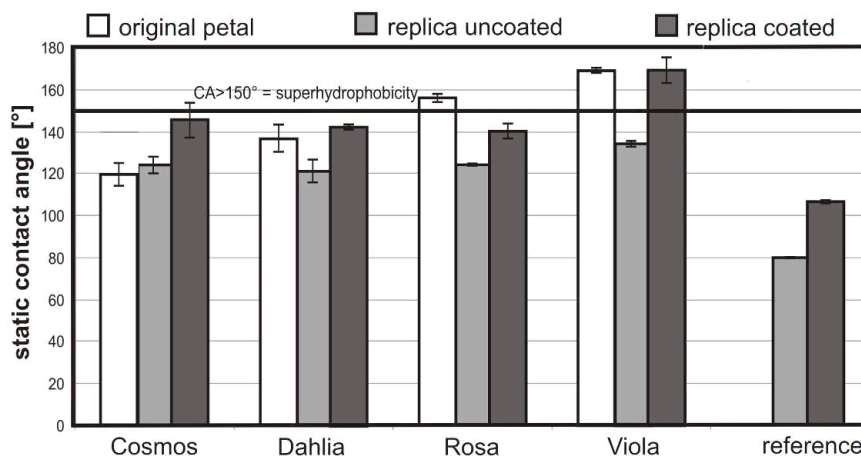
Figure 4: Static CAs of 5 µl water droplets on the surfaces of fresh (original) petals, their uncoated and coated polymer replicas and of the reference (uncoated and coated flat polymer; *n* = 10).
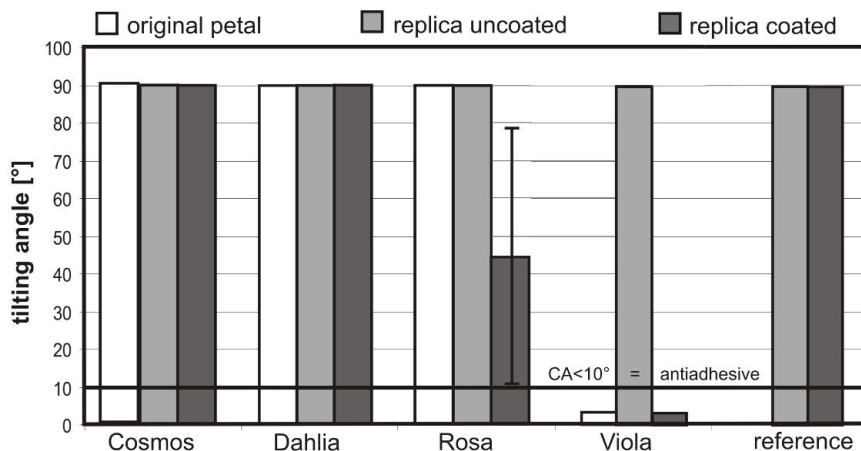
Figure 5: TAs of 5 µl water droplets on the surfaces of fresh (original) *Cosmos*, *Dahlia*, *Rosa* and *Viola* flowers, their uncoated and coated polymer replicas and the TA of the reference (uncoated and coated flat polymer; *n* = 10).

uncoated replicas. These data correlate well with the reported "petal effect". Feng et al. [17] showed that *Rosa* petal surface structures impart special properties to the flowers, in that small water droplets (1–10 µl) adhere to the petals whilst larger droplets (>10 µl) roll-off. On *Viola* petals and their coated replicas, applied droplets rolled off at TAs of <5°, even when droplets with a volume smaller than 10 µl (here 5 µl) were used (Figure 5).

The TA of the coated $Rosa_{cr}$ was very inhomogeneous. The average TA was 44° with high standard deviation (±34.4°). *Rosa* petals possess sharp micropapillae, the folds are relatively thick (410 ± 9 nm) and the micropapillae are only 13.8 ± 3.2 µm in height. With respect to wetting stages, air pocket formation on surfaces is important. By comparison of the microstructure of *Rosa* and *Viola*, we expect larger air pocket formation in *Viola,* based on the much higher micropapilla in *Viola* (40.2 µm in height). However, in roses sometimes air pocket formation might exist because some droplets rolled-off the surface at low inclination angles (TA 10°). These observations are in contrast to those of Feng et al. [17]. Over millions of years of co-evolution, different morphological adaptations have evolved in petals. Scanning electron microscopy studies also revealed large structural variations in petal microstructures. These surface microstructures cause optical signals [30,31] or function as a tactile cue for bees [32]. For us the "petal effect" or the repellence of petals seems to be a side effect and not the primary aim of the flower. A petal is a relatively short lived organ of plants, developed for pollinator attraction, but the short duration of petal lifetime makes a self-cleaning property for pathogen defence expendable. The last point might explain why water repellence is not widespread in petals.

Viola petals as a model for superhydrophobic, water repellent surfaces

Viola petals do not possess the "petal effect" and are anti-adhesive for water droplets. It is well known that hierarchical surface architecture represents optimized structures for superhydrophobic surfaces [11,33-36]. Based on the data presented here, we can describe two main superhydrophobic surface architectures for plant surfaces, the micropapillae with wax crystals [6] and micropapillae with cuticle folds. Some remarkable differences exist between the surface architecture of the lotus leaf and *Viola* petals. In *Viola* petals microstructures are larger (average height of 40.2 µm) than those of lotus leaves, which have microstructures with an average height of 15 µm [37]. The nanofolds in *Viola* have an average thickness of 0.26 µm, while the wax tubules of lotus are only 100 nm thick and ~0.5–3 µm in length [38]. Thus, the *Viola* petal possesses no three dimensional wax crystals, but a hydrophobic two dimensional wax film covering the micropapillae and nanofolds.

The distances between the structures also have an influence on the wetting stage. The average pitch value (peak to peak distances) of the lotus micropapillae is 22.6 ± 1.9 µm [37,38]. This is lower than the average pitch value of the *Rosa* micropapillae (31.1 ± 8.9 µm), but similar to the value of the *Viola* micropapillae (24.9 ± 3.8 µm). The dried rose petals investigated by Bhushan et al. [25] showed microstructures with larger pitch values than those found for the lotus leaf. On such petals water droplets seem to partially penetrate into the petal microstructures leading to a "Cassie impregnating wetting state". The low TA found for *Viola* petals indicates a Cassie–Baxter wetting regime, in which water droplets do not penetrate into the grooves of the micropapillae. Furthermore,

hysteresis can also be affected by the shape of the microstructures and adequate nano-sculpting on top. The combination of high (40.2 μm) and extremely peaked micropapillae with very fine folds (260 nm) on top apparently prevents water from penetrating into the structures by capillary force (Supporting Information File 1, Figure S2).

A high standard deviation in *Viola* micropapillae heights (σ: ±13.1 μm ≙ 33%, Table 1) demonstrates that large variations in cell height do exist. The percentage standard deviation of the micropapillae height of the other investigated species $Cosmos_r$ (σ: ±4.7 μm ≙ 23%), $Dahlia_r$ (σ: ±5.6 μm ≙ 26%) and $Rosa_r$ (σ: ±3.2 μm ≙ 23%) is much smaller. The higher standard deviation of the micropapillae height is correlated to a large reduction in papilla contact with the applied water droplet. Cryo-SEM-investigations (Figure 6) indicated that smaller micropapillae are not in contact with the applied liquid. Thus, cell height variations further decrease the liquid–solid contact area and consequently decrease the adhesion of the liquid to the surface. Additionally, a sharp papillae tip benefits more from a lower contact area than a flat, rounded papilla tip. For the "petal effect" Feng et al. [17] proposed that water droplets penetrate into the grooves between the micropapillae. *Viola* prevents water penetration into the micropapillae grooves by reducing the papillae peak to peak distance, which is on average 24.9 μm. Much larger peak to peak distances were found in $Rosa_r$ (31.1 μm), $Cosmos_r$ (41.0 μm) and $Dahlia_r$ (48.4 μm). The results presented here show that the combination of high micropapillae with high ar, sharp tips and small peak to peak distances is required for the design of biomimetic superhydrophobic petal surfaces with low hysteresis.
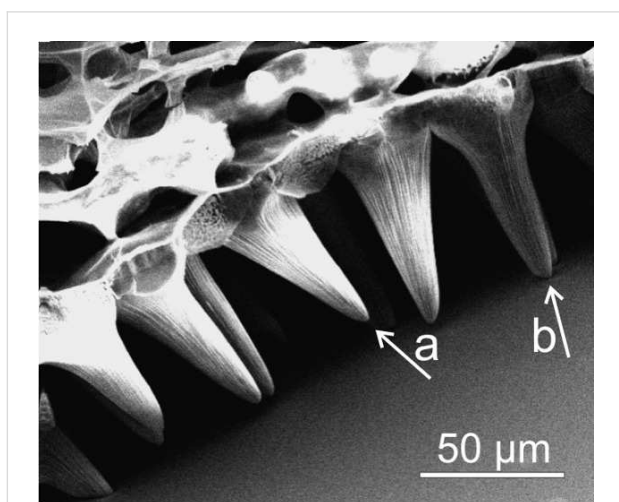
Figure 6: Cryo-SEM micrograph of the micropapillae of a *Viola* petal in contact with the surface of a water-glycerol droplet. Many micropapillae are not in contact with the droplet surface (a) while others are in contact with the droplet surface (b).

The cuticular folds also have an influence on the wetting stage. On $Viola_r$ the micropapillae are completely covered with fine nano-folds (260 ± 70 nm), arranged at a separation of 450 ± 120 nm, whilst the micropapillae of the $Rosa_r$ petals are only partially covered with broader folds (410 ± 90 nm), arranged at a separation of 210 ± 90 nm. Feng et al. [17] noted folds of 730 nm width on the micropapillae with an average diameter of 16 μm and a height of 7 μm (the differences probably result from the usage of different species). Their rose petals possess a CA of 152.4° and a TA of >90°. By replicating the flowers, they developed a polymer film with a CA of 154.6° and a high adhesion to water droplets (TA >90°). Hydrophobic replicas of the *Viola* petals have a CA of 169° and a TA of <5°. These results show that finer folds arranged at small separation seem to prevent the penetration of water into the folds by capillary forces.

Conclusion

Flower petals provide a new design strategy for the development of superhydrophobic, biomimetic materials. In contrast to superhydrophobic petals, where water droplets adhere, and which have been described before, we found a biological model (*Viola tricolor*) with a superhydrophobic, water repellent petal surface. Indeed, these flowers provide the typical surface architecture of petals (micropapillae with a folding on top), but a similar wetting behavior as that described for lotus leaves. By an easy and fast replication technique and subsequent hydrophobic coating, biomimetic replicas were fabricated. These replicas possessed the same surface structures and wettability as the biological models. The petal surface design of *Viola*, introduced here, seems to be easier and much more favourably to produce, e.g., by imprint processes, than the hierarchically organized structures which are found on the lotus leaf. In contrast to the lotus leaf structuring with randomly distributed nanocrystals the surface structures of *Viola* could be qualified, for example, for large area foil imprinting processes. Thus, a new surface design for the development of superhydrophobic, water repellent biomimetic materials is presented.

Experimental
Plant material
The upper surface (adaxial) sides of the petals of four different plant species were investigated. Plants were cultivated in the Botanic Gardens of the Rheinische Friedrich–Wilhelms-University of Bonn (BGB). Their scientific names are given together with their registration numbers of the BGB. Investigated species are the Chocolate Cosmos (*Cosmos atrosanguineus;* BGB 29614-8-2008), *Dahlia pinnata* (BGB 7960-9-1990), the China Rose (*Rosa chinensis;* BGB 3089-9-1979) and the Wild Pansy *Viola tricolor* (BGB 27262-4-2004).

Fabrication of the replicas

For the fabrication of the biomimetic polymer replicas, the replication technique introduced by Koch et al. [28] was used. Here, we briefly introduce the technique and mention the modifications made. The replication technique is a two-step moulding process, in which at first a negative is generated and then a positive. For generating the negative replicas, the master (biological sample) is moulded with polyvinylsiloxane dental wax (President light body Gel, ISO 4823, PLB; Coltene Whaldent, Hamburg, Germany). In the second step, the negative replicas were filled with a two-component epoxy resin (RECKLI Injektionsharz EP, RECKLI GmbH, Herne, Germany). The use of this material is a modification in the replication process introduced by Koch et al. [28] (replication performance of the RECKLI material; Supporting Information File 1, Figure S1). After spilling the negative replicas, the epoxy resin was dried for 48 h at 25 °C. After hardening, the positive replicas were peeled off from the negative replicas and further replicas were fabricated. In total, five petals of each species were replicated and examined afterwards.

Hydrophobization of the replicas

The replicas were dip-coated (30 sec) in a fluorine polymer (Antispread, E2/50 FE 60, Dr. Tillwich GmBH Werner Stehr) and then dried for 20 min at room temperature. Antispread is a commercially available Fluorocarbon 60 for surface hydrophobization. It forms approximately 40 nm thin layers on the substrate (producer information) and causes no additional nanostructuring on the replica surfaces. A smooth surface, dipcoated with Antispread has a static CA of 106°.

Surface characterization

The surface structures of the biological samples and their replicas were investigated by SEM. Images were recorded using a CAMBRIDGE Stereoscan 200 SEM (Zeiss GmbH, Oberkochen, Germany), a digital image processing system (DISS 5, Version 5.4.17.0, Point Electronic GmbH, Halle, Germany) was used to visualize and measure the surface structures of the petals. Fresh plant material was dehydrated with ethanol and dried in a critical point dryer (CPD 020, Balzers Union, Balzers–Pfeifer GmbH, Aßlar). On account of their stability, the replicas did not require special preparation. All samples were sputter-coated with a 30 nm gold layer (Balzers Union SCD 040, Balzers–Pfeifer GmbH, Aßlar) prior to SEM investigations.

Cryo-SEM examinations

To display an applied droplet in contact with the petal surface, the Cryo-SEM method, developed by Ensikat et al. [18], was used. In this method a sample–droplet (glycerol–water mixture of 1:3) complex was frozen with liquid nitrogen. A water–glycerol mixture was used as the liquid to prevent crystallization patterns on the droplet surface, which occur on pure water droplets. After this the sample was separated from the droplet (5 µl) and the surface imprint of the droplet was examined under a scanning electron microscope. All examinations were performed using a CAMBRIDGE Stereoscan 200 SEM (Zeiss GmbH, Oberkochen, Germany), equipped with a digital image acquisition system (DISS 5, Point Electronic, Halle, Germany).

Static contact angle and tilt angle measurements

The wettability of the biological samples and the replicas was characterized by CA and TA measurements with a computer controlled goniometer OCA 30 (Dataphysics SCA 2.02, Filderstadt, Germany). Five microliters of demineralized water droplets were automatically applied to the samples via syringe and CAs were automatically determined using the Laplace–Young fitting algorithm. TAs were measured by tilting the samples (with an applied droplet on the surface) and measuring the TA at which the droplets rolled off the surface. Each measurement was repeated 10 times.

Supporting Information

Supporting Information File 1
Additional figures.
[http://www.beilstein-journals.org/bjnano/content/supplementary/2190-4286-2-27-S1.pdf]

Acknowledgements

References

1. Koch, K.; Bhushan, B.; Barthlott, W. *Prog. Mater. Sci.* **2009,** *54,* 137–178. doi:10.1016/j.pmatsci.2008.07.003
2. Bargel, H.; Koch, K.; Cerman, Z.; Neinhuis, C. *Funct. Plant Biol.* **2006,** *33,* 893–910. doi:10.1071/FP06139
3. Barthlott, W.; Ehler, N. In *Tropische und Subtropische Pflanzenwelt;* Mainz, Akademie der Wissenschaften und der Literatur, Ed.; Steiner: Wiesbaden, 1977; Vol. 19, pp 367–467.

4. Barthlott, W.; Neinhuis, C. *Planta* **1997,** *202,* 1–8.
   doi:10.1007/s004250050096
5. Neinhuis, C.; Barthlott, W. *Ann. Bot. (Oxford, U. K.)* **1997,** *79,* 667–677.
   doi:10.1006/anbo.1997.0400
6. Koch, K.; Barthlott, W. *Philos. Trans. R. Soc. London, Ser. A* **2009,**
   367, 1487–1509. doi:10.1098/rsta.2009.0022
7. Barthlott, W.; Schimmel, T.; Wiersch, S.; Koch, K.; Brede, M.;
   Barczewski, M.; Walheim, S.; Weis, A.; Kaltenmaier, A.; Lederer, A.;
   Bohn, H. F. *Adv. Mater.* **2010,** *22,* 2325–2328.
   doi:10.1002/adma.200904411
8. Cerman, Z.; Striffler, B. F.; Barthlott, W. In *Functional Surfaces in
   Biology;* Gorb, S. N., Ed.; Springer: Berlin, Heidelberg, 2009; Vol. 1,
   pp 97–112. doi:10.1007/978-1-4020-6697-9_7
9. Roach, P.; Shirtcliffe, N. J.; Newton, M. I. *Soft Matter* **2008,** *4,* 224–240.
   doi:10.1039/b712575p
10. Barthlott, W.; Wollenweber, E.
    Tropische und subtropische Pflanzenwelt **1981,** *32,* 7–67.
11. Wenzel, R. N. *Ind. Eng. Chem.* **1936,** *28,* 988–994.
    doi:10.1021/ie50320a024
12. Cassie, A. B. D.; Baxter, S. *Trans. Faraday Soc.* **1944,** *40,* 546–551.
    doi:10.1039/tf9444000546
13. Lafuma, A.; Quéré, D. *Nat. Mater.* **2003,** *2,* 457–460.
    doi:10.1038/nmat924
14. Israelachvili, J. N.; Chen, Y.-L.; Yoshizawa, H. In *Fundamentals of
    adhesion and interfaces;* Rimai, D. S.; DeMejo, L. P.; Mittal, K. L., Eds.;
    VSP: Utrecht, 1994; pp 261–279.
15. Extrand, C. W. *Langmuir* **2002,** *18,* 7991–7999. doi:10.1021/la025769z
16. Wang, S.; Jiang, L. *Adv. Mater.* **2007,** *19,* 3423–3424.
    doi:10.1002/adma.200700934
17. Feng, L.; Zhang, Y.; Xi, J.; Zhu, Y.; Wang, N.; Xia, F.; Jiang, L.
    Langmuir **2008,** *24,* 4114–4119. doi:10.1021/la703821h
18. Ensikat, H. J.; Schulte, A. J.; Koch, K.; Barthlott, W. *Langmuir* **2009,** *25,*
    13077–13083. doi:10.1021/la9017536
19. Hong, X.; Gao, X.; Jiang, L. *J. Am. Chem. Soc.* **2007,** *129,* 1478–1479.
    doi:10.1021/ja065537c
20. Liu, M.; Zheng, Y.; Zhai, J.; Jiang, L. *Acc. Chem. Res.* **2010,** *43,*
    368–377. doi:10.1021/ar900205g
21. Bhushan, B.; Jung, Y. C.; Nosonovsky, M. In *Springer Handbook of
    Nanotechnology;* Bhushan, B., Ed.; Springer: Berlin, Heidelberg, New
    York, 2010; Vol. 3, pp 1437–1524. doi:10.1007/978-3-642-02525-9_42
22. Shi, F.; Chen, X.; Wang, L.; Niu, J.; Yu, J.; Wang, Z.; Zhang, X.
    Chem. Mater. **2005,** *17,* 6177–6180. doi:10.1021/cm051453b
23. Xi, J.; Jiang, L. *Ind. Eng. Chem. Res.* **2008,** *47,* 6354–6357.
    doi:10.1021/ie071603n
24. Bormashenko, E.; Stein, T.; Pogreb, R.; Aurbach, D. *J. Phys. Chem. C*
    2009, *113,* 5568–5572. doi:10.1021/jp900594k
25. Bhushan, B.; Her, E. K. *Langmuir* **2010,** *26,* 8207–8217.
    doi:10.1021/la904585j
26. Xia, Y.; Whitesides, G. M. *Angew. Chem., Int. Ed.* **1998,** *37,* 550–575.
    doi:10.1002/(SICI)1521-3773(19980316)37:5<550::AID-ANIE550>3.0.
    CO;2-G
27. Koch, K.; Dommisse, A.; Barthlott, W.; Gorb, S. N. *Acta Biomater.*
    2007, *3,* 905–909. doi:10.1016/j.actbio.2007.05.013
28. Koch, K.; Schulte, A. J.; Fischer, A.; Gorb, S. N.; Barthlott, W.
    Bioinspir. Biomim. **2008,** *3,* No. 04600210.
    doi:10.1088/1748-3182/3/4/046002
29. Schulte, A. J.; Koch, K.; Spaeth, M.; Barthlott, W. *Acta Biomater.* **2009,**
    5, 1848–1854. doi:10.1016/j.actbio.2009.01.028
30. Whitney, H.; Kolle, M.; Alvarez-Fernandez, R.; Steiner, U.; Glover, B. J.
    Commun. Integr. Biol. **2009,** *2,* 230–232. doi:10.4161/cib.2.3.8084

31. Zhang, Y.; Hayashi, T.; Inoue, M.; Oyama, Y.; Hosokawa, M.;
    Yazawa, S. *Acta Hort. (ISHS)* **2008,** *766,* 469–476.
32. Kevan, P. G.; Lane, M. A. *Proc. Natl. Acad. Sci. U. S. A.* **1985,** *82,*
    4750–4752. doi:10.1073/pnas.82.14.4750
33. Callies, M.; Quéré, D. *Soft Matter* **2005,** *1,* 55–61.
    doi:10.1039/b501657f
34. Sun, C.-H.; Gonzalez, A.; Linn, N. C.; Jiang, P.; Jiang, B.
    Appl. Phys. Lett. **2008,** *92,* 0511071–0511073. doi:10.1063/1.2841818
35. Nosonovsky, M.; Bhushan, B. *Ultramicroscopy* **2007,** *107,* 969–979.
    doi:10.1016/j.ultramic.2007.04.011
36. Bhushan, B.; Jung, Y. C.; Koch, K. *Philos. Trans. R. Soc., A* **2009,** *367,*
    1631–1672. doi:10.1098/rsta.2009.0014
37. Fürstner, R. In *Untersuchungen zum Einfluss von Struktur und Chemie
    auf die Benetzbarkeit und die Selbstreinigung superhydrophober
    Oberflächen;* Walzel, P., Ed.; Schriftenreihe Mechanische
    Verfahrenstechnik, Vol. 5; Shaker Verlag: Aachen, Germany, 2002;
    pp 151 ff.
38. Koch, K.; Dommisse, A.; Niemietz, A.; Barthlott, W.; Wandelt, K.
    Surf. Sci. **2009,** *603,* 1961–1968. doi:10.1016/j.susc.2009.03.019

Supporting Information

for

Hierarchically structured superhydrophobic flowers with low hysteresis of the wild pansy (*Viola tricolor*) – new design principles for biomimetic materials

Anna J. Schulte[*1], Damian M. Droste[1], Kerstin Koch[2] and Wilhelm Barthlott[1]

[1]Nees Institute for Biodiversity of Plants, University of Bonn, Meckenheimer Allee 170, Bonn, Germany and [2]Rhine-Waal University of Applied Sciences, Landwehr 4, Kleve, Germany

Email: Anna Julia Schulte - a.schulte@uni-bonn.de

[*]Corresponding author

Additional figures
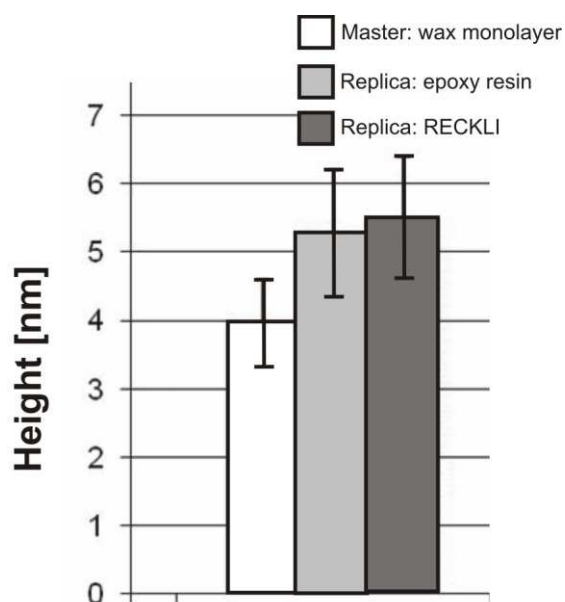
Figure S1: Replication of an octacosanol wax crystal multilayer with steps of 4 nm height. – Moulding performance of the replication material RECKLI compared to the replication performance of epoxy resin used in Koch et al. 2008 [1]. Measurements were performed by atomic force microscopy (n = 10).
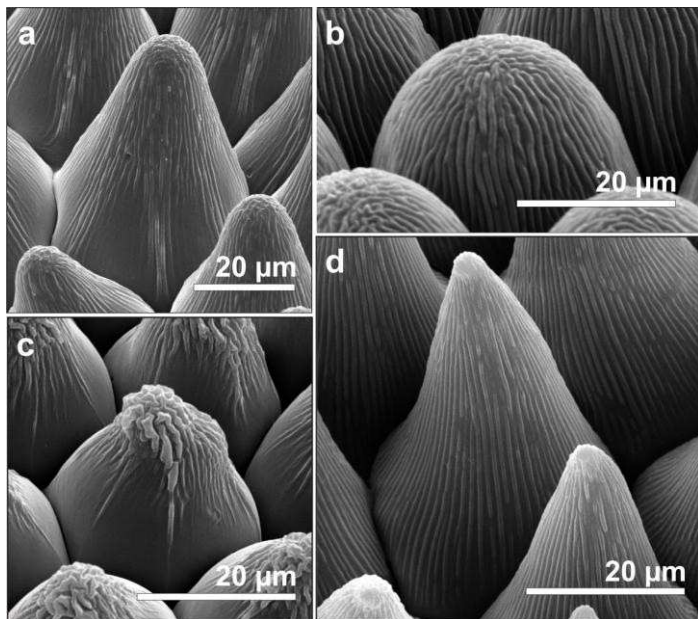
Figure S2: SEM micrographs of single epidermal cells and their cuticular folding on top: (a) *Cosmos*, (b) *Dahlia*, (c) *Rosa* and (d) *Viola*.
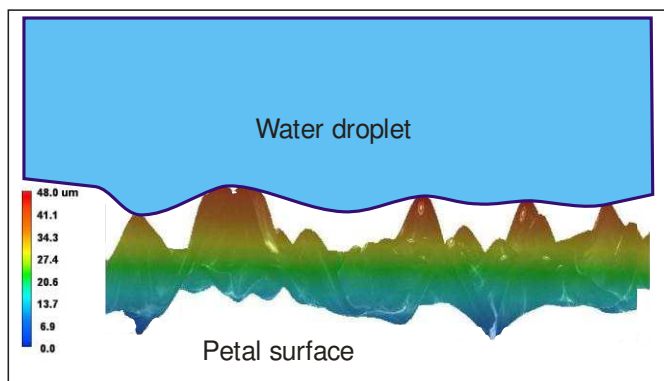
Figure S3: Schematic of the proposed wetting state of a water droplet on a 3d microscopy scan of the surface of a *Viola* petal (Cassie-Baxter state) when a water droplet is in contact with the surface of a *Viola* petal.

References

1. Koch, K.; Dommisse, A.; Barthlott, W.; Gorb, S. N. *Acta Biomater.* **2007,** *3,* 905–909. doi:10.1016/j.actbio.2007.05.013